Characterization of the role of host factors in the paramyxovirus life cycle

Dissertation
zur Erlangung des Doktorgrades
der Naturwissenschaften

vorgelegt beim Fachbereich Biochemie
der Johann Wolfgang Goethe-Universität
in Frankfurt am Main

von
Kristin Pfeffermann
aus Hünfeld

Frankfurt 2019

(D 30)

vom Fachbereich Biochemie der

Johann Wolfgang Goethe-Universität als Dissertation angenommen.

Dekan: Prof. Dr. Clemens Glaubitz

Gutachter: Prof. Dr. Robert Tampé, Institut für Biochemie, Goethe-Universität Frankfurt

Prof. Dr. Veronika von Messling, Paul-Ehrlich-Institut, Bundesinstitut für Impfstoffe und biomedizinische Arzneimittel, Abteilung Veterinärmedizin

Datum der Disputation: 18.10.2019

Regarde attentivement car ce que tu vas voir

n'est plus ce que tu viens de voir.

- Leonardo da Vinci -

CONTENTS

LIST OF ABBREVIATIONS

°C	degree Celsius
µg	microgram
µL	microliter
2-5A OAS	2-5′ oligoadenylate synthetase
^{35}S-Met/Cys	^{35}S-methionine/cysteine
4E-BP1	eIF4E-binding protein 1
5′ pppRNA	short hairpin dsRNA with triphosphorylated 5′ end
ABCE1	ATP-binding cassette sub-family E member 1
APS	ammonium persulfate
ATP	adenosine triphosphate
AUG	start codon
BALT	bronchus-associated lymphoid tissue
BeiPV	Beilong virus
BME	β-mercaptoethanol
bp	base pair
C	constant
CD150	cluster of differentiation 150
CDC	Centers for Disease Control and Prevention
cDNA	complementary DNA
CHX	cycloheximide
CNS	central nervous system
COPB2	coatomer protein complex subunit beta 2
CR	conserved region
CrPV	Cricket paralysis virus
CTP	cytidine triphosphate
CX3CR1	CX3 chemokine receptor 1
DAPI	4′,6-diamidino-2-phenylindole
DENV	Dengue virus
DMEM	Dulbecco's modified Eagle's medium
DMSO	dimethyl sulfoxide
DNA	deoxyribonucleic acid
dNTP	deoxynucleotide triphosphate
dsDNA	double-stranded deoxyribonucleic acid
DTT	dithiothreitol
E. coli	*Escherichia coli*
EBOV	Ebola virus
eEF2	eukaryotic elongation factor 2
EGF	epidermal growth factor
EGFP	enhanced green fluorescent protein
eIF	eukaryotic initiation factor
eIF1	eukaryotic initiation factor 1

eIF1A	eukaryotic initiation factor 1A
eIF2	eukaryotic initiation factor 2
eIF3	eukaryotic initiation factor 3
eIF3A	eukaryotic initiation factor 3A
eIF4A	eukaryotic initiation factor 4A
eIF4E	eukaryotic initiation factor 4E
eIF4F	eukaryotic initiation factor 4F
eIF4G1	eukaryotic initiation factor 4G1
eIF5	eukaryotic initiation factor 5
eIF5B	eukaryotic initiation factor 5B
eIFG	eukaryotic initiation factor G
EMCV	Encephalomyocarditis virus
eRF1	eukaryotic release factor 1
eRF3	eukaryotic release factor 3
esiRNAs	endoribonuclease-prepared siRNAs
F protein	fusion protein
FBS	fetal bovine serum
FDR	false discovery rate
FeS	iron sulfur
ffLuc	firefly luciferase
FIP	fusion inhibitory peptide
FOXP4	forkhead box P4
fwd	forward
G protein	glycoprotein
GAPDH	glyceraldehyde 3-phosphate dehydrogenase
ge	gene end
gs	gene start
GTP	guanosine triphosphate
H	hemagglutinin
h	hours
H1	hinge region 1
HCV	Hepatitis C virus
HEK293	human embryonic kidney 293 cells
HeLa	Henrietta Lacks
HEPES	4-(2-hydroxyethyl)-1-piperazineethanesulfonic acid
HeV	Hendra virus
HIV	Human immunodeficiency virus
HLH	helix–loop–helix
HN	hemagglutinin-neuraminidase
hpi	hours post-infection
HRC	heptad repeat region
HRP	horseradish peroxidase

HRSV	Human respiratory syncytial virus
HSD11B2	hydroxysteroid 11-beta dehydrogenase 2
hSLAM	human signaling lymphocytic activation molecule
HSPGs	heparan sulfate proteoglycans
ICAM-1	intercellular adhesion molecule 1
ICTV	International Committee on Taxonomy of Viruses
IFIT	interferon-induced with tetratricopeptide repeats
IFITM	interferon-induced transmembrane protein
IFN	interferon
Ig	immunoglobulin
IKKα	IκB kinase α
IRES	internal ribosomal entry site
IRF3	interferon regulatory factor 3
IRF7	interferon regulatory factor 7
ISG	IFN-stimulated genes
JAK-STAT	Janus kinase-signal transducers and activators of transcription
JPV	J paramyxovirus
kb	kilobases
KCl	potassium chloride
kDa	kilodalton
KH_2PO_4	potassium dihydrogen phosphate
KS strain	Khartoum-Sudan strain
KS test	Kolmogorov-Smirnov test
L protein	large protein
LB	Luria-Bertami
le	leader
LGP2	laboratory of genetics and physiology 2
M protein	matrix protein
MARV	Marburg virus
MDA5	melanoma differentiation associated factor 5
MeOH	methanol
Met-$tRNA_i$	initiator methionyl transfer RNA
MeV	Measles virus
mg	milligram
$MgCl_2$	magnesium chloride
min	minute
mL	milliliter
mM	millimolar
MMR	measles mumps rubella
MOI	multiplicity of infection

MoRE	molecular recognition element
mRNA	messenger RNA
MsigDB	Molecular Signatures Database
MuV	Mumps virus
Mx1	MX dynamin-like GTPase 1
N protein	nucleoprotein
Na_2HPO_4	sodium hydrogen phosphate
NaCl	sodium chloride
NaOAc	sodium acetate
NBD	nucleotide binding domain
NH_4Cl	ammonium chloride
NiV	Nipah virus
NP-40	Nonidet P-40
NSC	non-silencing control
nt	nucleotide
OAS	oligoadenylate synthase
OAS3	oligoadenylate synthase 3
OPP	O-propargyl-puromycin
P protein	phosphoprotein
PAMPS	pathogen-associated molecular patterns
PBMC	peripheral blood mononuclear cell
PCR	polymerase chain reaction
PDH E1α	pyruvate dehydrogenase E1α
PFA	paraformaldehyde
P_i	inorganic phosphate
PKK	protein kinase C-associated kinase
pmol	picomole
PNK	polynucleotide kinase
PRR	pattern recognition receptors
PRR15	proline rich 15
PVDF	polyvinylidine fluoride
qPCR	quantitative PCR
RBC	red blood cell
RBM22	RNA binding motif protein 22
renLuc	Renilla luciferase
rev	reverse
RIG-I	retinoic-acid inducible gene-I
RIPA buffer	radioimmunoprecipitation assay buffer
RISC	RNA induced silencing complex
RLRs	retinoic-acid inducible gene (RIG)-I like receptors
RNA	ribonucleic acid
RNase L	ribonuclease L

RNP	ribonucleoprotein complex
RP	ribosomal protein
rpm	revolutions per minute
RPV	Rinderpest virus
rRNA	ribosomal RNA
RT	reverse transcription
RT	room temperature
SAP	SLAM-associated protein
SDS-PAGE	sodium dodecyl sulfate-polyacrylamide gel electrophoresis
SH protein	small hydrophobic protein
SHCBP1	SHC SH2 domain-binding protein 1
shRNAs	small hairpin RNAs
siRNA	small interfering RNAs
SLAM	signaling lymphocytic activation molecule
SSPE	subacute sclerosing panencephalitis
STIKO	German Standing Committee on Vaccination (Ständige Impfkommission)
STP	serine-threonine-proline
SYBR green	N′,N′-dimethyl-N-[4-[(E)-(3-methyl-1,3-benzothiazol-2-ylidene)methyl]-1-phenylquinolin-1-ium-2-yl]-N-propylpropane-1,3-diamine
TAE	Tris-acetate-EDTA
TBS	Tris-buffered saline
TC	ternary complex
$TCID_{50}$	tissue culture infection dose 50
TEMED	tetramethylethylenediamine
TLR4	Toll-like receptor 4
TM	transmembrane
TNF-α	tumor necrosis factor alpha
TRBP	TAR-RNA-binding protein
Tris-HCl	Tris-hydrochloride
UPW	ultra-pure water
UTP	uridine triphosphate
UTR	untranslated region
UV	ultraviolet
V	variable
V	volt
VOC	valid object count
VSV	Vesicular stomatitis virus
w/v	weight/volume
WHO	World Health Organization
WNV	West Nile virus

ABSTRACT

Paramyxo- and pneumoviruses include many pathogens with great relevance for human and animal health. To identify common host factors involved in the *Paramyxo*- and *Pneumoviridae* life cycle as a basis for new insights in the biology of these viruses and the development of rationally designed therapeutics, genome scale siRNA screens with wild-type measles, mumps, and respiratory syncytial viruses in A549 cells, a human lung adenocarcinoma cell line, were performed. A comparative bioinformatics analysis yielded different members of the coatomer complex I, the translation factors ABCE1 and eIF3A, and several RNA binding proteins as cellular proteins with proviral activity for all three viruses. The strongest common hit, ABCE1, an ATP-binding cassette transporter member, was chosen for further study. We found that ABCE1 supports replication of all three viruses, confirming its importance for both virus families. While viral protein kinetics showed that ABCE1 knockdown resulted in a drastic decrease of MeV protein expression, viral mRNA kinetics are not directly affected by a reduction of ABCE1. The impact of ABCE1 on viral and global cellular translation was investigated using both ^{35}S metabolic labelling and non-radioactive fluorescent protein labelling. ABCE1 knockdown strongly inhibited the production of MeV proteins, while only modestly affecting global cellular protein synthesis and showed that ABCE1 is specifically required for efficient viral, but not general cellular, protein synthesis, indicating that paramyxo- and pneumoviral mRNAs may exploit specific translation mechanisms.

In a second approach the efficacy of the small-molecule polymerase inhibitor ERDRP-0519 against MeV was assessed in squirrel monkeys. Animals treated with the drug experienced less severe clinical disease compared to untreated controls, and this effect correlated with the onset of drug treatment. We observed a reduction of levels of PBMC-associated viremia and virus release in the upper airways, illustrating effective inhibition of virus replication by the drug treatment. ERDRP-0519 drug treatment also alleviated MeV-induced immunosuppression. In addition to providing proof-of-concept for the support of MeV eradication efforts by preventing disease and transmission with a small-molecule polymerase inhibitor, this dissertation provides a novel perspective on cellular proteins that impact the replication of MeV, MuV and HRSV and highlights the role of ABCE1 as host factor that is required for efficient paramyxo- and pneumovirus translation.

ZUSAMMENFASSUNG

Infektionskrankheiten zählen immer noch zu den häufigsten Todesursachen und haben aufgrund ihres Ausbruchscharakters hohe wirtschaftliche Bedeutung. Dabei stellen über die Luft übertragbare Erreger eine besondere Herausforderung für Gesundheitssysteme dar. Viren aus der Familie der Paramyxo- und Pneumoviren fallen in diese Gruppe und sind für hohe Morbiditäts- und Mortalitätsraten bei ihren Wirten verantwortlich. Zu den Vertretern der Paramyxo- und Pneumoviren gehören beispielweise das hochansteckende Masernvirus, die weit verbreiteten humanpathogenen Viren Mumpsvirus und Respiratorisches Synzytial-Virus, Vieh- und Geflügelzucht beeinträchtigende Viren wie das Newcastle-Disease-Virus und neu aufkommende Viren wie Hendra- und Nipahvirus. Die Familie *Paramyxoviridae* wird in vier Subfamilien unterteilt: *Avulavirinae*, *Metaparamyxovirinae*, *Orthoparamyxovirinae* und *Rubulavirinae*. Das Masernvirus (MeV) gehört zum Genus *Morbillivirus* (Subfamilie *Orthoparamyxovirinae)* und das Mumpsvirus (MuV) zum Genus *Orthorubulavirus* (Subfamilie *Rubulavirinae)* in der Familie der Paramyxoviren. Zu der Familie Pneumoviren gehören die zwei Genera *Metapneumovirus* and *Orthopneumovirus*, wobei das humane Respiratorische Synzytial-Virus (HRSV; formell *Humanes Orthopneumovirus*) ein Mitglied des Genus *Orthopneumovirus* ist (ICTV, 2019).

Paramyxo- und Pneumoviren sind behüllte Viren und haben ein nichtsegmentiertes, durchgehendes RNA-Genom in Negativstrangorientierung. Der Ribonukleoproteinkomplex wird aus Nukleoprotein (N), RNA-Genom, der RNA-abhängigen RNA-Polymerase (L), und dessen assoziiertem Kofaktor Phosphoprotein (P) gebildet. Das Matrixprotein (M) ist mit der inneren Hüllmembran verbunden und interagiert mit dem N-Protein. Auf der Oberfläche des Viruspartikels werden Glykoproteine exprimiert: das Fusionsprotein (F), das die Fusion von Virus und Wirtszelle vermittelt, und das Rezeptorbindungsprotein (H, HN, oder G), das für die Adsorption an die Zielzelle verantwortlich ist.

MeV, MuV und HRSV repräsentieren Paramyxo- und Pneumoviren mit hoher klinischer Relevanz, die durch Tröpfcheninfektion oder durch direkten Kontakt mit infizierten Personen übertragen werden. Während MeV- und MuV-Infektionen zu einer systemischen Erkrankung führen, ist HRSV auf eine Infektion des Respirationstraktes begrenzt. Die wirksamste präventive Maßnahme gegen MeV und MuV ist die Schutzimpfung, die zusammen mit Röteln als trivalenter Kombinationsimpfstoff MMR oder als Vierfach-Impfstoff mit Windpockenkomponente (MMRV) verabreicht wird. Eine antivirale Therapie gegen die beiden Erreger ist nicht verfügbar. Zur Prophylaxe von HRSV-Erkrankungen in Risikopatienten ist der humanisierte monoklonale Antikörper Palivizumab zugelassen, aber weitere zugelassene antivirale Therapien oder Impfstoffe

existieren nicht.

Um gemeinsame Wirtsfaktoren als Zielmoleküle für die Entwicklung von Breitband-Therapeutika zu identifizieren und Virus-Wirtinteraktionen zu analysieren, wurden genomweite siRNA Screens von MeV, MuV und HRSV in der A549 Lungenadenokarzinomzelllinie durchgeführt. Für die Screens wurden rekombinante Viren verwendet, die auf Sequenzen von Wildtypisolaten basieren und von einer zusätzlichen Transkriptionseinheit zwischen dem P und M Gen das EGFP Protein exprimieren, sodass infizierte Zellen anhand von Fluoreszenz direkt quantifiziert werden konnten. Die Screen Daten wurden mittels zwei verschiedener statistischer Ansätze bioinformatisch analysiert, um provirale Wirtsfaktoren für MeV, MuV und HRSV zu identifizieren. Dafür wurde zunächst jeder Screen individuell analysiert, gefolgt von zwei unabhängigen kombinierten Analysen aller Screens. Der Abgleich der Hitlisten dieser beiden Meta-Analysen ergab 24 Kandidaten, die in einem weiteren Validierungsscreen mit MuV bestätigt werden konnten. Unter Hinzunahme der Treffer eines bereits durchgeführten Screens mit dem verwandten Hendravirus (HeV), wurden die sechs Gene, ABCE1, COPB2, FOXP4, HSD11B2, PRR15 und RBM22, identifiziert, die sowohl für MeV, MuV, HRSV als auch für HeV eine Rolle spielen. Diese wurden durch einen weiteren Validierungsscreen mit MeV bestätigt.

Das Protein ABCE1, das in den siRNA Screens unter den besten Treffern war, wurde für eine tiefgreifende Charakterisierung ausgewählt. ABCE1 hat verschiedene zelluläre Funktionen und wurde als erstes als RNase L Inhibitor im Interferon-induzierbaren 2-5A/RNase L Signalweg beschrieben, der nach der Aktivierung und Dimerisierung von RNase L in mRNA Degradierung und Inhibition der Proteinsynthese resultiert. Es ist bekannt, dass ABCE1 ein Heterodimer mit RNase L bildet und somit die Bindung von dessen Aktivator 2-5A verhindern kann. Des Weiteren ist ABCE1 in die Teilung der Ribosomen in ihre Untereinheiten involviert, um blockierte 80S Ribosomen zu befreien und als Qualitätskontrolle, um maturierte 40S Ribosomen zu überprüfen. Eine besonders große Rolle spielt ABCE1 während der Termination der Translation in der Spaltung der 80S Ribosomen in 40S und 60S Untereinheiten, um Ribosomen zu recyceln und eine Reinitiation einzuleiten. Es konnte außerdem gezeigt werden, dass ABCE1 essentiell für die HIV Partikelbildung ist.

In der hier vorgelegten Arbeit wurde die Rolle von ABCE1 im Lebenszyklus der Paramyxo- und Pneumoviren systematisch untersucht. Um den Einfluss von ABCE1 auf den viralen Lebenszyklus zu analysieren, wurden A549-hSLAM Zellen mit einer Kontroll-siRNA (NSC) und einer ABCE1-spezifischen siRNA (ABCE1_6) transfiziert. Nach 48 Stunden wurden die Zellen für eine mehrstufige Wachstumskinetik mit einer MOI von 0,1 infiziert und zell-assoziiertes und freies Virus wurden alle 12 Stunden bis

zum 72 Stunden Zeitpunkt quantifiziert. Zell-assoziierte Masernvirusproduktion war in ABCE1_6-transfizierten Zellen um 12 Stunden verzögert und spätere Zeitpunkte zeigten 100-fach niedrigere Titer im Vergleich zur Kontrolle. Während die MuV Titer nur 10-fach reduziert waren, zeigten HRSV und MeV beide eine 100-fache Reduktion im freigesetztem Virustiter, was bestätigt, dass ABCE1 für die effiziente Replikation von MeV, MuV und HRSV notwendig ist. Um die Interaktion von ABCE1 mit dem viralen Lebenszyklus genauer zu untersuchen, wurden Protein- und mRNA-Kinetiken durchgeführt. Dabei zeigte sich, dass die virale Transkription nicht direkt von ABCE1 abhängig ist, während ABCE1 die Expression viraler Proteine stark reduziert und auf Translationsebene agiert. Die erste N-Protein Expression konnte nach 24 Stunden detektiert werden und stieg in Kontrollzellen kontinuierlich an, während nur minimale Level an N-Protein in Zellen mit reduzierter ABCE1 Expression vorhanden war. Ein ähnlicher Effekt auf die virale Proteinsynthese wurde mit HRSV und MuV beobachtet. Dabei waren in der Abwesenheit von ABCE1 HRSV N-Protein Level kaum detektierbar und die MuV N-Protein Expression war um 50% reduziert.

Weiterführende Untersuchungen mittels metabolischer Fluoreszenz-Markierung zeigten, dass ABCE1 in der Synthese zellulärer Proteine eine untergeordnete Rolle spielt. In der Abwesenheit von ABCE1 war die globale Proteinsynthese sowohl in nicht infizierten, als auch in MeV-, MuV- und HRSV-infizierten Zellen nur geringfügig beeinträchtigt. “Pulse-Chase“ Experimente mit ^{35}S radioaktiver Markierung ergab, dass ABCE1 für eine effiziente virale Proteinsynthese unerlässlich ist. ABCE1 Knockdown zeigte keinen Effekt auf die *de novo* Proteinsynthese der zellulären Proteine β-actin und PDH E1α, zwei Proteine mit moderater und schneller “Turnover Rate“. Die virale Proteinsynthese, repräsentiert durch die MeV M- und F-Proteine, war hingegen um 30-50% reduziert verglichen mit den Expressionsleveln in Anwesenheit von ABCE1. Ein Vergleich der zellulären und viralen Proteinexpressionslevel in Zellen, die mit der Kontroll- oder ABCE1-spezifischen siRNA transfiziert waren, zeigte zum Zeitpunkt 30 Minuten nach radioaktiver Markierung eine Reduktion von 60% für das MeV M-Protein und 40% für das MeV F-Protein.

Die Bedeutung von ABCE1 für die Translation der Paramyxo- und Pneumoviren wurde durch ein “Chase“ Experiment nach Aufhebung der Translationshemmung durch den Inhibitor Cycloheximide weitergehend analysiert. 24 Stunden nach Infektion der zuvor translationsgehemmten Zellen, wurde der Inhibitor entfernt und die *de novo* Synthese des N-Proteins von MeV, MuV und HRSV zu verschiedenen Zeitpunkten in An- und Abwesenheit von ABCE1 untersucht. Eine Reduktion der ABCE1 Level führte zu einer signifikanten Inhibition der *de novo* Synthese viraler Proteine und bestätigte somit die spezifische Rolle von ABCE1 in der Translation der mRNAs von Paramyxo- und

Pneumoviren. Die spezielle Bedeutung von ABCE1 für die virale Translation impliziert, dass Paramyxovirus und Pneumovirus mRNAs spezielle Translationsmechanismen nutzen.

Wir vermuten, dass virale Proteine in Zellen mit normalem ABCE1 Level bevorzugt gegenüber zellulären Proteinen translatiert werden. Liegt jedoch eine Reduzierung des ABCE1 Levels vor, ist die virale Proteinsynthese drastisch von diesem Effekt betroffen, während die Translation zellulärer Proteine die Abwesenheit von ABCE1 tolerieren kann.

Die Ergebnisse dieses Projektes geben neue Einblicke in die Rolle zellulärer Prozesse in Paramyxovirus und Pneumovirus Infektionen und beschreiben die Wichtigkeit des Wirtsfaktors ABCE1 für eine effiziente virale Translation.

Neben der Identifikation von Wirtsfaktoren als mögliche antivirale Ziele, wurde in einer zweiten Studie die antivirale Wirksamkeit des niedermolekularen Polymerase-Inhibitors ERDRP-0519 in MeV-infizierten Totenkopfäffchen (*Saimiri sciureus)* getestet. ERDRP-0519 weist im Vergleich zum Vorgängermolekül AS-136a eine verbesserte Wasserlöslichkeit und erhöhte orale Bioverfügbarkeit im Ratten-Pharmakokinetikmodel auf. Der antivirale Inhibitor bindet an die katalytische Domäne des MeV L-Proteins, die für die Bildung der Phosphodiesterbindung zuständig ist, und reduziert deren Aktivität. Um die antivirale Wirksamkeit des Inhibitors zu überprüfen, wurden 20 Totenkopfäffchen in vier Gruppen von je fünf Tieren aufgeteilt und zweimal täglich für eine Gesamtdauer von zwei Wochen behandelt. Dabei wurde eine Gruppe prophylaktisch und zwei Gruppen zu unterschiedlichen Zeitpunkten nach MeV-Infektion behandelt und eine Gruppe blieb unbehandelt. Körpertemperatur und Gewicht wurde täglich gemessen, und klinische Symptome wurden ebenfalls täglich überprüft. Zusätzlich wurden zu vorab festgelegten Zeitpunkten Blutproben genommen, um zellassoziierte Virämie und neutralisierende Antikörperantworten zu messen. Die Schwere der MeV-induzierten Immunsuppression wurde durch die Bestimmung der Leukozytenzahlen evaluiert. Außerdem wurden Rachenabstriche titriert, um die Virusausscheidung vom oberen Respirationstrakt zu analysieren.

Die Studie zeigte einen deutlich milderen Krankheitsverlauf bei ERDRP-0519 behandelten Tiere im Vergleich zu unbehandelten Tieren, wobei die Schwere der Krankheit mit dem Behandlungsbeginn korrelierte. Außerdem wurde eine Reduzierung der Viruslast in PBMCs und in den oberen Atemwegen festgestellt, was die effektive Inhibition der viralen Replikation bestätigt und darauf hindeutet, dass auch die Übertragung verringert ist. Eine stabile Leukozytenzahl in behandelten Tieren, zeigte des Weiteren, dass die Behandlung mit ERDRP-0519 die MeV-induzierte Immunsuppression reduziert. Es konnte somit zum ersten Mal die antivirale

Wirksamkeit des Polymerase-Inhibitors ERDRP-0519 in einem nicht-menschlichen Primaten bei MeV-Infektionen gezeigt werden.

Antivirale Therapien, wie die Gabe des niedermolekularen Polymerase-Inhibitors ERDRP-0519, stellen somit eine wichtige Option dar, schwere Krankheitsverläufe nach MeV-Infektionen zu verhindern und Transmissionen zu verringern.

Diese Arbeit bietet einen neuen Überblick über zelluläre Wirtsfaktoren, die die Replikation von MeV, MuV und HRSV beeinflussen, und zeigt die Bedeutung des Wirtsfaktors ABCE1 für eine effiziente Translation von Paramyxo- und Pneumoviren auf. Zusammen mit der Wirksamkeitsstudie des niedermolekularen Polymerase-Inhibitors ERDRP-0519 leistet sie einen wichtigen Beitrag zu unserem Verständnis von Paramyxo- und Pneumovirus-Wirts-Interaktionen und zur Entwicklung neuer antiviraler Medikamente gegen diese Viren.

1. INTRODUCTION

1.1. *Paramyxoviridae* and *Pneumoviridae*

The *Paramyxoviridae* family has recently been re-organized, and its members have been re-classified into two families: *Paramyxoviridae* and *Pneumoviridae,* which are part of the larger order *Mononegavirales*. The *Paramyxoviridae* family includes four subfamilies, *Avulavirinae*, *Metaparamyxovirinae, Orthoparamyxovirinae* and *Rubulavirinae.* Measles virus (MeV; formally *Measles morbillivirus*) and mumps virus (MuV; formally *Mumps orthorubulavirus*) are both members of the family *Paramyxoviridae*. MeV is further sub-classified in the genus *Morbillivirus* (subfamily *Orthoparamyxovirinae*), while MuV is part of the genus *Orthorubulavirus* (subfamily *Rubulavirinae*). The family *Pneumoviridae* contains two genera, *Metapneumovirus* and *Orthopneumovirus*. Human respiratory syncytial virus (HRSV; formally *Human orthopneumovirus*) is a member of the genus *Orthopneumovirus* in the family *Pneumoviridae*. (ICTV, 2019). Both families include a broad range of pathogens responsible for high morbidity and variable mortality among humans and animals. This includes highly prevalent and extremely infectious viruses such as human respiratory syncytial virus (HRSV), mumps virus (MuV), measles virus (MeV) and human metapneumovirus, as well as viruses which impact poultry and livestock such as Newcastle disease virus (NDV; formally Avian orthoavulavirus 1) and the newly identified emerging zoonotic viruses Hendra virus (HeV) and Nipah virus (NiV). MeV, MuV, and HRSV are representatives of the *Paramyxo-* and *Pneumoviridae* families with high clinical relevance. All three viruses are transmitted by aerosols or large droplets as well as through direct contact and fomites. While MeV and MuV result in systemic infections, HRSV remains restricted to the respiratory tract (Collins and Karron, 2013).

Paramyxo- and pneumoviruses are enveloped and have non-segmented negative-sense single-stranded RNA genomes. The RNA genome is encapsidated by the nucleocapsid (N) protein, which is also associated with the viral RNA-dependent RNA polymerase (L) protein and the phosphoprotein (P) polymerase co-factor. Together, these viral proteins and RNA form the ribonucleoprotein (RNP) complex. The matrix (M) protein is associated with the inner leaflet of the viral particle membrane and at least two major integral membrane proteins are expressed on the virion surface: the fusion (F) protein, which mediates fusion between the viral and host cell membranes; and the attachment protein (named either H, HN, or G), which binds receptors on the host cell to initiate infection. Rubulaviruses, respiroviruses, avulaviruses, ferlaviruses, and aquaparamyxoviruses encode a hemagglutinin-neuraminidase (HN) protein, which both recognizes sialic acid receptors on the cell surface for virus attachment during entry,

and also cleaves sialic acids during budding to facilitate virion release. Morbilliviruses encode a hemagglutinin (H) protein that recognizes the cell surface protein receptors signaling lymphocyte activation molecule (SLAM; also known as CD150) (Tatsuo *et al.*, 2000) and nectin-4 (Mühlebach *et al.*, 2011), but lacks neuraminidase activity. Henipaviruses encode an attachment protein that has neither hemagglutinating nor neuraminidase activity, named the G protein (Chua, 2000), that binds to the cellular receptors ephrin-B2 and ephrin-B3 (Bonaparte *et al.*, 2005; Negrete *et al.*, 2005). Pneumoviruses also possess a G protein, which promotes virus attachment through interaction with glycosaminoglycans (Collins and Karron, 2013). Pneumoviruses (Collins and Karron, 2013) and some paramyxoviruses, including some rubulaviruses (Elango *et al.*, 1989), the rodent paramyxoviruses J virus (JPV) and Beilong virus (BeiPV) (Jack *et al.*, 2005), encode an additional glycoprotein called the small hydrophobic (SH) protein. SH is a type II transmembrane (TM) protein and is thought to inhibit tumor necrosis factor alpha (TNF-α) signaling (Li *et al.*, 2011). JPV and BeiPV also encode a TM protein that promotes cell-cell fusion by the F and G proteins (Jack *et al.*, 2005; Li *et al.*, 2015). The paramyxovirus M protein plays a central role in morphogenesis by interacting with the integral membrane proteins, the lipid bilayer, and the nucleocapsid (Lamb and Parks, 2013) to initiate virus assembly and budding (Harrison, Sakaguchi and Schmitt, 2010). Pneumoviruses encode two additional unique nonstructural proteins, NS1 and NS2, which have a role in innate immune response evasion (Ramaswamy *et al.*, 2004; Spann *et al.*, 2004; Lo, Brazas and Holtzman, 2005).

Paramyxovirus replication is initiated by the viral polymerase, which transcribes the N protein-encapsidated genomic RNA into 5′ capped and 3′ polyadenylated messenger RNA (mRNA). Initiation of mRNA synthesis occurs at the 3′ end of the (-)-sense genome and the transcription of the genes into mRNAs occurs in a sequential manner by termination and reinitiation at each gene junction. At the beginning and end of each gene are short (~10–13 nt) conserved signals termed *gene start* (*gs*) for capping (Stillman and Whitt, 1999; Ogino *et al.*, 2005; Wang, McElvain and Whelan, 2007) and transcription initiation of the following gene and *gene end* (*ge*) signals, where polyadenylation takes place by reiterative copying of four to seven uridines (Whelan, 2008), resulting in mRNA. Between each gene is a short, non-transcribed intergenic region. Polymerase failure during termination and reinitiation leads to a gradient of mRNA synthesis whereby transcripts of genes located further downstream toward the 3′ end of the genome are less abundant (Cattaneo *et al.*, 1987). The viral genome is flanked by a *leader* (*le*) promoter region at the 3′ terminus which is ~40–55 nt long, and a trailer (tr) region at the 5′ terminus which varies in length depending on the virus. To replicate the genome, the polymerase also initiates RNA synthesis at the *le* promoter. In the first

step of replication, a positive-sense antigenome is synthesized from the negative-sense genomic template, while the second step consists of the production of negative-sense genomes from the positive-sense antigenomic template (Lamb and Parks, 2013). During replication, the polymerase does not respond to the gene junction signals and reads through these sequences. The infection cycle is completed when newly-synthesized viral proteins and RNPs assemble at the plasma membranes of the host cell and are subsequently released.

1.1.1. Measles virus

1.1.1.1. MeV structure

MeV is a member of the *Morbillivirus* genus in the family *Paramyxoviridae*. The 16-kb genome encodes six structural proteins: N, P, M, F, H, L, and two non-structural proteins, V and C, both encoded by the P gene (Figure 1A). The envelope of the virion consists of the M, F, and H proteins (Figure 1B). The H protein is one of the two glycoproteins on the virion surface and it binds to the cellular receptors SLAM, which is expressed on monocytes, lymphocytes, macrophages and dendritic cells (Tatsuo *et al.*, 2000), and nectin-4, which is expressed on epithelial cells (Mühlebach *et al.*, 2011). The second glycoprotein, the F protein, is essential for the fusion of the viral envelope with the host cell membrane, enabling entry of viral RNPs into the cell cytoplasm (Griffin, 2013).

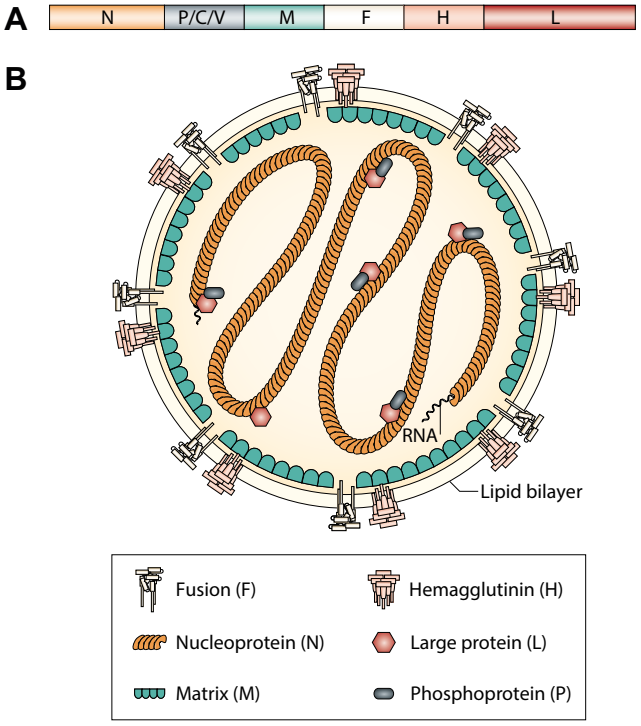

Fig. 1 | Schematic depiction of the measles virus genome and virus particle. A) The 16-kb genome encodes six structural proteins, the nucleoprotein (N), phosphoprotein (P), matrix (M), fusion (F), hemagglutinin (H), large polymerase protein (L), and two non-structural proteins V and C encoded by the phosphoprotein gene. **B)** The virion envelope is composed of the M protein and the two gylcoproteins F and H. Viral genomic RNA is encapsidated by the N protein and, together with the L polymerase protein and its P cofactor, form the ribonucleoprotein complex (Moss and Griffin, 2006). Adapted by permission from Springer Nature: Nature, Nature Reviews Microbiology, Global measles elimination, Moss and Griffin, © 2006.

1.1.1.2. MeV proteins

The N protein is approximately 60 kDa in size. It stabilizes the helical structure of the viral genome and is required for transcription and replication. MeV N consists of a 400-residue N-terminal RNA-binding core, which determines the spatial organization of the nucleocapsid (Bankamp *et al.*, 1996; Desfosses *et al.*, 2011), and a hypervariable C-terminal 125-residue N-tail domain. The C-terminal tail is variable, intrinsically disordered and mediates interactions with several host proteins and viral binding partners. A molecular recognition element (MoRE) domain mediates binding of the C-terminal domain of the phosphoprotein (Bourhis *et al.*, 2004).

The 72 kDa P protein is a polymerase cofactor, whose function is modulated by phosphorylation. It mediates attachment of the polymerase complex to the encapsidated viral RNA genome by linking the N and L proteins for transcription and replication (Curran *et al.*, 1995). The phosphorylated N-terminus of the P protein is unstructured, and it binds the N protein and is essential for viral replication. The conserved C-terminus contains all domains required for transcription support, including an oligomerization domain and a domain important to bind and induce folding of the N-tail (Huber *et al.*, 1991; Curran *et al.*, 1995; Kingston, Baase and Gay, 2004).

In addition to the P protein, the P gene encodes two accessory proteins, V and C, which play important roles in controlling both the induction of the interferon (IFN) response and downstream IFN pathway signaling. The V protein (46 kDa) is translated using the P initiation codon and reading frame, but a non-templated guanosine residue is inserted by the viral polymerase in the mRNA at position 751 in a process known as co-transcriptional editing. This leads to a C-terminal shift of the reading frame downstream of residue 231, which yields a unique cysteine-rich 68-aa C-terminus (Cattaneo *et al.*, 1989). The MeV V protein interacts with retinoic-acid inducible gene-I (RIG-I)-like receptors, melanoma differentiation associated factor 5 (MDA5) and LGP2, and is suggested to be a positive regulator of RIG-I and MDA5-mediated antiviral responses (Satoh *et al.*, 2010), thereby inhibiting IFN induction (Andrejeva *et al.*, 2004; Rodriguez and Horvath, 2014). It also interacts with interferon regulatory factors 3 (IRF3) and 7 (IRF7) to block their transcriptional activity, as well as with IκB kinase α (IKKα) via the V protein's cysteine-rich C-terminal domain to downregulate IRF7 (Pfaller and Conzelmann, 2008).

The 20 kDa and 186 aa C protein is encoded by the P mRNA, but is translated from an alternate reading frame upstream of the P gene start codon (Bellini *et al.*, 1985). The C protein is known to have two major functions, innate immune response modulation and regulation of genome replication and transcription (Reutter *et al.*, 2001; Bankamp *et al.*, 2005). The MeV C protein also regulates viral RNA synthesis through host factor

SHC SH2 domain-binding protein 1 (SHCBP1)-mediated interaction with the MeV RNP complex (Ito *et al.*, 2013). Furthermore, MeV C can impair cellular immune pathways including RIG-I signaling and protein kinase R (PKR) activation via decrease of defective copyback viral dsRNA (Pfaller *et al.*, 2014).

The 40 kDa M protein is located at the inner surface of the viral envelope and plays a key role in virus assembly, budding, and modulation of viral RNA synthesis. It has been shown that the M protein regulates assembly and viral RNA synthesis via its interaction with the N protein (Iwasaki *et al.*, 2009). The protein annexin A2 interacts with the N-terminal region of the M protein and mediates its localization at the plasma membrane where MeV particles are formed. It has also been shown that the M protein associates with the inner surface of the plasma membrane and interacts with cytoplasmic domains of H and F to facilitate virus assembly (Cathomen *et al.*, 1998; Cathomen, Naim and Cattaneo, 1998; Tahara, Takeda and Yanagi, 2007).

The F protein is a type I integral transmembrane protein with a C-terminal cytoplasmic tail, which is initially synthesized as an inactive 60 kDa precursor (F_0). F_0 is proteolytically cleaved by furin within the trans-Golgi network, producing the mature fusion-competent F protein which consists of the disulfide-linked 41 kDa F_1 and the 18 kDa F_2 subunits. The F protein has a short stalk region and a globular head domain. F_1 includes the transmembrane domain as well as the N-terminal hydrophobic fusion peptide, whereas F_2 possesses a heptad repeat region (HRC) involved in the modulation of syncytia formation (Plemper and Compans, 2003). Functional F proteins associate on the virion surface as trimers. Upon binding of H to the cellular receptor, prefusion F trimers undergo a series of conformational changes, resulting in relocation and insertion of the fusion peptide into the target membrane, followed by further conformational changes that bring the viral and host membranes in close proximity to enable lipid mixing.

The 75-80 kDa H protein is a type II transmembrane protein with a short N-terminal cytoplasmic tail and a large C-terminal ectodomain. It is comprised of a large globular head atop a long stalk. The H protein consists of antiparallel β-strands that form a six-bladed structure known as a β-propeller (Colf, Juo and Garcia, 2007). H dimers are formed by two covalently bound monomers via two disulfide bonds located in the upper stalk region (Cys-139 and Cys-154) (Plemper, Hammond and Cattaneo, 2000), and these dimers then form tetramers via non-covalent hydrophobic interactions with other dimers. The H protein is responsible for attachment to the cellular receptors SLAM, expressed on immune cells, and nectin-4, expressed on epithelial cells.

The 250 kDa L protein performs all enzymatic functions necessary for viral RNA synthesis, including nucleotide polymerization, 5′ end capping, cap methylation, and

3′ polyadenylation of viral transcripts. MeV L has six conserved regions (CR I through CR VI) which are found in all other members of the order *Mononegavirales* (Poch *et al.*, 1990; Sidhu *et al.*, 1993). CR I (aa 217-408) is thought to interact with P to form an active enzyme complex (Horikami *et al.*, 1994; Cevik *et al.*, 2004). CR III contains the catalytic GDNQ motif present in the polymerases of many negative-strand RNA viruses and is the active center for phosphodiester bond formation during RNA synthesis (Duprex, Collins and Rima, 2002; Chattopadhyay and Shaila, 2004). CR V and VI are important for the cap synthesis and methylation of newly-synthesized viral mRNAs (Sourimant and Plemper, 2016).

1.1.1.3. Cellular receptors

MeV uses distinct receptors to enter different host cells and to facilitate transmission to new hosts via the respiratory epithelium. Upon infection, MeV enters the upper airway and initially infects immune cells using SLAM. SLAM (70 kDa) belongs to the immunoglobulin (Ig) super family and is composed of an extracellular domain containing a variable (V) and a constant (C2) immunoglobulin-like repeat domain, and a cytoplasmic domain, which is associated with SLAM-associated protein (SAP) (Yanagi *et al.*, 2002; Sidorenko and Clark, 2003). SLAM is expressed on a broad range of immune cells such as activated T and B cells, macrophages, and mature dendritic cells (Schwartzberg *et al.*, 2009). The H protein amino acids Y529, D530, and R533 are important for binding to the V domain of SLAM. At later stages after initial infection, MeV-infected immune cells infiltrate the upper airway epithelium, where they use nectin-4 to infect epithelial cells (Mühlebach *et al.*, 2011; Noyce and Richardson, 2012). Nectin-4 also belongs to the Ig superfamily and is composed of a V region and two C2 domains (Noyce and Richardson, 2012). Laboratory-adapted and vaccine strains of MeV can also use CD46 as a receptor, which is expressed on all nucleated human cells (Noyce and Richardson, 2012). CD46 is a human complement regulatory protein composed of four sushi/short consensus repeat domains, a serine-threonine-proline (STP) rich domain, a transmembrane domain, and a cytoplasmic region (Noyce and Richardson, 2012). However, only SLAM-positive cells are infected after intramuscular injection of vaccine viruses into nonhuman primates, which suggests that CD46 usage is a laboratory artifact that has little relevance for the viral life cycle and pathogenesis (Rennick *et al.*, 2015).

1.1.1.4. MeV life cycle

Binding of MeV to the host cell surface is mediated by the tetrameric H protein via interaction with one of the respective receptors, which triggers a series of conformational

changes in the F protein, leading to relocation and insertion of the fusion peptide into the target membrane and refolding of the HRB domains in the stalk domain to form the typical post-fusion six-helix bundle core structure (Russell, Jardetzky and Lamb, 2001; Yin *et al.*, 2006; Lamb and Parks, 2013). The cascade of F protein structural rearrangements is proposed to bring the TM domain embedded in the viral envelope and the fusion peptide inserted into the target membrane into close proximity, leading to membrane curvature and membrane fusion (Plattet *et al.*, 2016). Upon release of the viral RNP into the cytoplasm, the viral RNA-dependent RNA polymerase transcribes the genomic RNA template to produce 5′-capped and 3′-polyadenylated mRNAs, which can then be directly translated by the host translation machinery to produce viral proteins (Figure 2). Transcription begins at the 3′ end of the viral genome and genes are sequentially transcribed moving toward the 5′ end of the genome by a "stop–start" mechanism described in Chapter 1.1. Multiple cycles of transcription results in a gradient of viral mRNAs, whereby transcripts of genes located further downstream toward the 5′ end of the genome (e.g., L) are less abundant than those derived from the 3′ end such as N (Cattaneo *et al.*, 1987). It has been suggested that upon sufficient accumulation of N proteins, the viral polymerase switches its activity to a replication mode, where the transcriptional termination signals are no longer recognized and full-length positive-sense antigenomes are produced (Plumet, Duprex and Gerlier, 2005). This antigenomic RNA then serves as a template for the synthesis of negative-sense genomes, which are immediately encapsidated. Newly assembled RNP complexes are transported to the plasma membrane, and further interactions first with M protein and then with the glycoproteins lead to virus assembly and budding (Runkler *et al.*, 2007; Dietzel, Kolesnikova and Maisner, 2013). Infected cells expressing H and F can also fuse with other susceptible host cells, resulting in the formation of large multinucleated cells (syncytia) which allow direct transfer of viral RNPs into new cells.

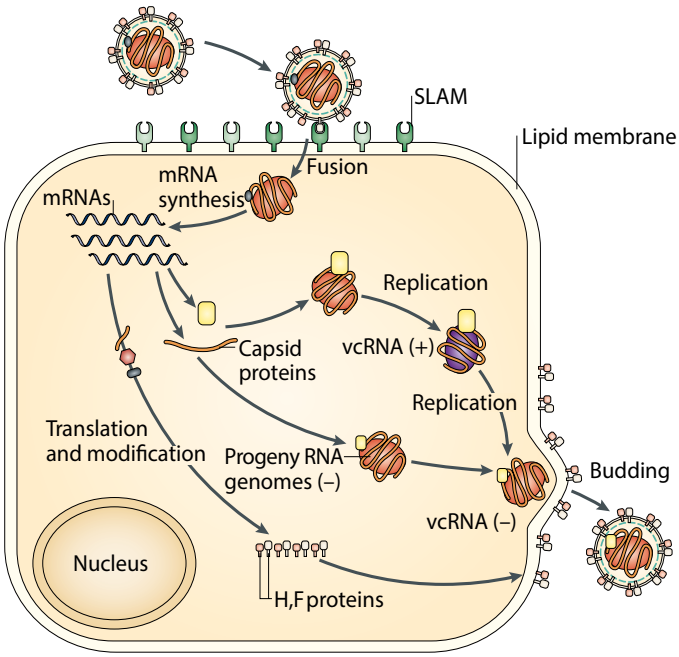

Fig. 2 | Measles virus replication cycle. MeV binds to the host cell surface via interaction of H and host cell receptor SLAM expressed on immune cells. Binding of H triggers F protein-mediated fusion of the viral envelope and the host cell membrane. Upon transcription of genomic RNA into 5' capped and 3' polyadenylated mRNAs by the viral RNA-dependent RNA polymerase and translation of viral proteins using the host cell machinery, the viral polymerase produces positive-sense antigenomes, which serves as template for the synthesis of negative-sense genomes during replication. Newly synthesized viral proteins and RNPs assemble together at the plasma membrane, followed by virion budding and release (Moss and Griffin, 2006). Adapted by permission from Springer Nature: Nature, Nature Reviews Microbiology, Global measles elimination, Moss and Griffin, © 2006.

1.1.1.5. Clinical features, pathogenesis, and pathology of MeV

MeV enters the respiratory tract and initially infects dendritic cells in the upper respiratory tract, or dendritic cells or alveolar macrophages of the lower respiratory tract using SLAM as the cellular receptor. A second possible MeV entry route is through infection of myeloid or lymphoid cells in the conjunctiva (Seo *et al.*, 2010). The infected immune cells transport the virus to draining lymph nodes and bronchus-associated lymphoid tissue (BALT), where MV replicates vigorously and is then transmitted to lymphocytes, including B cells and memory $CD4^+$ and $CD8^+$ T cells (Hall *et al.*, 1971; White and Boyd, 1973; Sakaguchi *et al.*, 1986; McChesney *et al.*, 1997; De Swart *et al.*, 2007; de Vries *et al.*, 2012; Ludlow *et al.*, 2015). Viral dissemination occurs predominantly by cell-to-cell transmission (Koethe, Avota and Schneider-Schaulies, 2012; Mateo *et al.*, 2015; Singh *et al.*, 2015). During viremia, infected immune cells enter the circulation and MeV spreads systemically to immune cells in other organs and tissues, such as the gastrointestinal tract, kidney, liver, and skin (Ludlow, Allen and Schneider-Schaulies, 2009).

The resulting close contact between infected immune and neighboring epithelial cells

leads to spread to epithelial airways via interaction of the viral H protein with nectin-4 expressed on epithelial cells (Mühlebach *et al.*, 2011). Nectin-4 is part of the adherens junction complex, which is located on the basolateral side of the tight junction. Infection of epithelia is associated with the onset of clinical signs approximately 10 days after initial infection. Progeny virus particles in the upper and lower respiratory tract epithelium are released into the lumen of the respiratory tract and are expulsed by coughing and sneezing. MeV is extremely contagious, with a basic reproductive number R_0 of 12-18, which means that one infected individual will infect an average of 12-18 people in a susceptible population. Measles clinical disease typically starts with mild non-specific symptoms including moderate fever, cough, runny nose, conjunctivitis, and coryza, and is later characterized by immunosuppression and typical maculopapular skin rash that spreads from the face and trunk to the extremities. Infection is associated with lymphopenia during its acute phase, in which the numbers of T and B cells, circulating and homing to lymphoid tissues decreases dramatically (Arneborn and Biberfeld, 1983; Bachmann *et al.*, 1996; Kobune *et al.*, 1996; Ryon *et al.*, 2002). The rash is a manifestation of the virus-specific cellular immune response by the host where $CD4^+$ and $CD8^+$ T cells infiltrate infected dermal epithelial layers or keratinocytes, and of subsequent virus clearance (Permar *et al.*, 2003; Griffin, 2013). MeV infection results in a transient but profound immune suppression, which increases the susceptibility to secondary infections. Severe complications can also include secondary viral or bacterial pneumonia, otitis media, stomatitis, and encephalitis. Subacute sclerosing panencephalitis (SSPE) is a very rare, but fatal progressive neurodegenerative disease that can occur many years after initial MeV infection (Griffin, 2013). Complications mostly arise in immunocompromized patients, pregnant women, and infants less than 1 year of age (Tannous, Barlow and Metcalfe, 2014).

1.1.1.6. MeV epidemiology and vaccination

There is no specific antiviral therapy for measles, so treatment is largely supportive and focused on the management of symptoms. In the pre-vaccination era, major epidemics occurred at intervals of 2-5 years with around 2.6 million deaths annually. In 1963 the first vaccine, based on the MeV-Edmonston-B strain, isolated in 1954 from a blood sample of a 13 year-old MeV-infected boy, was licensed in the United States. Several live-attenuated MeV vaccines, often derived from the Edmonston seed strain, are produced around the world. MeV vaccines are available either as monovalent vaccines or most often in combination with vaccines against other viruses such as the trivalent measles-mumps-rubella (MMR) vaccine. A 2-dose series is recommended by the German Standing Committee on Vaccination or Ständige Impfkommission (STIKO), with the

first dose given at ages 11-14 months of age and the second dose at 15-23 months. After the implementation of vaccination programs, global MeV deaths have continuously decreased from 555,100 deaths in 2000 to 111,000 in 2017 (WHO, 2018a). However, the WHO vaccination campaign was unsuccessful in its initial goal of eradicating measles by 2015. Under the revised Global Vaccine Action Plan, MeV has now been targeted for elimination in at least five WHO Regions (the Americas, Eastern Mediterranean, European, South East Asia, African, and Western Pacific Regions) by 2020 (WHO, 2018b). Since MeV is highly contagious, vaccination rates exceeding 95% are required to interrupt transmission cycles and maintain herd immunity, which makes achieving these vaccination goals very challenging (WHO, 2018c).

1.1.2. Mumps virus

1.1.2.1. MuV structure

Mumps virus (MuV) is a member of the *Othorubulavirus* genus in the family *Paramyxoviridae*. The genome is 15,384 nucleotides long and encodes the N, P, M, F, SH, HN, and L proteins. The particle consists of an RNP complex for virus replication which includes a non-segmented, single-stranded RNA of negative polarity encapsidated by the N protein in association with the viral RNA polymerase complex. The HN glycoprotein is responsible for attachment of the virus via its sialic acid receptor, and together with the F glycoprotein, mediates virus-to-cell fusion and cell-to-cell membrane fusion, facilitating virus spread (Rubin *et al.*, 2015). The M protein is involved in localizing the viral RNP to regions of the host cell membrane, where the glycoproteins have accumulated promoting budding of the infectious virions from infected cells. The SH protein has been reported to interfere with innate immunity by inhibiting TNF-α-mediated apoptosis and NF-κB activation by interacting with tumor necrosis factor receptor 1, interleukin-1 receptor 1, and Toll-like receptor 3 complexes (Xu *et al.*, 2011; Franz *et al.*, 2017). For rubulaviruses, the unedited mRNA encodes the V protein, while P is produced by translation of an mRNA containing a two-G co-transcriptional insertion by the polymerase, and addition of one G nucleotide produces an mRNA encoding the I protein (Lamb and Parks, 2013). The V protein is important for inhibiting IFN-mediated antiviral responses by blocking IFN signaling and limiting IFN production (Lara-Sampablo et al. 2012). WHO currently recognizes 12 genotypes, designated A through N (there are no E or M genotypes), which are based on the nucleotide sequences of SH and HN genes.

1.1.2.2. Clinical features, pathogenesis, and pathology of MuV

Humans are the only natural host for MuV. MuV replicates in the upper respiratory tract and is transmitted by direct contact or by airborne droplets. MuV is able to disseminate systemically in the body. After infection of the upper respiratory mucosa, it spreads to regional lymph nodes, and then via viraemia to epithelia throughout the body. The average incubation time is 16-18 days, with a range of 12 to 25 days. Approximately one-third of infections are asymptomatic or the infection results in mild respiratory symptoms, sometimes accompanied by fever (Philip, Reinhard and Lackman, 1959; Brunell *et al.*, 1968; Cooney, Fox and Hall, 1975; Rubin *et al.*, 2015). The prodromal phase is characterized by non-specific mild clinical signs such as headache, malaise, and mild fever. In the ensuing early acute phase of infection, infected individuals likely become viremic with swelling of the parotid salivary glands, one of the classical clinical signs of mumps disease. Swelling usually peaks 1 to 3 days after first appearance and then subsides during the following week. Virus can be excreted into the saliva from one week prior to salivary gland swelling, and up to two weeks afterward (Rubin *et al.*, 2015). The acute phase of disease may result in serious complications such as orchitis, an inflammation of the testicles, which occurs in approximately 15-30% of infections in post-pubertal men (Philip, Reinhard and Lackman, 1959; Postovit, 1983). MuV is also highly neurotropic and can cause meningitis in 1-10% of cases, and encephalitis in fewer than 1%. Other complications of mumps include deafness, myocarditis, nephritis, and pancreatitis (Mandell, 2010). Symptoms of mumps disease normally resolve within 2 weeks and coincide with the development of a MuV-specific humoral response. MuV infection can be contagious 7 days before to 9 days after the appearance of swelling of the parotid salivary glands (RKI, 2013).

1.1.2.3. MuV epidemiology and vaccination

As with MeV, there is no specific antiviral therapy for mumps, and treatment is mostly supportive and focused on the management of clinical signs. There are combined live-attenuated vaccines available for measles, mumps, and rubella (MMR), which are highly effective and are the primary methods of reducing the number of cases caused by these viruses along with associated morbidity and mortality (Tannous, Barlow and Metcalfe, 2014). All currently available MuV vaccines consist of live-attenuated strains (Rubin, 2018). Jeryl Lynn and Urabe Am9 strains are most common, followed by the Leningrad-Zagreb, Leningrad-3, and Rubini strains; the newer RIT 4385 strain has been derived from the Jeryl Lynn strain (Naim, 2015). Prior to the implementation of widespread MuV immunization programs, 95% of adults had serologic evidence of exposure to MuV with peak acquisition during childhood (Mortimer, 1978; Centers for Disease Control

and Prevention (CDC), 1986). Following implementation of MuV vaccination programs in the 1960s in the United States, disease incidence declined dramatically. By 2001, the disease was nearly eliminated with fewer than 0.1 cases/100,000 population (McNabb *et al.*, 2007). However, in the last decade, several resurgent mumps outbreaks have been reported, including in populations with very high vaccination coverage (Centers for Disease Control and Prevention (CDC), 2006, 2010; Watson-Creed *et al.*, 2006; Park *et al.*, 2007; Boxall *et al.*, 2008; Cortese *et al.*, 2008; Marin *et al.*, 2008; Bangor-Jones *et al.*, 2009; Roberts *et al.*, 2009; Rota *et al.*, 2009). The reason for the lower than expected efficacy of MuV vaccination is not fully understood. Several explanations have been proposed, including waning immunity in vaccinated populations, as well as the emergence of vaccine escape mutants where antigenic changes in outbreak strains allow these viruses to evade the vaccine-induced humoral immune response (Rubin *et al.*, 2012).

1.1.3. Human respiratory syncytial virus

HRSV is a member of the *Orthopneumovirus* genus in the family *Pneumoviridae*. HRSV consists of an enveloped negative-sensed single-stranded RNA genome of 15,191 nucleotides. Its 10 genes encode 11 proteins since two overlapping open reading frames in the M2 mRNA yield two distinct matrix proteins, the M2-1 antitermination protein, and M2-2, which is involved in transcription/replication regulation. Two nonstructural proteins, NS1 and NS2, involved in evasion of the innate immune response, are unique for HRSV (Ramaswamy *et al.*, 2004; Spann *et al.*, 2004; Lo, Brazas and Holtzman, 2005). It has the key internal structural proteins N and M, and the proteins required for a functional polymerase complex P and L, in common with MeV and MuV. As surface glycoproteins, HRSV encodes SH, G, and F proteins (Fields, Knipe and Howley, 2013).

HRSV infection starts by attachment of the virus to the host cell and the subsequent entry process. Several studies indicated that G is not required for infection (Techaarpornkul, Barretto and Peeples, 2001; Teng, Whitehead and Collins, 2001). It has also been shown, that the contribution of G to binding, entry, and infection depends on the respective F protein (Meng *et al.*, 2016). Many candidate HRSV receptors have been proposed, including annexin II (Malhotra *et al.*, 2003), CX3 chemokine receptor 1 (CX3CR1) expressed on the apical surface of ciliated bronchial epithelial cells (Tripp *et al.*, 2001; Harcourt *et al.*, 2006; Jeong *et al.*, 2015; Johnson *et al.*, 2015; Stobart *et al.*, 2015), epidermal growth factor (EGF) receptor (Currier *et al.*, 2016), calcium-dependent lectins (Malhotra *et al.*, 2003), Toll-like receptor 4 (TLR4) expressed on ciliated bronchial epithelial cells in the airway (Kurt-Jones *et al.*, 2000; Marchant *et al.*, 2010; Marr and Turvey, 2012), intercellular adhesion molecule 1 (ICAM-1) (Behera *et al.*, 2001), nucleolin (Tayyari *et al.*, 2011; Holguera, Villar and Muñoz-Barroso,

2014), and heparan sulfate proteoglycans (HSPGs) (Krusat and Streckert, 1997). While nucleolin has been confirmed as a functional HRSV receptor *in vivo* (Tayyari *et al.*, 2011), no other candidate receptor has been validated as a functional receptor. Host cell macropinocytosis is also a route of entry for HRSV (Krzyzaniak *et al.*, 2013). Virus internalization depends on actin rearrangement, phosphatidylinositol 3-kinase activity, and host cell early endosomal $Rab5^{+}$ vesicles (Krzyzaniak *et al.*, 2013). In the early endosome, proteolytic cleavage activates the HRSV F protein, triggering the fusion reaction in the endosome (Griffiths, Drews and Marchant, 2017). Upon completion of entry, virus particle contents are released into the host cell and L, P and M2-1 proteins, together with the encapsidated viral genome form the replication complex (Griffiths, Drews and Marchant, 2017). The HRSV RNA-dependent RNA polymerase transcribes viral mRNA transcripts and synthesizes full-length, positive-sense antigenomes in a manner similar to paramyxoviruses.

1.1.3.1. Clinical features, pathogenesis, and pathology of HRSV

HRSV is a leading cause of respiratory tract infections in infants, resulting in high rates of hospitalization and mortality. The infection is transmitted via inhalation of infectious droplets or through direct contact with respiratory or ocular mucosa (Hall *et al.*, 1981; Teng, Whitehead and Collins, 2001). The virus then targets ciliated airway epithelial cells in the nasopharyngeal or conjunctival mucosa. Symptoms can range from mild cold-like signs including cough, rhinitis, fever, and nasal congestion (Hacking and Hull, 2002; Collins and Melero, 2011; Hall, Simoes and Anderson, 2013), to more serious clinical scenarios such as bronchiolitis, pneumonia, and respiratory failure. HRSV affects nearly 70% of infants in their first year of life and almost 100% of children have been exposed by 2 to 3 years of age (Domachowske and Rosenberg, 1999; Mejías *et al.*, 2005; Collins and Graham, 2008). Children under the age of one year are at the highest risk of severe HRSV disease that requires hospitalization and can even be deadly (Borchers *et al.*, 2013). HRSV is the most common cause of childhood acute lower respiratory infection, causing approximately 200,000 deaths per year (Nair *et al.*, 2010). Risk factors that pre-dispose children to HRSV infections include low birth weight, cardiopulmonary disease, bronchopulmonary dysplasia, and immunodeficiency (Welliver, 2008). In young children, 2% of those infected show symptoms of central nervous system (CNS) alterations such as apnea, seizures, lethargy, and encephalopathy (Whimbey *et al.*, 1995; Eisenhut, 2006, 2007; Torres *et al.*, 2010). Apart from a humanized monoclonal antibody against HRSV F (Palivizumab), the treatment of HRSV infection is symptomatic and no vaccine has been licensed.

1.2. RNAi Screening

In the past decade, RNA interference, a cellular mechanism that uses sequence-specific degradation of messenger RNA transcripts, has become an effective tool to identify and characterize gene function. First discovered in *Caenorhabditis elegans (Fire et al., 1998)*, several genome-scale RNAi high-throughput screens have been done in *Drosophila* and mammalian cultured cells to explore the effects of gene silencing on biological phenotypes, including biological processes such as intracellular signaling, cancer biology, and host cell response to viral infections. These innovative unbiased approaches provide insights into the complexity of biological systems, as well as the identification of components involved in these processes, and have helped to understand functional networks in cells. Since results of RNAi high-throughput screens are acutely sensitive to reagent design and delivery, as well as assay design and data analysis, important caveats apply and should be taken into consideration when performing and interpreting RNAi screens.

1.2.1. Steps involved in RNAi screening

RNAi screening relies either on genome-wide screens which identify all possible inhibitors and activators of a biological process or on category-restricted approaches, identifying a protein in a specific pathway (Figure 3). The biological question of interest also determines species choice and delivery of RNAi. Small interfering RNAs (siRNAs), endoribonuclease-prepared siRNAs (esiRNAs) or small hairpin RNAs (shRNAs) are typically used for mammalian cell screens. Long dsRNA molecules have been successfully used in non-mammalian organisms, since the absence of the defensive type I IFN response facilitates greater knockdown of target proteins. shRNA screens can be conducted in a pooled format (Boettcher and Hoheisel, 2010; Mohr, Bakal and Perrimon, 2010), introducing a shRNA library into bulk populations of cells, thus allowing rapid analysis of large gene sets or parallel analyses of cell types. Cells are infected with pools of shRNA encoding lentiviruses or retroviruses to yield on average one stably integrated shRNA per cell. The next step involves the selection for loss or acquisition of a given phenotype by comparison of experimentally treated cells with control cells, followed by collection of the desired phenotype, preparation of RNA and deconvolution using microarrays or NGS of enriched or depleted shRNA sequences.

Array-formatted screens enable targeting of individual genes by reagents in individual wells of a microtiter plate, such as a 96- or 384-well plate, facilitating a wide variety of manipulations and readouts. Arrayed plate reader screens require robotic liquid handling and high-throughput readout instruments and can be easily combined with the addition of drug treatment, infectious agents such as viruses, stress, or a metabolic

substrate (for examples see (Bauer *et al.*, 2010; Gonsalves *et al.*, 2011; Seyhan *et al.*, 2011; Zhu *et al.*, 2011)). Assays can be customized to a multiwell plate reader format via measuring whole-well intensity of colorimetric, fluorescence, or luminescent readouts, to a microscopy-based format in which a robotic camera reads several positions in each well of a multiwell plate, or to a flow cytometry–based format. Prior to primary screening, pilot experiments should be performed to validate the read-out and to determine siRNA dose, incubation times, infection rates and other assay variables to further optimize assay response to negative and positive control siRNAs. Control values determine baseline, signal and standard deviation and are thus important for the development of robust, reliable, and reproducible assays. Technical considerations in an appropriate primary screen include establishment of the number of unique siRNAs per gene and number of replicates to yield meaningful data (Boutros and Ahringer, 2008; Falschlehner *et al.*, 2010; Booker *et al.*, 2011), suitable positive and negative controls, which should ideally be included on every plate to monitor quality control during screening, early assessment of data quality to detect plate-or well-level problems such as dispensing errors, data normalization, setting appropriate cutoff values for significant results (Kaplow *et al.*, 2009) and elimination of false positives. Secondary screens that narrow down the primary hit list and that refine and characterize a functional gene set should be performed to validate the primary screen.

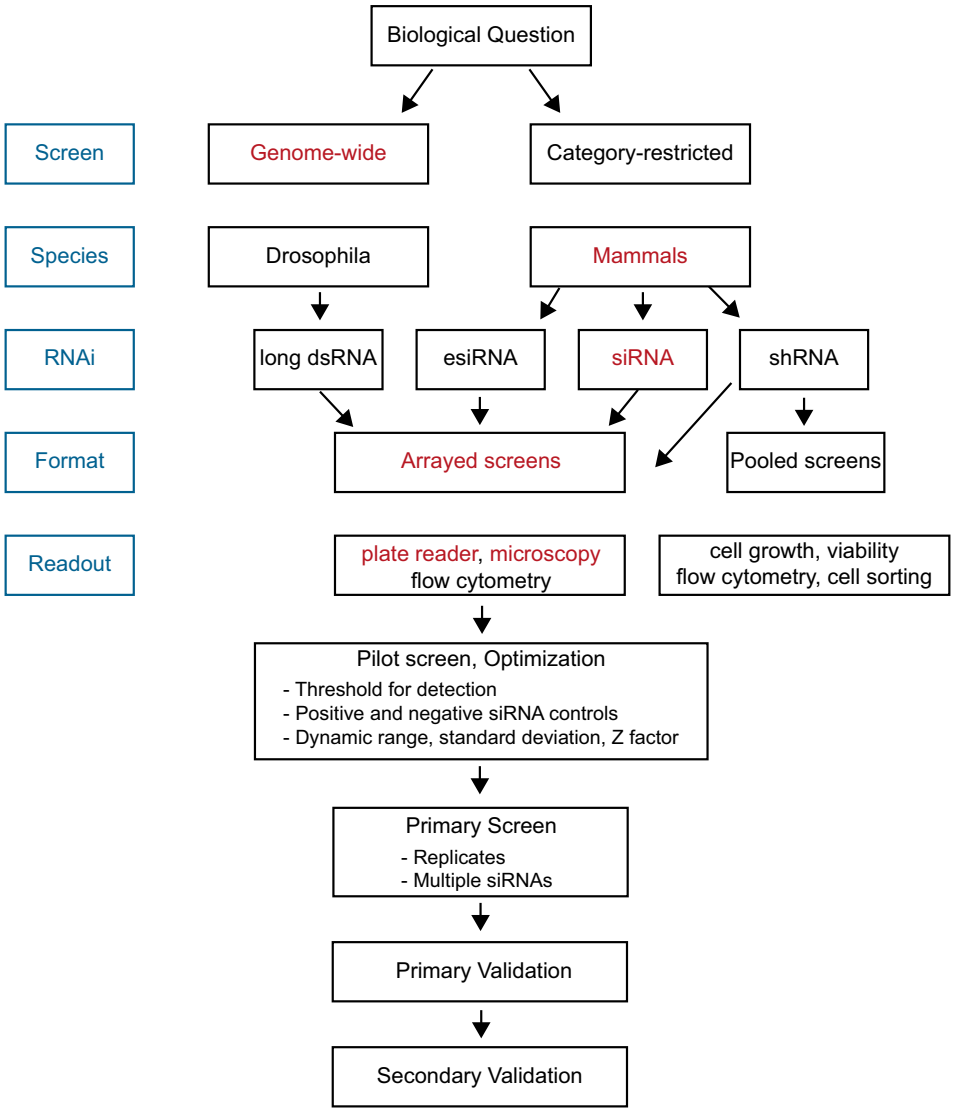

Fig. 3 | Steps involved in RNAi screens. Steps marked in red indicate the genome-wide siRNA approach that is described in the dissertation (Sharma and Rao, 2009). Adapted by permission from Springer Nature: Nature, Nature Immunology, RNAi screening: tips and techniques, Sharma and Rao, © 2009.

1.2.2. Readout, statistical analysis, and off-target effects

Assay quality assessed by strong signal/background ratio and low variation (Zhang, Chung and Oldenburg, 1999), can be indicated by the Z-factor, which is calculated through the use of many replicates with positive and negative controls. An ideal value of >0.7 indicates a suitable difference between signal and background values and low variability. Off-target effects are a major challenge of RNAi-based screens and may contribute to false discovery of candidate protein hits (Echeverri *et al.*, 2006). False positive effects can be either sequence-independent or sequence-specific. Sequence-independent effects include toxicity of the reagent delivery approach or activation of antiviral type I IFN response even by short siRNAs in mammalian cells (Sledz and

Williams, 2004; Echeverri and Perrimon, 2006; Echeverri *et al.*, 2006). Sequence-specific recognition of transcripts other than the intended target, and the resulting degradation of the unrelated mRNA, may lead to misinterpretation of the phenotype and produce a false-positive result. Off-target effects are also seen when the seed region of an siRNA pairs with a weakly complementary sequence in the 3′ untranslated region (UTR) of an unrelated mRNA. Then, the siRNA, acting like a microRNA, causes depletion of that non-target protein via mRNA degradation or translational block (Birmingham *et al.*, 2006; Echeverri *et al.*, 2006). Off-target effects can be limited by effective screen design. Regions in the target sequences that have 19 or more base pairs of contiguous nucleotide identity to another mature transcript should be avoided, since a 19-mer is sufficient to induce RNAi knockdown. Non-targeting siRNA sequences and C911 controls (Buehler, Chen and Martin, 2012) should be used, and general cellular and IFN responses to siRNA delivery should also be monitored. Multiple siRNAs applied in pools should be used for each target gene to maximize knockdown and at least two siRNAs in the pool should recapitulate the phenotype. If possible, alternative loss-of-function methods using pharmacological inhibitors, gene mutants, or CRISPR/Cas should be used to confirm the results obtained by siRNA-mediated knockdown. The 'gold standard' test for an on-target effect is a functional rescue by reintroducing an siRNA-resistant version of the target gene product into depleted cells and observing recovery of function (Lassus, Rodriguez and Lazebnik, 2002; Sarov and Stewart, 2005).

1.2.3. RNAi mechanisms

Upon introduction in the cell, long dsRNAs form a complex with the dsRNA-specific RNase III enzyme Dicer that processes them into 20–25 bp siRNAs with a 3′ dinucleotide overhang. The cleaved products are then incorporated into the RNA-induced silencing complex (RISC), consisting of the Argonaute-2 protein (Liu *et al.*, 2004; Meister *et al.*, 2004) together with PACT (Lee *et al.*, 2006), TAR-RNA-binding protein (TRBP), and Dicer (Bernstein *et al.*, 2001). RISC association involves duplex separation, selection of one strand to be removed from the RISC complex and selection of the other strand for stable incorporation into the RISC complex (Schwarz *et al.*, 2003). Binding to the target mRNA in a sequence-specific manner, mediated by complementary base pairing, then results in cleavage of the target mRNA (Hammond *et al.*, 2000; Schwarz *et al.*, 2002). The introduction of shRNA into mammalian cells through infection with viral vectors allows for stable integration of shRNA into the genome and long-term knockdown of the targeted gene. After expression in the nucleus, shRNAs, which consist of a stem region of paired 19–22 bp antisense and sense strands connected by 4–11 nt unpaired nucleotides that make up a loop, are processed by Drosha and its dsRNA-binding partner DGCR8, resulting in pre-shRNAs. The pre-shRNA is exported to the cytoplasm

by Exportin-5 (Yi *et al.*, 2003), followed by association with dicer and removal of the loop sequence. After this point they are processed in the same manner as siRNAs.

1.2.4. siRNA screens to identify host factors in viral life cycles

The development of antiviral therapeutics has focused on virus-specific targets, but high mutations rates of many viruses, especially RNA viruses, impede the treatment of infections. If a treatment is robust and viral fitness is impaired sufficiently, viral genome replication is inhibited, while an ineffective treatment can allow sufficient genome replication for rapid adaptation toward resistance. An alternative therapeutic strategy that may greatly reduce the emergence of viral resistance is the development of host-factor-directed antiviral therapies. While broad-spectrum antibiotics have long been identified and have proven efficacious against bacterial pathogens, broad-spectrum antivirals have been more elusive. The development of unbiased genome-wide siRNA screens has enabled the identification of host functions that are subverted by viruses leading to a deeper understanding of virus-host interactions during the viral replication cycle. These screens thus have enormous potential to yield new cellular therapeutic targets that are less prone to resistance development. Genome-wide siRNA libraries that target all genes in a given host cell enable the identification of cellular proteins that either promote or inhibit infection in a relatively unbiased way. Genome-wide siRNA screens for pro- and anti-viral factors in human cells have been performed with many viruses, including West Nile virus (WNV) (Krishnan *et al.*, 2008), hepatitis C virus (HCV), human immunodeficiency virus (HIV) (Brass *et al.*, 2008; König *et al.*, 2008; Zhou *et al.*, 2008), influenza A virus (König *et al.*, 2010) and VSV (Lee, Burdeinick-Kerr and Whelan, 2014). Antibodies directed against viral proteins or genetically-modified viruses expressing the green fluorescent protein (GFP) are used to quantify the extent of infection. Alternatively, enzyme activity of reporter genes proportional to viral protein production can be measured using viruses engineered to express reporter genes such as luciferase or β-galactosidase.

Screen design, read-out approach, as well as multiplicity of infection and time post-siRNA transfection and infection, can influence which stages of the viral life cycle are investigated. For example, to identify cellular proteins associated with the early stages of WNV infection, including viral entry and intracellular translation of viral RNA, siRNA screens were performed at 24 h post-infection, thereby excluding later stages of the viral life cycle such as replication, assembly, or release (Krishnan *et al.*, 2008).

A genome-wide analysis of virus-host interactions affecting the early steps of HIV-1 infection was performed using a single-cycle, replication-defective HIV vector pseudotyped with a VSV-G envelope glycoprotein in HEK293 cells at 24 h post-infection

(König *et al.*, 2008). Thus, host factors involved in the early stages of replication, including virion uncoating, reverse transcription, and integration were elucidated, while host factors involved in CD4-mediated viral entry, as well as host molecules that regulate late-stage HIV replication were not investigated. Brass *et al.* developed a two-part HIV screen to identify host proteins needed from viral entry through to Gag-mediated translation, and in the second phase to identify late-acting factors (Brass *et al.*, 2008). In a third HIV genome-scale siRNA screen, viral replication was evaluated at either 48 h and 96 h post-infection measuring β-gal as a surrogate for viral infection (Zhou *et al.*, 2008). Interestingly, only a few hits were in common between the different HIV screens, illustrating the importance of the assay design. The identification of cellular factors required for early stage influenza virus replication was performed by infecting cells with modified influenza virus expressing the *Renilla* luciferase (WSN-Ren), followed by luciferase measurements at 12 h, 24 h and 36 h post-infection (König *et al.*, 2010).

1.2.5. Inhibiting virus-host interactions

Viruses use host proteins at multiple stages of their life cycles. Strategies to target host factors can include intervention in early infection stages, such as viral attachment, fusion or endocytosis, replication, assembly and budding, or activating cellular defenses. Viral attachment to host cells is the first critical interaction between viral surface proteins and their cellular receptors. Sialic acids linked to glycoproteins and gangliosides are used by many viruses as cell entry receptors, including influenza, parainfluenza, and MuV (Matrosovich, Herrler and Klenk, 2013). The use of sialidases, which hydrolyze cell surface sialic acids, has been shown to prevent attachment. The compound DAS181, a bacterial sialidase linked to amphiregulin, which contains an epidermal growth factor-like domain for the effective targeting of respiratory epithelium, has been shown to effectively protect mice from infection with different influenza strains and parainfluenza virus, and also prevents animals from secondary infections such as pneumonia (Hedlund *et al.*, 2010; Nicholls, Moss and Haslam, 2013). Instead of targeting the viral RNA polymerase, replication can be inhibited by interrupting the biosynthesis of pyrimidine, to generate uracil essential for replication of viral RNA and DNA (Evans and Guy, 2004). The compound A3 was identified in a high-throughput screen for inhibitors of influenza virus replication (Hoffmann, Palese and Shaw, 2008). A3 targets dihydroorotate dehydrogenase, an important enzyme involved in *de novo* pyrimidine biosynthesis. This resulted in the inhibition of replication of negative-strand RNA viruses (influenza A and B viruses), positive-strand RNA viruses (HCV, DENV, and WNV), DNA viruses (VACV), adenovirus, and retroviruses (HIV) (Hoffmann *et al.*, 2011). The guanosine analog ribavirin has been used to inhibit viral RNA synthesis

(Parker, 2005) and is approved for the treatment of HRSV and HCV infections (Naik and Tyagi, 2012). Due to drug toxicity and minimal clinical benefit it has not been recommended for routine clinical use to treat HRSV (RKI, 2015; Drysdale, Green and Sande, 2016). It has also been shown that inhibiting the cellular mitochondrial electron transport chain and *de novo* pyrimidine synthesis by antimycin A controls infections by various RNA viruses *in vitro* (Raveh *et al.*, 2013). Depletion of ATP-sensitive intracellular Ca^{2+} stores by the commercial antiprotozoal agent Nitazoxanide leads to Nitazoxanide-mediated Ca^{2+} mobilization including chronic sub-lethal ER stress as well as perturbation of viral protein glycosylation and trafficking (Ashiru, Howe and Butters, 2014). This inhibits the replication of several viruses including influenza, DENV, HCV, HBV, and JEV (Rossignol, 2014). Further host-dependent steps of the viral life cycle which can be targeted are viral assembly and egress. For example, after replication of influenza virus genomic RNA in the nucleus, the vRNP complexes are translocated into the cytoplasm, which is mediated by the interaction of the protein XPO1 with NS2, the viral nuclear export protein (Neumann, 2000). It has been shown that a small molecule antagonist of XPO1, KPT-335, effectively inhibits replication of influenza A and B strains including pandemic H1N1, highly pathogenic AIV H5N1, and H7N9. *In vitro* studies and *in vivo* administration in mice has demonstrated protection against representative strains of circulating influenza A virus subtypes H1N1 (A/California/04/09) and H3N2 (A/Philippines/2/82-X79) and reduction of viral particle production (Perwitasari *et al.*, 2014). The ESCRT pathway is used by enveloped viruses, such as EBOV, to release progeny virus from infected cells. It has been shown that the phenolic compound FGI-104 targets the TSG101 subunit of ESCRT-1 (Luyet *et al.*, 2008) and blocks viral budding of EBOV, and also demonstrates broad-spectrum *in vitro* inhibition of HCV, HBV, HIV, VEE and cowpox (Kinch *et al.*, 2009).

Host immune defense mechanisms are also potential targets for new antivirals. Innate immune responses are initially activated by the detection of pathogen-associated molecular patterns (PAMPs) via pattern recognition receptors (PRR) (Creagh and O'Neill, 2006; Kawai and Akira, 2010) including MDA-5 and RIG-I like receptors (RLRs) (Kato *et al.*, 2006). Sensing of viral infections by PRRs then leads to IRF3, IRF7 and NFκB activation, resulting in the production of type I IFN-α/β, as well as inflammatory cytokines. Secreted type I IFNs bind to type I IFN receptors, activating the JAK-STAT pathway and resulting in upregulation of IFN-stimulated genes (ISGs) such as ISG15, IFIT, IFITM, and 2-5′ oligoadenylate synthetase (2-5A OAS). An analog of 5′ pppRNA has been shown to induce IFN expression and multiple antiviral responses, including IRF3, IRF7, and STAT signaling. Activation and induction of inflammatory and IFN stimulated genes (ISGs) thus controls infection by influenza A, DENV, VSV, HCV, and

VACV, as well as other pathogens (Goulet *et al.*, 2013; Olagnier *et al.*, 2014). IFIT and IFITM proteins also show antiviral activity against a range of human viruses (Diamond and Farzan, 2013). Inhibition of viral infection via IFIT occurs through multiple mechanisms such as suppression of translation initiation via IFIT1 and IFIT2 (Hui *et al.*, 2003), binding of IFIT1 to incomplete or uncapped viral RNA (Pichlmair *et al.*, 2011), and translocation of viral proteins or RNA in the cytoplasm by IFIT1 (Terenzi, Saikia and Sen, 2008). IFITM proteins, which are enriched in endosomes and lysosomes, prevent several enveloped viruses from crossing endosomal or lysosomal membranes and penetrating into the cytoplasm (Diamond and Farzan, 2013). The entry processes of MARV, EBOV, influenza, and SARS-CoV are specifically restricted by IFITM proteins (Huang *et al.*, 2011). Upon activation by viral dsRNA, 2-5′ oligoadenylates (2-5A) are synthesized by 2-5A OAS from ATP. 2-5A binds to the inactivated monomeric RNase L, which results in dimerization and activation of RNase L, followed by degradation of viral RNA. Two RNase L activators have been identified by high-throughput screenings of chemical libraries with a FRET method, which demonstrated antiviral activity against RNA viruses including paramyxoviruses, rhabdoviruses, picornaviruses, and retroviruses (Thakur *et al.*, 2007).

1.2.6. Host factor ATP-binding cassette protein E1 (ABCE1)

1.2.6.1. Structure of ABCE1

The ATP-binding cassette sub-family E member 1 (ABCE1) protein belongs to the superfamily of ATP-binding cassette proteins and was first identified as an RNase L inhibitor (Bisbal *et al.*, 1995). It is an essential and highly conserved 599-aa protein with a molecular mass of 67 kDa, found in eukaryotes and archaea, but not in bacteria. ABCE1 consists of five structural domains: two nucleotide binding domains (NBDs), two hinge regions, and an iron–sulfur (FeS) cluster domain. The NBDs are arranged in the typical head-to-tail orientation and form nucleotide-binding sites for two ATP molecules. NBD1 contains a helix–loop–helix (HLH) structural motif. The NBDs harbor conserved motifs including Y loop, Walker A, Q loop, ABC signature motif, Walker B and H loop, and are interconnected by the hinge region 1 (H1), while another hinge region (H2) also exists at the C-terminus. The two hinge regions position the two NBDs in a V-like shape and both hinge domains and the HLH motif mediate interaction of NBDs with the ribosome (Becker *et al.*, 2012; Preis *et al.*, 2014; Brown *et al.*, 2015). ABCE1 has an N-terminal iron–sulfur (FeS) cluster domain, which contains two $[4Fe\text{-}4S]^{2+}$ clusters (Barthelme *et al.*, 2007; Karcher, Schele and Hopfner, 2008). Unlike most ABC domain proteins, ABCE1 lacks a membrane-spanning domain and therefore is unlikely to have transporter function (Kerr, 2004).

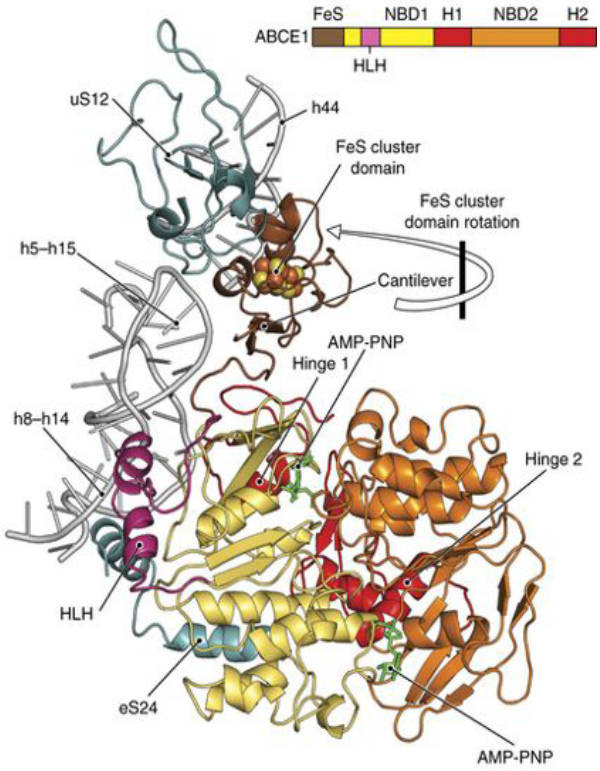

Fig. 4 | Structure of ABCE1 and an interacting small 40S ribosomal subunit. ABCE1 consists of an N-terminal iron–sulfur (FeS) cluster domain, two nucleotide-binding domains (NBDs) with a helix-loop-helix structural motif in NBD1, and two hinge regions. HLH and hinge regions contact 18S rRNA and the ribosomal protein eS24 and FeS cluster domain interacts with uS12 and rRNA helices h5 and h44 (Heuer *et al.*, 2017). Reprinted by permission from Springer Nature: Nature, Nature Structural & Molecular Biology, Structure of the 40S-ABCE1 post-splitting complex in ribosome recycling and translation initiation, Heuer et al., © 2017.

1.2.6.2. Functions of ABCE1

ABCE1 has several cellular functions (Figure 5). It was initially described as an RNase L inhibitor in the IFN-dependent 2-5A/RNase L pathway. Upon activation of the IFN-inducible 2′-5′-oligoadenylate synthase (OAS) by dsRNA, OAS converts ATP into a series of unique, 5′-phosphorylated, 2′-5′ linked oligoadenylates known as 2-5A. 2-5A binds to and converts RNase L from its inactivate monomeric state to a dimeric active state, resulting in mRNA degradation and further inhibition of protein synthesis (Floyd-Smith, Slattery and Lengyel, 1981). ABCE1 inhibits this binding of 2-5A by forming a heterodimer with RNase L (Bisbal *et al.*, 1995). ABCE1 is also involved in different aspects of ribosome recycling; it participates in ribosome splitting of vacant ribosomes assembled under nutrition stress. It disassembles 80S ribosomes in a translation-like cycle which serves as quality control checkpoint for maturing 40S ribosome subunits

(Strunk *et al.*, 2012). ABCE1 has also been implicated in the rescue of stalled elongating 80S ribosomes. Stalled ribosomes are released in the no-go and non-stop mRNA decay pathways, which are eukaryotic surveillance mechanisms that target damaged or structured (e.g., hairpins) mRNAs. The eRF1 and eRF3 paralogs Dom34 (yeast)/PELO (mammals) and Hbs1 (yeast)/HBS1L (mammals) are also implicated in these processes (Pisareva *et al.*, 2011). ABCE1 recycles terminating ribosomes and controls reinitiation of translation in the 3′UTR by unrecycled ribosomes (Young *et al.*, 2015).

ABCE1 has a crucial role in splitting 80S ribosomes into the small 40S and the large 60S subunit after translation termination. The 40S-ABCE1 complexes then associate with initiation factors eIF2, eIF5, and the multiprotein complex eIF3 in *Drosophila melanogaster* and *Saccharomyces cerevisiae*, suggesting that ABCE1 connects translational termination and initiation via ribosome recycling. A 3.9-Å-resolution EM structure of the 40S-ABCE1 post-splitting complex (Heuer *et al.*, 2017) and studies on the role of the two nucleotide-binding sites of ABCE1 (Nürenberg-Goloub *et al.*, 2018) have provided new insights into the dual role of ABCE1 in ribosome recycling and reinitiation. Canonical cap-dependent eukaryotic translation initiation is mediated by the 5′ 7-methyl-guanosine cap and the 3′ poly(A) tail of the mRNA. The cap recruits a multisubunit translation initiation complex eIF4F (Tuteja, 2009), composed of cap-binding protein eIF4E, RNA helicase eIF4A, and the adaptor protein eIFG, which mediates recruitment of the 43S preinitiation complex (PIC) and circularization of the mRNA through interaction with the poly(A) binding protein (PABP) bound to the 3′ poly(A) tail. Formation of the 43S preinitiation complex comprised of the small (40S) ribosomal subunit and the ternary complex (TC) consisting of initiator Met-tRNA$_i$ and the GTP-bound form of eIF2 is promoted by multiple eIFs (eIF1, eIF1A, eIF5, and the eIF3 complex). The 43S PIC binds to the 5′ end of the mRNA via interaction of eIF3 with eIF4G. AUG start codon recognition by the initiator Met-tRNAi within the ribosomal P site results in eIF2-bound GTP hydrolysis, release of P_i, and conformational changes in many eIFs (eIF2, eIF1A, eIF1, and eIF5B). A second GTP hydrolysis of eIF5B leads to the release of most protein factors and facilitates joining of the 60S subunit to form an elongation-competent 80S ribosome. During elongation, the ribosome actively moves along the mRNA, and aminoacylated tRNAs delivered by eEF1A bind to matching mRNA codon through base pairing in a GTP hydrolysis-dependent process. Peptide bond formation is followed by GTP hydrolysis-dependent translocation by eEF2 and delivery of the next tRNA. In eukaryotes, translation termination starts with the recognition of a stop codon in the A site of the 80S ribosome by eRF1 and the GTPase eRF3 with GTP, followed by hydrolysis of GTP and eRF3 dissociation and ABCE1 binding. Upon ATP binding to the pre-splitting complex and closure of the NBDs, the FeS cluster

domain contacting the C-terminal domain of eRF1 in the A-site, pushes eRF1 into the intersubunit space (Heuer *et al.*, 2017). Once eRF1 and the 60S subunit are unlocked, a repositioning of the FeS cluster domain occurs by 150° rotation to its new interaction site on the 40S subunit. After splitting, the translocated FeS cluster domain of ABCE1 prevents reassociation of the 60S and 40S subunits though steric hindrance. ABCE1 remains transiently bound to the 40S subunit. The structure of the native post-splitting complex reveals ABCE1 to be a component of the 43S pre-initiation complex including the initiation factors eIF1a, eIF2, eIF3 and the initiator tRNA (Heuer *et al.*, 2017) and is thus a link between translational termination and reinitiation.

It has been shown that ABCE1 is essential for HIV capsid assembly (Zimmerman *et al.*, 2002). The correct assembly of HIV-Gag (p55) polypeptides along the host cell plasma membrane is required to form the immature HIV-1 capsid. After specific recruitment to discrete sites at the plasma membrane, ABCE1 associates with Gag and forms Gag-ABCE1 complexes throughout capsid formation until the start of virus maturation (Dooher *et al.*, 2007).

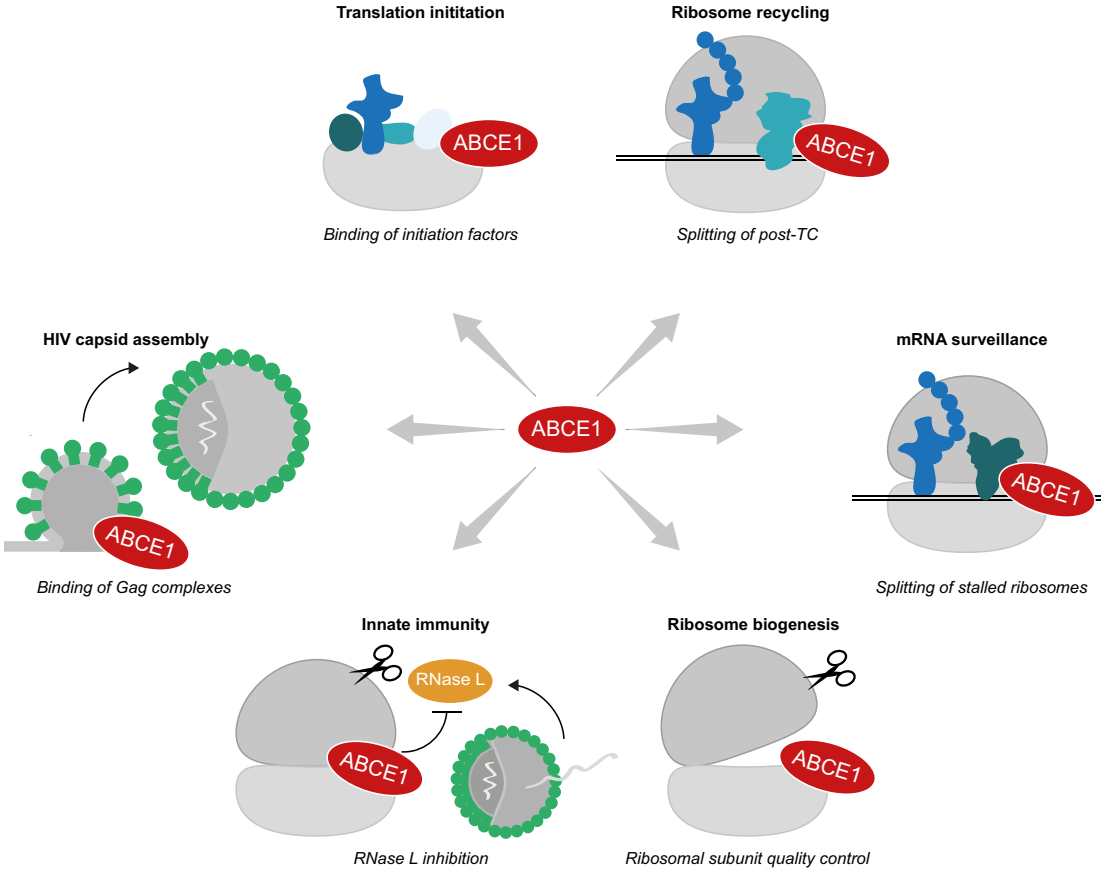

Fig. 5 | Functions of ABCE1. ABCE1 is known as RNase L inhibitor. It is involved in translation initiation and in HIV capsid assembly. ABCE1 splits ribosomes after translation termination, during ribosome recycling, and in mRNA surveillance. (Modified from (Nürenberg and Tampé, 2013)).

2. MATERIAL

2.1. Chemicals and Reagents

PRODUCT	SOURCE
^{35}S-Cys/Met mix	Hartmann Analytic, Braunschweig
Acetic acid (3%)	Paul-Ehrlich-Institute, Langen
Acrylamide/Bisacrylamide Rotiphorese	Bio-Rad Laboratories GmbH, München
Agarose	Carl Roth, Karlsruhe
Ammonium persulfate (APS)	Carl Roth, Karlsruhe
Ampicillin	Carl Roth, Karlsruhe
Atipamezole	Zoetis Austria, Wien
Complete Protease Inhibitor Cocktail EDTA-free	greiner bio-one, Kremsmünster
Cycloheximide (CHX)	Sigma-Aldrich, München
Cysteine/methionine-free DMEM	Invitrogen, Karlsruhe
Dialyzed FBS	Invitrogen, Karlsruhe
Dimethyl sulfoxide (DMSO)	Sigma-Aldrich, München
DNA gel loading dye 6×	Thermo Scientific, Karlsruhe
dNTPs	Agilent Technologies, Waldbronn
Dulbecco's modified Eagle medium (DMEM), 4.5 g/l Glucose	Lonza, Zurich
Ethanol, 96 %	Paul-Ehrlich-Institut, Langen
Fetal bovine serum (FBS)	Thermo Scientific, Karlsruhe
Formalin (3.7% formaldehyde in PBS)	VWR International, Gießen
Gel Loading Buffer II	Invitrogen, Karlsruhe
GelRed Nucleic Acid Stain, 10,000× in water	Biotium, Fremont
Gene Ruler 1 kb Plus DNA Ladder (0.5 µg/µl)	Thermo Scientific, Karlsruhe
GeneRuler 100 bp Plus DNA Ladder	Thermo Scientific, Karlsruhe
IFN-α (1.1×10^8 units/mL)	PBL Assay Science, Piscataway Township
Isoflurane CP 1 mL/mL (250 mL)	cp-pharma, Burgdorf
Isopropanol	Paul-Ehrlich-Institut, Langen
Ketamine (100 mg/mL)	Bela-Pharm GmbH & Co. KG, Vechta
LB Agar plates (100 µg/mL Ampicillin)	Paul-Ehrlich-Institut, Langen
L-glutamine (200 mM)	Biochrom AG, Berlin
Luria-Bertami (LB) Medium	Paul-Ehrlich-Institut, Langen
Medetomidine (1 mg/mL)	Orion Corporation, Espoo
Methanol	Paul-Ehrlich-Institut, Langen
Methylcellulose	Sigma-Aldrich, München
Nonidet P-40 (NP-40) substitute	Sigma-Aldrich, München
Nutribound	Virbac, Biot
Opti-MEM I reduced serum medium	Invitrogen, Karlsruhe
P3015 - Poly(ethylene glycol) (average mol wt 200)	Sigma-Aldrich, München
PageRuler Plus Prestained protein ladder	Thermo Scientific, Karlsruhe

Paraformaldehyde	Roth, Karlsruhe
PBS without magnesium and calcium, pH 7.1	Paul-Ehrlich-Institut, Langen
Penicillin-streptomycin (10,000 units penicillin / 10 mg streptomycin per mL)	Sigma-Aldrich, München
ProLong Gold Antifade Reagent with DAPI (4′,6-diamidino-2-phenylindole)	Life Technologies, Eugene
Protein A-agarose beads	Santa Cruz, Dallas
Random hexamers	New England Biolabs (NEB), Frankfurt
RNase OUT	Invitrogen, Karlsruhe
SevoFlo (250 mL)	Zoetis Belgium SA, Zaventem
Skim milk powder	Carl Roth, Karlsruhe
SOC Medium	Paul-Ehrlich-Institut, Langen
Sodium dodecylsulfate (SDS), 10× concentrate	Paul-Ehrlich-Institut, Langen
Tetramethylethylenediamine (TEMED)	Roth, Karlsruhe
Triton X-100	Sigma-Aldrich, München
Trypanblue solution (0.4%)	Sigma-Aldrich, München
Trypsin-EDTA, 0.05 % (w/v) Trypsin, 0.002 % (w/v) EDTA	Paul-Ehrlich-Institut, Langen
Tween-20 for SDS-PAGE	Carl Roth, Karlsruhe
Xylene	VWR International, Gießen
Zeocin	Sigma-Aldrich, München
β-mercaptoethanol (BME)	Sigma-Aldrich, München

2.2. Buffers

PRODUCT	**SOURCE**
Laemmli buffer 2×	25% 0.5 M Tris-HCl, pH 6.8 20% Glycerol 4% SDS 10% β-mercaptoethanol 0.004% Bromophenol blue in UPW, pH 8.3
LB-Medium (Paul-Ehrlich-Institut, Langen)	1% (w/v) Tryptone from Casein 0.5 % (w/v) Yeast extract 1% (w/v) NaCl in UPW, pH 7.0
Lysis buffer for metabolic labeling	50 mM Tris pH 7.5 150 mM NaCl 1% Triton X-100 in UPW 1 tablet of complete Protease Inhibitor Cocktail per 20 mL
PBS (Paul-Ehrlich-Institut, Langen)	137 mM NaCl 2.7 mM KCl 1.5 mM KH_2PO_4 8.1 mM Na_2HPO_4 in UPW, pH 7.1

Red blood cell (RBC) lysis buffer (Paul-Ehrlich-Institut, Langen)	0.8 M NH_4Cl 50 mM Tris-HCl in UPW, pH 7.5
RIPA-complete buffer	150 mM NaCl 50 mM Tris-HCl, pH 8 1% NP-40 substitute 0.5% Sodium deoxycholate 0.1% SDS in UPW 1 tablet complete Protease Inhibitor Cocktail per 10 mL
SDS gel-loading buffer for metabolic labeling	62.5 mM Tris-HCl pH 7.5 1% SDS 8.75% glycerol 0.125% bromophenol 5% β-mercaptoethanol in UPW
SDS running buffer 10× (Paul-Ehrlich-Institut, Langen)	250 mM Tris 192.1 mM Glycine 1% SDS in UPW
SOC Medium (Paul-Ehrlich-Institut, Langen)	2% (w/v) Tryptone from Casein 0.5% (w/v) Yeast extract 10 mM $MgCl_2$ 10 mM Mg_2SO_4 10 mM NaCl 2.5 mM KCl 20 mM D(+)-Glucose in UPW, pH 7.0
TBS-T buffer for Western blot (Paul-Ehrlich-Institut, Langen)	10% 10× TBS buffer 1% (v/v) Tween 20 in UPW
Transfer buffer for Western blot	10% 10× Tris/Glycine buffer 20% MeOH 0.375% SDS in UPW, pH 8.3
Tris buffered saline (TBS) 10×	50 mM Tris base 150 mM NaCl, in UPW, pH 7.4
Tris-HCl 1.5 M, pH 6.8 (PEI Medienküche, Langen)	1.5 M Tris base in UPW, pH 6.8
Tris-HCl 1.5 M, pH 8.8 (PEI Medienküche, Langen)	1.5 M Tris base in UPW, pH 8.8
Wash buffer for metabolic labeling	50 mM Tris pH 7.5 300 mM NaCl 0.2% Triton X-100 5 mM EDTA in UPW

2.3. Kits, Substrates and Enzymes

PRODUCT	SOURCE
Amersham ECL Prime Western Blotting Detection Reagent	GE Healthcare, Backinghamshire
Click-iT Plus OPP Alexa Fluor 594 Protein Synthesis Assay Kit	Thermo Scientific, Karlsruhe
HiScribe T7 High Yield RNA Synthesis Kit	New England Biolabs (NEB), Frankfurt
HotStar HiFidelity Polymerase Kit	Qiagen, Hilden
Lipofectamine 2000 Reagent	Life Technologies, Eugene
Lipofectamine 3000 Reagent	Life Technologies, Eugene
Lipofectamine RNAiMAX Reagent	Life Technologies, Eugene
Pierce BCA Protein Assay Kit	Thermo Scientific, Karlsruhe
Qiagen Plasmid Midi Kit	Qiagen, Hilden
QIAprep Spin Miniprep Kit	Qiagen, Hilden
QIAquick PCR Purification Kit	Qiagen, Hilden
QIAquick Gel Extraction Kit	Qiagen, Hilden
QuantiTect SYBR Green PCR Kits	Qiagen, Hilden
RNeasy Mini Kit	Qiagen, Hilden
SuperScript III Reverse Transcriptase	Thermo Scientific, Karlsruhe
T4 DNA ligase	Thermo Scientific, Karlsruhe
TOPO TA Cloning Kit	Life Technologies, Eugene
TurboFect Transfection Reagent	Thermo Scientific, Karlsruhe

2.4. Consumables

PRODUCT	SOURCE
Cell culture flasks, tissue culture treated (T25, T75, T175)	Greiner bio-one, Frickenhausen
Cryo tubes (Cryo S)	Greiner bio-one, Frickenhausen
Falcons (15 and 50 mL)	Greiner bio-one, Frickenhausen
Immobilon-P PVDF Membrane	Merck Millipore, Darmstadt
Mini-Protean 10% TGX gels	Bio-Rad Laboratories GmbH, München
Multiwell-plates (6-, 12-, 24- and 96-well plates)	Nunc, Rochester
PCR reaction tubes, 0.2 mL	Thermo Scientific, Karlsruhe
Pipette filter tips (10, 100, 300 and 1000 µL)	4titude Ltd., Berlin
Pipette tips (20, 200 and 1000 µL)	Eppendorf, Hamburg
Polycarbonate ultracentrifuge tube	Beckman Coulter, Krefeld
Reaction tubes	Sarstedt, Nürnbrecht
Serological pipettes (5, 10, 25 mL)	Greiner bio-one, Frickenhausen
Single-use reagent reservoir, 50 mL	Roth, Karlsruhe
Sterican canulae 100	B.Braun, Emmenbrücke
VACUETTE K2EDTA (2 mL)	Greiner bio-one, Frickenhausen
VACUETTE Z Serum Clot Activator (2 mL)	Greiner bio-one, Frickenhausen

Whatman chromatography paper	GE Healthcare, Backinghamshire

2.5. Equipment and Instruments

PRODUCT	**SOURCE**
Accu-jet pro	Brand, Wertheim
cassette-K BaFBr:Eu phosphor screen	Kodak, Hemel Hempstead
Cell culture incubator Heracell 150i	Thermo Scientific, Karlsruhe
Centrifuge Eppendorf 5418 equipped with rotor FA-45-18-11	Eppendorf, Hamburg
Centrifuge Eppendorf 5810 equipped with swinging bucket rotor A-4-81	Eppendorf, Hamburg
Centrifuge Varifuge RF	Heraeus Sepatech, Hanau
Chemiluminescent imaging system: MicroChemi 4.2, camera MicroLine ML 4022	DNR Bio Imaging Systems, Jerusalem
Class II biological safety cabinet	Thermo Scientific, Karlsruhe Labotec, Ormond Beach, Florida
DITABIS HLC Heating Thermo Shaker MHR 13	DITABIS Digital Biomedical Imaging Systems AG, Pforzheim
Electrophoresis power supply PowerPac HC	Bio-Rad Laboratories GmbH, München
Finnpipette F2 Multichannel Pipettes	Thermo Scientific, Karlsruhe
Fluorescence/Absorbance plate reader: Genios plus	Tecan Group Ltd., Männedorf
Freezer (-20 °C) GG4010-20	Liebherr, Biberach an der Riss
Freezer (-80 °C) HERAfreeze Top	Thermo Scientific, Karlsruhe
Fridge FKS 1800-20	Liebherr, Biberach an der Riss
Gel Dryer Model 583	Bio-Rad Laboratories GmbH, München
Gel electrophoresis chamber: Mini-Protean	Bio-Rad Laboratories, München
Gel electrophoresis chamber: RunOne Electrophoresis Cell	EmbiTec, San Diego, CA
Heidolph Reax top test tube shaker	Heidolph Instruments GmbH & Co. KG, Schwabach
Highspeed-centrifuge Avanti J-26XP equipped with rotor JA-25.50	Beckman Coulter, Krefeld
Incubator shaker Innova 42	New Brunswick Scientific, Edison (NJ)
Microscope Nikon ECLIPSE Ti-S equipped with camera Nikon DIGITAL SIGHT DS-QiIMc-U3	Nikon GmbH, Düsseldorf
Microscope Nikon Eclipse TS100-F	Nikon GmbH, Düsseldorf
Microwave: 7809	Severin, Sundern
Mr. Frosty Freezing container	Thermo Scientific, Karlsruhe
MSC-Advantage BSC	Thermo Scientific, Karlsruhe
NanoDrop 2000c Spectrophotometer	Thermo Scientific, Karlsruhe
Neubauer chamber: Neubauer Brightlight	LO-Laboroptik, Friedrichsdorf
Northern Vaporizers, Isoflurane, 5090	Shor-Line, Kansas City
Oxygen concentrator JAY-5	Longfian Scitech Co.,Ltd, Baoding
Personal Molecular Imager (PMI) System	Bio-Rad Laboratories GmbH, München

Pipettes: Reference 2 (0.1–0.5 µl, 0.5–10 µl, 10–100 µl, 20–200 µl, 100– 1000 µl)	Eppendorf, Hamburg
Sevoflurane Vapor 19.3	Dräger, Lübeck
Shaker SSL4	Stuart, Villepinte
Thermo Scientific Heraeus microbiological incubator B 6060	Thermo Scientific, Karlsruhe
Tissue culture hood MSC-Advantage 1.2	Thermo Scientific, Karlsruhe
TProfessional TRIO Thermocycler	Biometra/Analytik Jena, Göttingen
Trans-Blot SD Semi-Dry Transfer Cell	Bio-Rad Laboratories GmbH, München
TW8 Water Bath	JULABO GmbH, Seelbach
Vacuum pump TopStream 3000	Fastbiotech, Frankfurt
VWR Signature Rocking Platform Shaker	VWR International GmbH, Darmstadt
Water bath	GFL, Burgwedel

2.6. Software

SOFTWARE	SOURCE
ImageJ	National Institutes of Health, USA
Magellan 7.1 Sp1	Tecan Group Ltd., Männedorf
Nis-Elements 4.20.00 LO	Nikon GmbH, Düsseldorf
Prism 7 for Windows, Version 7.04, 2017	GraphPad Software, Inc., La Jolla (CA)
Quantity One 1-D Analysis software package	Bio-Rad Laboratories GmbH, München
Sequencher 5.4.6	Gene Code Corporation

2.7. Eukaryotic Cell Lines

CELLS	ATCC	DESCRIPTION
A549-hSLAM	ATCC CCL-185	Human lung adenocarcinoma cell line constitutively expressing the human SLAM molecule
HEK293T	ATCC CRL-3216	Human embryonic kidney 293 cells
HeLa	ATCC CCL-2	Human cervical adenocarcinoma cell line
HEp-2	ATCC CCL-23	Human HeLa contaminant
Vero-hSLAM	ATCC CCL-81	African green monkey kidney cell line constitutively expressing the human SLAM molecule

2.8. Plasmids

PLASMID	SOURCE	DESCRIPTION
pCG-ABCE1-FLAG (N and C-terminal)	Prof. Dr. Veronika von Messling, Paul-Ehrlich-Institut, Langen	ABCE1 with an N- or C-terminal FLAG tag, cloned into the pCG1-IRESZeomut vector
siRNA-resistant pCG-ABCE1-FLAG	derived from pCG-ABCE1-FLAG	pCG-ABCE1-FLAG derivative carrying 7-10 silent mutations in the ABCE1_5 and ABCE1_6 siRNA target sequences
pCG-MeV-FLAG-N	Dr. Bevan Sawatsky, Paul-Ehrlich-Institut, Langen	MeV N protein with a FLAG-tag (DYKDDDDK) at the N-terminus, cloned into the pCG1-IRESZeomut vector

2.9. Viruses

VIRUS	SOURCE	DESCRIPTION
MeV Anchorage #1 P2	Prof. Dr. Veronika von Messling, Paul-Ehrlich-Institut, Langen	MeV wild type isolate, passage 2
MeV	Dr. Paul Duprex, National Emerging Infectious Diseases Laboratories, Boston University; Center for Vaccine Research, University of Pittsburgh	rMV^{KS}EGFP(3) is a recombinant virus, based on the Khartoum-Sudan (KS) strain of MeV, expressing EGFP from an additional transcription unit inserted between the P and M genes
MuV	Dr. Paul Duprex, National Emerging Infectious Diseases Laboratories, Boston University; Center for Vaccine Research, University of Pittsburgh	$rMuV^{G09}$EGFP(3) is a recombinant virus, based on the sequence of MuV present in clinical material from a genotype G MuV infection from the 2009 New York mumps outbreak, expressing EGFP from an additional transcription unit inserted between the P and M genes
MV/FrankfurtMain.DEU/17.11	Prof. Dr. Annette Mankertz, Robert Koch Institut, Berlin	MeV wild-type isolate from Germany
HRSV	Prof. Dr. Paul Duprex, National Emerging Infectious Diseases Laboratories, Boston University; Center for Vaccine Research, University of Pittsburgh	$rHRSV^{B05}$EGFP(5) is a recombinant virus, based on the sequence of HRSV present in a tracheal rinse from an HRSV-positive infant during the 2004-2005 HRSV season, expressing EGFP from an additional transcription unit inserted between the P and M genes

2.10. Antibodies

ANTIBODY	SOURCE
Anti-beta actin monoclonal antibody (ab8226)	Abcam, Cambridge
Anti-FLAG polyclonal antibody produced in rabbit	Sigma Aldrich, München
Anti-measles monoclonal antibody, nucleoprotein, clone 83KKII (MAB8906)	Merck Millipore, Darmstadt
Anti-measles blend antibody, hemagglutinin, clones CV1, CV4 (MAB8905)	Merck Millipore, Darmstadt
Anti-measles blend antibody, matrix protein, clones CV8, CV9 (MAB8910)	Merck Millipore, Darmstadt
Anti-mumps nucleoprotein antibody (ab9878)	Abcam, Cambridge
Anti-pyruvate dehydrogenase E1-alpha subunit (phospho S293) antibody (ab92696)	Abcam, Cambridge
Anti-respiratory syncytial virus nucleoprotein antibody (ab94806)	Abcam, Cambridge
eIF3A Antibody #2538	Cell Signaling Technology, Cambridge
Goat anti-mouse HRP conjugate	Jackson Immunoresearch, Cambridgeshire
Goat anti-rabbit IgG (H+L) secondary antibody, HRP conjugate	Life Technologies, Eugene
Monoclonal ANTI-FLAG M2	Sigma Aldrich, München
Mouse anti-GAPDH monoclonal antibody	Cell Biolabs, Inc, San Diego
Rabbit anti-peptide antisera against the MeV F	Prof. Dr. Veronika von Messling, Paul-Ehrlich-Institut, Langen
Rabbit anti-peptide antisera against the MeV M	Prof. Dr. Veronika von Messling, Paul-Ehrlich-Institut, Langen
Rabbit anti-peptide antisera against the MeV N	Prof. Dr. Veronika von Messling, Paul-Ehrlich-Institut, Langen
Rabbit anti-ABCE1 hyperimmune sera #9 and #10	Prof. Jaisri Lingappa, University of Washington, USA Prof. Dr. Veronika von Messling, Paul-Ehrlich-Institut, Langen

2.11. siRNAs

siRNA	SOURCE
ABCE1_5 20 µM	Custom siRNA oligos, Sigma-Aldrich, München Target sequence (5′-3′): TTCCGTGGATCTGAATTACAA Sense strand (5′-3′): CCGUGGAUCUGAAUUACAA[dT][dT] Anti-sense strand (5′-3′): UUGUAAUUCAGAUCCACGG[dT][dT]

ABCE1_6 20 µM	Custom siRNA oligos, Sigma-Aldrich, München Target sequence (5′-3′): TGGCGCCTTATCAATTGTCAA Sense strand (5′-3′): GCGCCUUAUCAAUUGUCAA[dT][dT] Anti-sense strand (5′-3′): UUGACAAUUGAUAAGGCGC[dT][dT]
Hs_ABCE1_5_C9l1	Custom siRNA oligos, Sigma-Aldrich, München Target sequence (5′-3′): TTCCGTGGATCTGAATTACAA Sense strand (5′-3′): CCGUGGAUGACAAUUACAA[dT][dT] Anti-sense strand (5′-3′): UUGUAAUUGUCAUCCACGG[dA][dA]
Hs_ABCE1_6_C9l1	Custom siRNA oligos, Sigma-Aldrich, München Target sequence (5′-3′): TGGCGCCTTATCAATTGTCAA Sense strand (5′-3′): GCGCCUUAAGUAUUGUCAA[dT][dT] Anti-sense strand (5′-3′): UUGACAAUACUUAAGGCGC[dC][dA]
Hs_EIF3S10_6	FlexiTube siRNA against human EIF3A (SI03019107), Qiagen, Hilden Target sequence (5′-3′): GAGGATCTAGATAATATTCAA
Hs_EIF3S10_7	FlexiTube siRNA against human EIF3A (SI04200063), Qiagen, Hilden Target sequence (5′-3′): ATGGCTAAACAGGTTGAACAA
non-silencing control (NSC) 20 µM	AccuTarget Negative Control siRNA, 20 µmol, BioNeer Corp., South Korea

2.12. Primer

Real-time PCR primers

		SEQUENCE
β-actin	fwd	5′-GGAAATCGTGCGTGACATTAAG-3′
	rev	5′-AGCTCGTAGCTCTTCTCCA-3′
PDH E1α	fwd	5′-GGAGGATGGGCTCAAATACTAC-3′
	rev	5′-GACCATCACACAAGTGACAGA-3′
GAPDH	fwd	5′- GAGTCAACGGATTTGGTCGT-3′
	rev	5′- TTGATTTTGGAGGGATCTCG -3′
MeV N	fwd	5′- TGGGAGTAGGAGTGGAACTT -3′
	rev	5′- CCTTACCATCTCTTGCCCTAATC -3′
MeV M	fwd	5′- AAAGGGTCGATCGCTCCGATACAA-3′
	rev	5′- TCCTTCCTATCACCTAGACCAGGA -3′

MeV F	fwd	5′-GCGAGCCTGGAAACTACTAATC-3′
	rev	5′-ACACCCTGAACAGCCAATATC-3′
ABCE1	fwd	5′-ACCTTGGAAAGTACGATGATCC-3′
	rev	5′-ATCTGGTCTACATATTGAGGTTTGA-3′

PCR primers for cloning

		SEQUENCE
β-actin	fwd	5′-CACCATGGATGATGATATCGCCGCGC-3′
	rev	5′-CCGCCTAGAAGCATTTGCGGTGG-3′
PDH Elα	fwd	5′-TGTGCTTCATGAGGAAGATGCTCGCC-3′
	rev	5′-CCCCTTAACTGACTGACTTAAACTTGATCC-3′
MeV N	fwd	5′-GGGACATCCGAGATGGCCACAC-3′
	rev	5′-CGCACCTAGTCTAGAAGGTCTCT-3′
MeV M	fwd	5′-GCAAAGTGATTGCCTCCCAAGCTCC-3′
	rev	5′-CGGTCTACAGAACTTTGAAGAGTCCTTGG-3′
MeV F	fwd	5′-CCATCATGGGTCTCAAGGTGAACGT-3′
	rev	5′-GAGGATCAAAGCGACCTTACATAGG-3′
ABCE1 (BamHI)	fwd	5′-GATCGGATCCATGGCAGACAAGTTAACGAGAATTGC-3′
(SphI)	rev	5′-GATCGCATGCCTAATCATCCAAGAAAAAGTAGTTTCC-3′

Mutagenesis primers for construction of siRNA-resistant ABCE1 mutant protein

		SEQUENCE
ABCE1_5	fwd	5′-TTTAGGGGGAGCGAGCTGCAAAATTACTTTACAAAGATTCTAGAAGATG-3′
	rev	5′-TTGCAGCTCGCTCCCCCTAAAATAAGTCAAAATCTCCTGCCAGTC-3′
ABCE1_6	fwd	5′-GGGGCGTTGTCGATAGTGAATCTACCAAGCAACTTGGAAAAAG-3′
	rev	5′-TTCACTATCGACAACGCCCCGAAGGGGCATTTCTTAATACAGATAC-3′

Sequencing primers

		SEQUENCE
β-actin	fwd	5′-AGCGGGAAATCGTGCGTGAC-3′
	rev	5′-CGTAGATGGGCACAGTGTGG-3′
PDH Elα	fwd	5′-ATGGCGATGGTGCTGCTAAC-3′
	rev	5′-CAGACGTTCCCATTCCATAG-3′
MeV N	fwd1	5′-AAGACCCTGAGGGCTTCAAC-3′
	fwd2	5′-TAGGGCAAGAGATGGTAAGG-3′
	rev1	5′-CAAGTTCCACTCCTACTC-3′
	rev2	5′-TGTGTCTGGAGCCGTAACCG-3′
MeV M	fwd	5′-TCTGATACCGCTGGATACCC-3′
	rev	5′-CGGTGTAATACCCGTTATCC-3′
MeV F	fwd1	5′-AGAGCGAGCCTGGAAACTAC-3′
	fwd2	5′-TGTGCTCGTACACTCGTATC-3′

	rev1	5′-GACCCGGATACGAGTGTACG-3′
	rev2	5′-ATCATCTCCTGCCCTGCTTG-3′
ABCE1	fwd1	5′-GGAGGAGAGTTGCAGAGATTTG-3′
	fwd2	5′-CTGATGAAGGAGGAGAAG-3′
	rev1	5′-GTCTTCCAGCAAGCATTC-3′
	rev2	5′-GCAGCCTTAGGAATCTGGTC-3′

3. METHODS

3.1. Molecular Biology Methods

3.1.1. RNA-isolation for RT-qPCR

For isolation of total RNA, uninfected or infected cells were lysed by adding RLT buffer containing 1% β-mercaptoethanol and lysates were homogenized via centrifugation through a QIAshredder spin column. For RNA purification and isolation, the RNeasy Mini Kit (QIAGEN) was used according to the manufacturer's instructions.

3.1.2. Reverse transcription (RT)

Single-stranded complementary DNA was reverse transcribed from total RNA using the SuperScript III Reverse Transcriptase according to the manufacturer's instructions. RNA (10 pg–5 µg total) was mixed with random hexamers and dNTPs, and heated to 65 °C for 5 min before incubation on ice. For DNA strand synthesis, 5× first strand buffer, DTT, RNase Inhibitor and Superscript III were added and incubated for 5 min at 25 °C followed by 60 min at 50 °C. Enzyme inactivation was performed for 15 min at 70 °C. Reaction components and RT program are described in Table 1 and Table 2.

Table 1 | Reverse transcription reaction mix.

Reaction Mix	**Volume**
Random hexamers NEB	1µL
10 mM dNTP Mix	1 µL
Total RNA (10 pg–5 µg)	1 µL
H_2O	10 µL
5× First Strand buffer	4 µL
0.1 M DTT	1 µL
RNase OUT	1 µL
SuperScript III RT (200 units/µL)	1 µL
Total	20 µL

Table 2 | Standard reverse transcription program.

Step	**Temperature**	**Time**
Primer annealing	65 °C	5 min
	4 °C	1 min
DNA polymerization	25 °C	5 min
	50 °C	60 min
Enzyme deactivation	70 °C	15 min
Cooling	4 °C	∞

3.1.3. Polymerase chain reaction (PCR)

PCRs were performed to amplify specific viral (MeV N, M, F) and cellular (β-actin, and PDH E1α) gene segments using the HotStar HiFidelity Polymerase Kit with the reaction components described in Table 3 and standard temperature cycle program shown in Table 4.

Table 3 | PCR reaction mix.

Reaction mix	**Volume**
RNase-free water	27 µL
Primer fwd (10 µM)	5 µL
Primer rev (10 µM)	5 µL
Template DNA	2 µL
5× HotStar HiFidelity PCR Buffer	10 µL
HotStar HiFidelity DNA Polymerase	1 µL
Total reaction volume	50 µL

Table 4 | PCR standard temperature cycle program.

Step	Temperature	Time	
Initial denaturation	95 °C	5 min	
Denaturation	94 °C	15 sec	30× (ΔT -0.3 °C)
Annealing	52 °C	1 min	
Elongation/Extension	72 °C	2 min	
Final Extension	72 °C	10 min	
Cooling		∞	

PCR amplification products were purified using the QIAquick PCR Purification Kit according to the manufacturer's instructions.

3.1.4. Agarose gel

Gel electrophoresis was used to separate DNA fragments of different sizes to detect PCR products or to purify DNA fragments. Electrophoresis was performed using 1% Agarose gels in 1× TAE buffer and Gel-Red (1:2500 dilution) to stain dsDNA. Samples and marker (Gene Ruler 1 kb Plus DNA Ladder) were prepared by adding an appropriate volume of 6× Loading Dye. The electrophoresis was performed at 100 V for 20 min and the DNA bands were then visualized with a UV-transilluminator and appropriate DNA fragments were excised from the gel and purified with the QIAquick Gel Extraction Kit according to the manufacturer's instructions.

3.1.5. TOPO-TA Cloning

The PCR-amplified viral (MeV N, M, F) and cellular (β-actin and PDH E1α) gene segments were cloned into the pCR2.1-TOPO vector for use in further steps for the generation of synthesized RNA RT-qPCRs standards. TOPO TA Cloning provides an efficient one-step cloning strategy for the direct insertion of PCR products, amplified by polymerases with nontemplate-dependent terminal transferase activity that adds a single deoxyadenosine (dA) to the 3′ ends of PCR products (Taq and HotStar HiFidelity), into a plasmid vector.

3.1.6. Transformation

Plasmid DNA was transformed into chemically competent *E. coli* Top10 bacteria by heat shock. Towards this, 5-10 µl of the ligation product were added to 25 µL *E. coli* Top10 cells and incubated on ice for 30 min. For uptake of plasmid DNA, a 45 s heat-shock at 42 °C was performed and the tubes were afterward immediately incubated on ice. After the addition of 250 µL of SOC medium, cultures were incubated for 1 h at 37 °C with shaking at 200 revolutions per minute (rpm). Transformations were plated in 100 µL and 150 µL aliquots on agar plates containing 100 µg/mL ampicillin, and plates were incubated overnight at 37 °C. The next morning, single colonies were picked and grown overnight in 5 mL Luria-Bertami broth (LB) medium containing 100 µg/mL ampicillin at 37 °C with shaking at 200 rpm.

3.1.7. Plasmid DNA preparation

For plasmid DNA preparation of overnight bacterial cultures, bacteria were pelleted by centrifugation at 6000× g, 4 °C for 15 min. Isolation and purification of plasmid DNA was performed using the QIAprep Spin Miniprep Kit (5 mL cultures) or the QIAGEN Plasmid Midi Kit (100 mL cultures) according to the manufacturer's protocol and DNA was either eluted in 50 µl (Miniprep) or resuspended in 250 µL (Midi) elution buffer. DNA concentrations were determined using the Nanodrop 2000c spectrophotometer. Clones were verified by Sanger sequencing by GATC Biotech AG/A Eurofins Genomics Company. Sequencing results were analyzed with Sequencher 5.4.6. Positive Miniprep clones were used to prepare Midi preps.

3.1.8. In vitro transcription of RNA

RNA standards of MeV N, M, F and β-actin and PDH E1α for RT-qPCR were prepared by *in vitro* transcription of RNA using T7 RNA polymerase. The RNA synthesis was performed using the HiScribe T7 High Yield RNA Synthesis Kit according to the manufacturer's instructions. The plasmids were linearized by digestion with SpeI for 3 h at 37 °C. The sizes of the digested plasmids were verified by agarose gel

electrophoresis, and the buffer for the digested plasmids was exchanged using the PCR Purification Kit according to the manufacturer's instructions and was eluted in 30 µL EB buffer. The DNA concentration was determined with the Nanodrop 2000c Spectrophotometer. For *in vitro* transcription, reaction components were mixed as described in Table 5 and incubated for 2 h at 37 °C.

Table 5 | *In vitro* transcription reaction mix.

Reaction mix	Volume
H_2O	variable
10× Reaction Buffer	2µL
ATP (100 mM)	2 µL
GTP (100 mM)	2 µL
CTP (100 mM)	2 µL
UTP (100 mM)	2 µL
Template DNA	1 µg
T7 RNA Polymerase Mix	2 µL
Total	20 µL

To remove template DNA, 70 µl nuclease-free water, 10 µl of 10× DNase I reaction buffer, and 1 µl of DNase I were mixed with the RNA sample and incubated for 15 minutes at 37 °C. Synthesized RNA was purified using the RNeasy Mini Kit according to the manufacturer's instructions.

3.1.9. Quantitative PCR (qPCR)

Quantitative Reverse Transcriptase-PCR (RT-qPCR) was used for viral und cellular mRNA quantification. Copy numbers of viral, β-actin, and PDH E1α mRNAs, and relative expression levels of OAS3, IFNβ, Mx1, and RNase L in samples isolated at different times after infection of NSC- or ABCE1-knockdown cells were quantified by qPCR using QuantiFast SYBR Green PCR kit after reverse transcription with SuperScript III Reverse Transcriptase. cDNA (10 ng) was mixed with 2× QuantiFast SYBR Green PCR Master Mix, primers and RNase-free water were mixed as shown in Table 6 and incubated according to the qPCR cycle conditions shown in Table 7.

Table 6 | qPCR reaction mix.

Reaction mix	Volume
2× QuantiFast SYBR Green PCR Master Mix	12. 5 µL
Primer fwd	1 µL
Primer rev	1 µL
cDNA	1 µL

RNase-free water	9.5 µL
Total reaction volume	25 µL

Table 7 | qPCR standard temperature cycle program.

Step	Time	Temperature
PCR initial activation step	95 °C	5 min
Denaturation	95 °C	5 sec
Combined annealing/ extension	60 °C	10 sec

3.1.10. Generation of the siRNA-resistant pCG-ABCE1-FLAG plasmid

The ABCE1_5 and ABCE1_6 siRNAs bind to different sites in the ORF. To rescue the RNAi effect by expressing a siRNA-resistant form of ABCE1, silent mutations (7-10 bases) were introduced into the ABCE1_5 and ABCE1_6 siRNA target sites in the pCG-ABCE1-FLAG plasmid using overlap extension PCR. Mutations were introduced by performing the following three PCRs: one PCR to amplify the 5′ end of the ORF up to the first siRNA target site, the second PCR from the first target site to the second target site, and the third PCR from the second siRNA target site to the end of the ORF. The PCR products were purified using the QIAquick PCR Purification Kit according to the manufacturer's instructions and DpnI digestion was performed to remove methylated template DNA. Towards this, 30 µL of the PCR product were incubated with 1 µL DpnI and 4 µL Tango buffer at 37 °C overnight. To join the fragments, an overlap PCR was performed without primers and in a second step, primers binding to the far ends of the joined fragment were added in a purification PCR to obtain and amplify one complete assembled fragment. Reaction components and PCR programs are shown in Table 8 and Table 9.

Table 8 | Overlap and purification PCR reaction mix.

Reaction mix overlap PCR	Volume
RNase-free water	27 µL
Template DNA	2 µL (0.5 µL fragment 1, 0.5 µL fragment 2, 1 µL fragment 3)
5× HotStar HiFidelity PCR Buffer	10 µL
HotStar HiFidelity DNA Polymerase	1 µL
Reaction mix purification PCR	
FLAG-ABCE1 BamHI fwd (10 µM)	5 µL
ABCE1 SphI rev (10 µM)	5 µL

Table 9 | Overlap and purification PCR program.

Step overlap PCR	**Temperature**	**Time**	
Initial denaturation	95 °C	2 min	
Annealing	40 °C	3 min	
Elongation/Extension	72 °C	3 min	
Step purification PCR			
Denaturation	95 °C	10 sec	30× (ΔT -0.3 °C)
Annealing	52 °C	30 s	
Elongation/Extension	72 °C	2 min 30 s	
Final Extension	72 °C	10 min	
Cooling	4 °C	∞	

3.1.11. Restriction digestion

To clone the purified PCR-amplified siRNA-resistant ABCE1 mutant gene fragment into the pCG1-IRESzeomut vector, the PCR product and vector were digested with the restriction enzymes BamHI and SphI for 2-3 h at 37 °C as described in Table 10.

Table 10 | Restriction digestion reaction mix.

Reaction mix	**Volume (PCR product)**	**Volume (vector)**
RNase-free water	-	14 µL
PCR product/ vector	30 µL	2 µL
10× cut smart buffer	4 µL	2 µL
Enzyme 1 (BamHI)	1 µL	1 µL
Enzyme 2 (SphI)	1 µL	1 µL
Total	36 µL	20 µL

The digested PCR product and vector were loaded on an agarose gel and respective bands were gel extracted using the QIAquick Gel Extraction Kit according to the manufacturer's instructions. The vector pCG was dephosphorylated by incubating 12.5 µL of vector with 1.5 µL 10× FastAP buffer and 1 µL FastAP Thermosensitive Alkaline Phosphatase for 1 h at 37 °C, followed by heating at 75 °C for 15 min to inactivate the enzyme.

3.1.12. Ligation

For the subsequent ligation of the siRNA-resistant ABCE1 mutant PCR fragment and the pCG vector, digested with the same restriction endonucleases, ligation reactions were

performed with the bacteriophage T4 DNA Ligase in 10× T4 Ligase buffer as shown in Table 11. The ligation reaction was incubated for 20-30 min at RT.

Table 11 | Ligation reaction mix.

Reaction mix	Volume
RNase-free water	8 µL
T4 ligase buffer	2 µL
vector	1 µL
insert	7 µL
T4 ligase	2 µL
Total reaction volume	20 µL

Transformation, plasmid DNA preparation and sequencing of the obtained siRNA-resistant pCG-ABCE1-FLAG plasmid were performed as described in Chapters 3.1.6 and in 3.1.7.

3.1.13. siRNA transfection

A549-hSLAM cells were seeded into 24-, 12-, or 6-well plates and transfected with ABCE1-specific, eIF3A-specific, or control siRNAs. C911 siRNAs were used to control for off-target effects with the ABCE1 siRNAs. Target sequence mismatches were introduced into the ABCE1_5 and ABCE1_6 siRNAs using the C911 Calculator Version 1 (http://rnai.nih.gov/haystack/C911Calc.html), to generate the ABCE1_5_C911 and ABCE1_6_C911 siRNAs, respectively. For the 24-well plate format, 100 µL/well of OptiMEM was combined with 0.75 µL/well siRNA at 20 µM working concentration and 1 µL/well of Lipofectamine RNAiMAX transfection reagent, vortexed, and incubated at RT for 15 min. The siRNA:OptiMEM mixture was added to the plated A549-hSLAM cells, which were then incubated at 37 °C. siRNA transfection mixtures are shown in Table 12. After 48 h, cells were infected with the respective viruses at a MOI of 0.01 or 1. At different time points thereafter, medium and cells were harvested for virus titrations, and cells were lysed in RIPA buffer for protein analysis, or RNA isolation buffer for RNA analysis.

Table 12 | siRNA transfection mix in 24-, 12- and 6-well plates.

Transfection Mix	24-well plate	12-well plate	6-well plate
Opti-MEM	100 µl	200 µL	400 µL
Lipofectamine RNAiMAX	1 µl	2 µL	4 µL
siRNA (20 µM)	0.75 µl	1.5µL	3 µL

3.1.14. Translation inhibition by cycloheximide

A549-hSLAM cells were reverse transfected with NSC or ABCE1_6 siRNA as previously described. After 48 h, cells were treated with 100 µg/mL cycloheximide (CHX) for 30 min before infection. Cells were infected with MeV at a MOI of 1 for 1 h, washed twice with PBS and 100 µg/mL CHX was again added. For mRNA analysis, total cytoplasmic RNA was isolated at 1 h, 12 h or 24 h post-infection using the RNeasy Kit and analyzed by qPCR using QuantiFast SYBR Green PCR kit after reverse transcription with the SuperScript III Reverse Transcriptase. Samples without addition of CHX were used as controls. Log_2-transformed groups were analyzed using one-way ANOVA and Sidak's multiple comparisons test. For CHX pulse chase experiments, 24 h post-infection, CHX was removed, cells were washed with PBC and cultured in medium. At 1 h, 12 h, 16 h, 20 h and 24 h post-CHX removal lysates were harvested and analyzed via Western Blots.

3.1.15. Plasmid transfection

For transfection in siRNA-transfected A549-hSLAM cells in 12-well dishes, 2 µg of plasmid was mixed with 3 µL of Lipofectamine 2000 in 100 µL/well OptiMEM. Transfection mixtures were vortexed and incubated at room temperature for 20 min. After incubation, 100 µL of transfection mixture was added to the appropriate well and incubated at 37 °C for 5 h, after which the medium was aspirated and replaced with fresh DMEM containing 5% FBS and 1% L-glutamine.

3.2. Cell Culture Methods

3.2.1. Cultivation of cell lines

All cell lines were maintained at 37 °C in a humidified incubator ventilated with 5% CO_2. HEK293T cells, HEp-2 cells, and Vero-hSLAM cells were cultivated in DMEM supplemented with 5% FBS and 200 mM L-glutamine. A549-hSLAM cells were cultivated in DMEM with 10% FBS and 200 mM L-glutamine. hSLAM expression was maintained by treatment with 500 µg/mL Zeocin.

3.2.2. Cryo-preservation and thawing of cells

For cryo-preservation of mammalian cells, trypsin-EDTA detached cells were pelleted at 4 °C and 2,000 rpm for 5 min. Cells were resuspended in freezing medium containing 80% FBS, 10% DMSO and 10% DMEM and aliquoted into cryotubes. Vials were placed in a Mr. Frosty Freezing container filled with isopropanol at -80 °C for 24 h before storage at -80 °C. For thawing, cells were placed for 2 min in a 37 °C water bath and transferred into a cell culture flask containing pre-warmed medium supplemented with 10% FBS and 1% L-glutamine. After 24 h, medium was exchanged and cells were cultured as

previously described.

3.2.3. Cell lysate preparation for Western blot analysis

Cells were washed with PBS and lysed with 250 µL RIPA buffer for 20 min at 4 °C. Cell lysates were cleared by centrifugation for 15 min at 4 °C at 13,000 rpm before storage at -20 °C.

3.2.4. Virus production

MeV was propagated in Vero-hSLAM cells in DMEM containing 5% FBS, while MuV and HRSV were grown on HEp-2 cells in DMEM supplemented with 5% FBS. When widespread cytopathic effect and EGFP expression was attained, MeV and HRSV infected cells were scraped and virus suspension was aliquoted and stored at -80 °C. MuV infected cells were scraped and supernatant was clarified by centrifugation at 3,000 rpm for 10 min at 4 °C. The clarified virus supernatant was aliquoted and stored at -80 °C.

3.2.5. Virus titration

To determine viral titers, 1×10^6 A549-hSLAM cells and 5×10^5 Vero-hSLAM cells were seeded in a 96-well plate and quadruplicate wells were inoculated with 10-fold serial dilutions of the virus. After 3 days of incubation at 37 °C and 5% CO_2, cytopathic effect and EGFP-expression was assessed with a fluorescence microscope, or titers were read using syncytium formation as evidence of infection. The virus titer was calculated and expressed as the 50% tissue culture infective dose ($TCID_{50}$/mL) according to Spearman und Kärber.

$$logTCID_{50} = x_k + \frac{d}{2} - d\sum p$$

x_k = decadic logarithm of the highest dilution in which all wells show a cytopathic effect/ EGFP expression

d = decadic logarithm of the dilution factor

p = amount of wells showing a cytopathic effect/EGFP expression in higher dilutions than x_k.

3.3. Animal Experiments

3.3.1. Squirrel monkeys

While humans are the only reservoir for MeV, certain non-human primates are also susceptible to MeV infection. Squirrel monkeys (*Saimiri sciureus*) develop a course of disease that is similar to that observed in humans (Delpeut *et al.*, 2017), so they are

well-suited to assess the *in vivo* efficacy of drugs against MeV. Animals were obtained from CNRS 0846 Primatologie (D56,13790 Rousset, France). Female and male squirrel monkeys both weighed around 600-800 g, ensuring that sufficient blood could be collected. A total of 20 animals were used for drug efficacy study and were divided into 4 groups of five animals each. Each treatment group was housed separately and within the groups, animals of same sex were grouped-housed together.

3.3.2. Study design for assessment of ERDRP-0519 antiviral efficacy

The study was approved by RP Darmstadt, F107-1032. Squirrel monkeys were divided into four groups (Figure 6). One group was treated prophylactically, 12 h prior to infection, and two groups were treated therapeutically, one starting at day 3 and the other at day 7 post-infection. Days 3 and 7 post-infection represent time points, where first virus is usually detectable and when first clinical signs are observed, respectively. Groups were treated orally twice daily for two weeks. The control group received only 2.5 mL of Nutribound liquid supplemental animal feed.

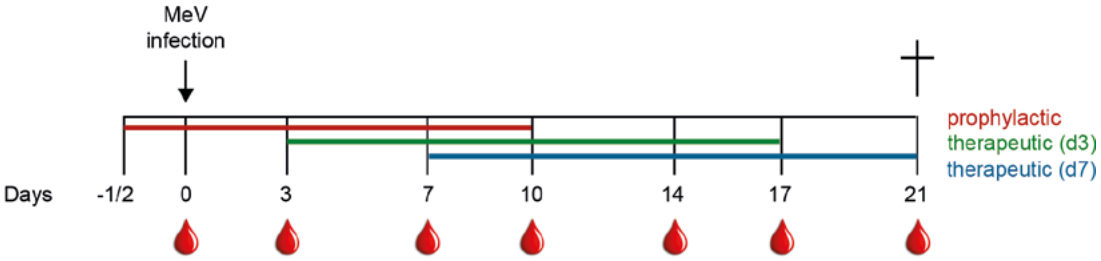

Fig. 6 | Overview of the study design for antiviral efficacy assessment of ERDRP-0519 in squirrel monkeys. Animals were divided into 4 groups including one untreated group (not shown) and three different treatment groups which are indicated in red, green, and blue. All groups were infected with MeV isolate MV/FrankfurtMain.DEU/17.11 on day 0. Blood and throat swabs were collected on days 0, 3, 7, 10, 14, 17 and 21 post-infection. Animals were euthanized by exsanguination on day 21.

Animals were infected intranasally with $1x10^6$ $TCID_{50}$/mL of MV/FrankfurtMain.DEU/17.11 in a volume of 200 µL DMEM/per animal after anesthesia with 0.125 mg/kg medetomidine (1 mg/mL) and 0.8 mg/kg ketamine (100 mg/mL) by intramuscular injection. Anasthesia was reversed by injection of 1 mg/kg atipamezole. The animals were monitored daily in the morning for clinical signs, and body weight and rectal temperature were measured immediately after administration of inhalation anesthesia using either sevoflurane or isoflurane. Cages were checked daily for evidence of diarrhea as an indication of drug toxicity or gastrointestinal signs of clinical disease. The drug was administered intragastrically through a 3.0 × 4.1 mm feeding tube at a dose of 50 mg ERDRP-0519/kg bodyweight in a volume of 3 mL. ERDRP-0519 working solution was prepared by dissolving 100 mg of the compound in 1 mL of poly(ethylene glycol)-200 (100 mg/mL), which was then stored in the dark to prevent light-induced degradation. Immediately before treatment, the working stock was diluted 1:10 by the addition of

0.5% methylcellulose, followed by vortexing to prevent precipitation. The feeding tube was flushed with 2.5 mL of Nutribound after treatment to account for the dead volume. On days 3, 7, 10, 14, 17, and 21, blood was collected from the vena saphena magna (2 mL tubes coated with K_3-EDTA) for leukocyte count, peripheral blood mononuclear cell (PBMC) titration, and neutralizing antibody titer assessment. Throat swabs were collected until day 17 with polyester-tipped swabs to assess viral load in the upper respiratory tract. At 21 days post-infection, animals were euthanized via anesthesia with 0.125 mg/kg medetomidine (1 mg/mL) and 0.8 mg/kg ketamine (100 mg/mL), followed by exsanguination from the cranial vena cava. Necropsies were performed to assess inflammation and gross pathologies and to collect the following organs and tissues for histological exanimation: lung, trachea, liver, spleen, kidney, intestine, bladder, cervical and mandibular lymph nodes, tonsils, testicles/ovaries, cerebrum, cerebellum, brain stem, bone marrow, and dura mater. Brain tissues were fixed in 10% formaldehyde solution, all other tissues were fixed in 4% formaldehyde solution.

3.3.3. Titration of throat swabs

Throat swabs were collected and placed into tubes containing 150 µL DMEM and 3% penicillin/streptomycin. The throat swab supernatants were titrated as described in 3.2.5.

3.3.4. Isolation of squirrel monkey PBMCs

For PBMC isolation, cells and plasma were separated by centrifugation at 3,000 rpm for 15 min. Plasma samples were frozen at -20 °C for further usage. Cells were resuspended in RBC lysis buffer and incubated at RT for 10 min, until lysis of erythrocytes led to a dark red color change. Cells were centrifuged at 2,000 rpm for 5 min, washed with PBS, and resuspended in 1 mL DMEM supplemented with 2% FBS and 1% L-glutamine. PBMCs were counted in a Neubauer chamber using trypan blue.

3.3.5. White blood cell count

For the leukocyte count, 10 µL of whole blood was mixed with 990 µL of 3% acetic acid. White blood cells were counted in a Neubauer chamber, using 10 µL of the suspension, and number of white blood cells per 1 mL blood was calculated.

3.4. Immunological Methods

3.4.1. Immunofluorescence staining

A549-hSLAM cells were seeded on coverslips in 24-well plates and infected with MeV at a MOI of 1. After 1 h of infection, the culture medium was removed and replaced

with medium including 20 µM Z-fFG (fusion inhibitory peptide (FIP)). At 24 h post-infection, cells were fixed with 4% paraformaldehyde in PBS for 15 min and subsequently permeabilized with 0.1% Triton X-100 in PBS for 15 min at room temperature. Cells were stained with the respective primary and secondary antibodies and coverslips were mounted onto glass slides using ProLong Gold Antifade Mountant containing DAPI. Images were obtained using a Zeiss LSM 510 confocal laser scanning microscope with a αPlanApochromat 100× oil objective. Images were collected at 1,008 × 1,008-pixel resolution and processed using ImageJ and Photoshop.

3.4.2. Sodium Dodecyl Sulfate-Polyacrylamide Gel Electrophoresis (SDS-PAGE)

For verification of protein expression, proteins were separated by molecular weight via SDS-PAGE, followed by transfer onto polyvinylidine fluoride (PVDF) membrane, which was then incubated with labeled antibodies specific to the protein of interest. Cell lysates were mixed with 2× Lämmli-buffer containing 10% β-mercaptoethanol and heated at 75 °C for 5 min to fully denature the proteins. Proteins were then separated by a 10% SDS-PAGE for 1 h at 160 V. The PageRuler Plus Prestained Protein Ladder was used as standard.

3.4.3. Western blot analysis

For antibody-mediated detection of the specific proteins, separated proteins were transferred onto PVDF membranes for 30 min at 12 V using a semi-dry transfer system. PVDF membranes were briefly activated in methanol, and the membranes and gels were then equilibrated for 10 min in transfer buffer. Whatman filter papers were soaked in transfer buffer and then arranged in layers on the transfer electrode. After protein transfer, membranes were incubated overnight at 4 °C in TBS-T containing 5% skim milk powder to block nonspecific binding sites. For the detection of viral proteins, mouse monoclonal antibodies against the MuV N protein or the HRSV N protein, or rabbit anti-peptide antisera against the MeV N, M, and F proteins, respectively were used. Mouse monoclonal antibodies against β-actin, PDH E1α, and GAPDH were used to visualize cellular proteins. The rabbit anti-peptide serum against ABCE1 was produced by immunizing rabbits with the peptide N-NSIKDVEQKKSGNYFFLDD-C, corresponding to 19 amino acids at the C terminal of human ABCE1, coupled to keyhole limpet hemocyanin. Goat anti-rabbit and goat anti-mouse antibodies conjugated to HRP were used as secondary antibodies. The FLAG tag was detected with the mouse monoclonal anti-FLAG M2 antibody and a donkey anti-mouse secondary antibody conjugated to HRP. The membrane was incubated with the primary antibodies diluted in TBS-T at RT for 1-2 h and was washed three times with TBS-T for 5 min each. After

incubation with the secondary antibodies diluted in TBS-T for 1 h at RT, three washing steps with TBS-T for 5 min each were performed. Membranes were incubated for 5 min with the ECL Prime Western Blotting Detection Reagent before visualizing the signals with a MicroChemi 4.2 gel documentation system. The bands from these images were quantified from underexposed TIF images using ImageJ Analysis Software package.

3.4.4. Metabolic labeling assay

For the analysis of *de novo* viral and cellular protein synthesis, metabolic labeling assays using ^{35}S were performed. A549-hSLAM cells were seeded in 6-well plates and treated with the respective siRNAs for 48 h and were then infected with MeV at an MOI of 0.1. After 24 h, the medium was removed and replaced with 1 mL per well of cysteine/methionine-free DMEM containing 5% dialyzed FBS and 1% L-glutamine for 1 h at 37 °C, after which the starvation medium was removed and the cells were washed with PBS. Infected cells were labeled with 0.1 mCi (3.7 MBq) per well of ^{35}S-Cys/Met mix in a total volume of 0.5 mL per well. After the respective labeling time, the medium was removed and the cells were washed with PBS, and lysed in 600 µL per well of Lysis Buffer at 4 °C. The whole cell lysates were clarified by centrifugation at 13,000 rpm for 10 min. Lysates were divided in two samples and mixed with 20 µL protein A-agarose beads and either 1 µL mouse monoclonal anti-actin antibody or 1 µL of a polyclonal rabbit antiserum against either the MeV M or F proteins. After overnight incubation at 4 °C, the beads were washed three times with 500 µL per tube of Wash, and the proteins were eluted by incubation in 50 µL SDS gel-loading buffer at 95 °C for 5 min. Samples were separated on Mini-Protean 10% TGX gels for 45 min at 200 V, and the gels were then dried onto Whatman 3 mm CHR filter paper for 3 h at 83 °C using a Bio-Rad Model 583 Gel Dryer. Dried gels were exposed to Kodak cassette-K BaFBr:Eu phosphor screens overnight and imaged using the Bio-Rad Personal Molecular Imager System. Bands were quantified using the Bio-Rad Quantity One 1-D Analysis software package.

3.5. RNAi Screens

3.5.1. Primary genome-wide siRNA screens

The screens were performed at the Duke University Functional Genomics Facility using the Qiagen genome siRNA library v 1.0 consisting of four distinct siRNAs (A, B, C, and D) targeting 21,705 known and putative human genes. The four siRNAs were grouped into two pools, each containing two siRNAs (set AB and set CD), which allowed each gene to be tested by two independent siRNA sets. Each screen consisted of 148 384-well plates. Black, clear bottom 384-well tissue culture plates (Corning) were pre-arrayed

with 1 pmol of siRNA per well by using the Velocity Bravo liquid, and Lipofectamine RNAiMAX (0.05 µL per well) was mixed with 10 µL of OptiMEM. After 15 min of complex formation, cells were dispensed at a density of 1,500 cells per well using a Matrix WellMate dispenser and reverse transfection was performed by adding 15.4 nM final concentration of siRNAs to 65 µL of total media volume per well. Plates were incubated at 37 °C with 5% CO_2 for 48 h and were then infected with 20 µL of virus diluted in DMEM supplemented with 10% FBS. Virus infections were performed using different MOIs, and varying lengths of time after infection to identify suitable conditions for the high-throughput screens (30-50% of total cells infected per well). Cells infected with MeV were incubated for 33 h and those infected with MuV and HRSV for 72 h at 37 °C in a 5% CO_2. To identify factors involved in all stages of the paramyxovirus life cycle, the screen was optimized to allow for multiple rounds of infection.

3.5.2. Validation screens

To validate the top hits identified by comparative analysis of the three primary screens, multiple siRNAs targeting the respective genes were used. Whenever available, siRNAs that differ from those used in the primary screens, were chosen. Each individual siRNA was represented in replicates of 4 in each plate. Validation screens, image collection, and analysis were performed as described for the primary screen.

3.5.3. Automated image analysis

At 33 h post MeV and 72 h post MuV and HRSV infection, cells were fixed with 4% PFA in PBS, permeabilized with 0.1% Triton X-100 in PBS and stained with Hoechst 33342 in PBS for 30 min. Cells were imaged and analyzed using the Cellomics ArrayScan VTI automated microscope, whereas uninfected cells served as a reference population for background fluorescence. Four fields per well of 384-well plates were imaged at 10× magnification and analysis was performed using the Compartmental Analysis Bioapplication. After autofocusing on nuclear staining in channel 1, cells were first identified and indicated as valid object count (VOC) in channel 1 and then the percentage of infected cells was assessed by presence of EGFP signal in channel 2.

3.5.4. General statistical methods used for RNAi screen analysis

Since distribution of percent infection for genomic population for the AB and CD pools did not follow a normal distribution, raw percent infection measurements were normalized by converting to robust Z. Primary data from the Cellomics Oracle database was retrieved and raw percent infection measurements were converted to robust Z scores within each plate using custom Python scripts. To identify host factor genes, the distribution of normalized well values for each gene relative to the overall

distribution of all wells, were evaluated using the Kolmogorov-Smirnov (KS) test. The false discovery rate (FDR) method was used to correct for multiple hypothesis testing. A similar approach to the gene level analysis was employed to identify pathways enriched for either negative or positive selection. All pathways were collected from the 'Curated Pathways' subset of the Molecular Signatures Database (MsigDB), and the KS test was used to evaluate the distribution of normalized values belonging to all genes of each pathway against the entire distribution of normalized values.

4. PERSONAL CONTRIBUTIONS

Except where stated otherwise by reference or acknowledgment, the work presented was generated by myself under the supervision of my advisors during my doctoral studies. All contributions from colleagues are explicitly referenced in the thesis and described in that chapter. Whenever a figure, table, or text is identical to a previous publication, it is stated explicitly in the thesis that copyright permission and /or co-author agreement has been obtained.

4.1. Characterization of the role of host factors in the paramyxovirus life cycle

I was introduced to the genome-wide siRNA screens and the investigation of the role of ABCE1 in the paramyxovirus life cycle during my Masters internship under the supervision of Dr. Danielle Anderson at Duke-NUS Medical School in Singapore. During my Master's thesis at the Paul-Ehrlich-Institut, I continued working on that project and focused on the influence of paramyxovirus infections on the subcellular localization of ABCE1 using immunofluorescence staining and co-localization analysis. After finishing my Master's thesis together with Prof. Dr. Veronika von Messling and the collaborating groups at Duke-NUS Medical School in Singapore and at UTMB in Galveston, TX, USA, we decided that the characterization of host factors in the paramyxovirus life cycle warranted further investigation as a way to gain insight into the biology of these viruses and for the potential development of broad-spectrum therapeutics.

The primary genome-wide siRNA screens and the corresponding bioinformatics analyses were performed by Dr. Danielle Anderson and Dr. So Young Kim, respectively. To further confirm the 24 top common hits, I planned a MuV validation screen, which was performed by Yvonne Krebs at the Paul-Ehrlich-Institut and Dr. Danielle Anderson performed the MeV validation screen of top proviral hits also identified in the HeV screen (Deffrasnes *et al.*, 2016). I designed and performed the experiments to characterize the role of ABCE1 in different steps of the viral life cycles including the validation of the specificity of antibodies, siRNAs, and knockdown. I also performed viral growth kinetics, Western blot analysis, and RT-qPCRs to analyse the influence of ABCE1 on viral replication, viral translation, viral transcription, and innate immune response activation. The Bachelor's student Oliver Siering, who worked under my supervision, and Yvonne Krebs helped to prepare and run the RT-qPCRs. Dr. Bevan Sawatsky performed the dual-luciferase reporter gene assay and the fluorescent labelling of newly synthesized cellular proteins and showed me how to perform the ^{35}S radiolabelling experiments to compare the amount of newly synthesized viral and cellular proteins. As shared first author of the manuscript "Comparative loss-of-function screens reveal

ABCE1 as an essential cellular host factor for efficient translation of *Paramyxoviridae* and *Pneumoviridae*" published in mBio, I produced and analyzed most of the data that are shown in the manuscript and designed the figures. Dr. Danielle Anderson, Prof. Dr. Veronika von Messling and Prof. Dr. Mariano Garcia-Blanco wrote the first draft and Dr. Bevan Sawatsky and I wrote the materials and methods section, figure legends, and finalized the manuscript. The progress of the project was discussed monthly via Skype meetings with Dr. Danielle Anderson and Prof. Dr. Mariano Garcia-Blanco from our collaborating groups.

4.2. Assessment of the antiviral efficacy of the compound ERDRP-0519 against MeV *in vivo*

During my PhD thesis, I participated in the supervision of a Master's student, Kevin Wittwer, and contributed to his project, the assessment of antiviral efficacy of a small-molecule viral polymerase inhibitor against MeV in squirrel monkeys. I was responsible for setting up the *in vivo* study including training of the squirrel monkeys, preparation of cages, surgery, and equipment. Prof. Dr. Veronika von Messling and I tested the experimental set-up before the study began to obtain measurements and samples of the animals prior to infection and treatment. During the study, I was involved in MeV infection of the animals, drug administration, regular blood sampling, throat swab collection, temperature and weight measurements and clinical assessments. I also supported Kevin Wittwer in sample processing, including PBMC and throat swab titration and leukocyte count. Dr. Roland Plesker and Kevin Wittwer euthanized the animals on day 21, and I participated in the necropsies to examine organs for evidence of virus or drug-related inflammation or gross pathologies and in collecting and fixing organs for histological examinations.

5. RESULTS

5.1. Characterization of the role of host factors in the paramyxovirus life cycle

5.1.1. Project background and preliminary data

Paramyxo- and pneumoviruses include a broad range of respiratory viruses with great relevance for human and animal health. Genome-wide RNA interference screens have been shown to be a powerful technique for the identification of host factors required by several RNA viruses (Brass *et al.*, 2008; König *et al.*, 2008; Krishnan *et al.*, 2008; Zhou *et al.*, 2008; Li *et al.*, 2009; Sessions *et al.*, 2009; Tai *et al.*, 2009). To identify common host factors involved in the *Paramyxo*- and *Pneumoviridae* life cycle as a basis for new insights in the biology of these viruses and the development of rationally-designed therapeutics, primary genome-wide siRNA screens with wild type measles, mumps and respiratory syncytial viruses in A549 cells were performed at the Duke University Functional Genomics Facility using the Qiagen genome siRNA library v 1.0 targeting 21,705 known and putative human genes (Figure 7).

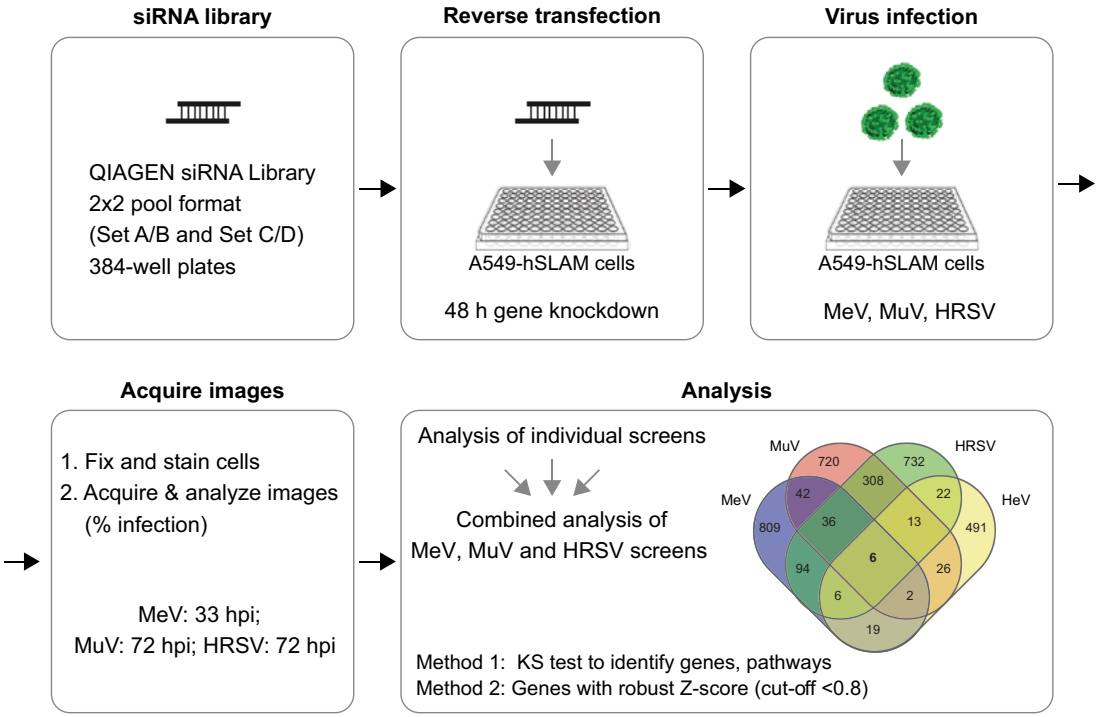

Fig. 7 | Schematic overview of the genome-wide siRNA screens. Individual RNAi screens for MeV, MuV, and HRSV were performed as depicted. A combined analysis of all screens was performed after analyzing individual screens.

5.1.1.1. Genome-scale siRNA screens

Four siRNAs were used to interrogate each gene, grouping two siRNAs each into one pool (set AB and set CD). This 2×2 pool design allows each gene to be tested by two independent siRNAs sets. All screens were performed in the lung adenocarcinoma cell line A549 that stably expresses the MeV receptor SLAM (A549-hSLAM) and shares key features with the respiratory epithelial cells targeted during a natural infection. Recombinant viruses based on wildtype sequences, expressing EGFP from an additional transcription unit inserted between the P and M genes, were used to facilitate quantification of infected cells by detection of green fluorescence (Figure 8) (Anderson *et al.*, 2019).

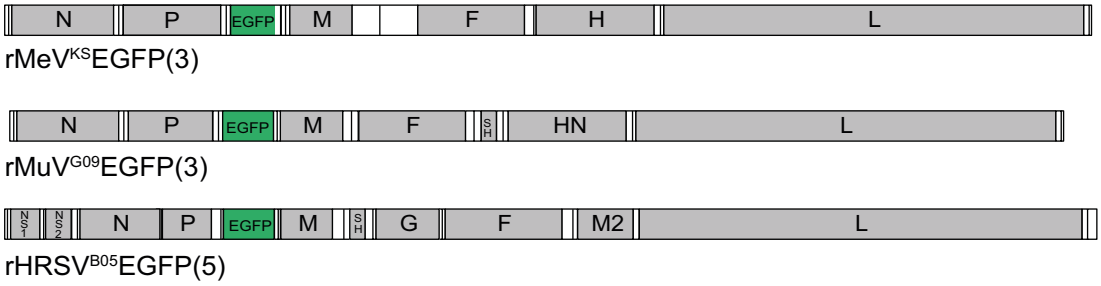

Fig. 8 | Schematic illustration of recombinant EGFP-expressing viruses. Grey and white boxes show open reading frames and UTRs, respectively. Genes are indicated by their respective abbreviation. The inserted EGFP genes between the viral P and M genes are shown in green (Anderson *et al.*, 2019).

Prior to infection with the respective virus at a MOI determined to lead to an infection rate of approximately 50%, A549-hSLAM cells were transfected with the siRNAs for 48 h. At 33 h after MeV infection and 72 h post MuV and HRSV infection, the infection rate was analyzed using a Cellomics ArrayScan VTI automated microscope (Figure 9A) Positive control siRNAs against EGFP resulted in a dramatic reduction in EGFP-expression for all viruses, which was close to the level of uninfected cells and negative controls showed infection levels ranging from 45-65%. The distribution of the siRNA-treated wells in the MeV and HRSV histograms showed a shift towards lower infection levels, whereas the MuV screen distribution was normal (Figure 9B) (Anderson *et al.*, 2019).

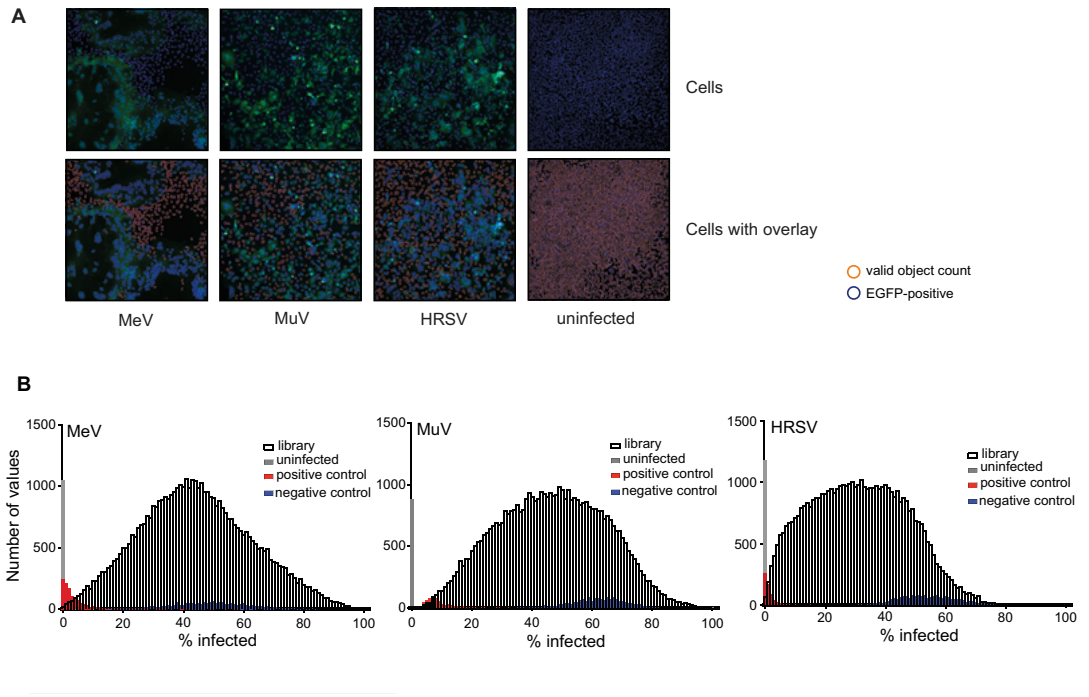

Fig. 9 | Analysis of infection levels and distributions in individual siRNA screens. A) Representative images of NSC-siRNA-treated and infected cells acquired and analyzed with a Cellomics ArrayScan VTI automated microscope. After infection, cells were fixed and stained with Hoechst 33342. Uninfected cells were used as reference population for background fluorescence. The top images depict raw images of infected cells from channel 1 (Nuclei, Hoechst), indicated as valid object count, and channel 2 (EGFP), indicating percentage of infected cells with the EGFP-expressing virus, and the bottom images show overlays from the analyzed channel 1 and channel 2. The overlays indicate valid object counts highlighted in orange and EGFP-positive cells highlighted in blue. **B)** Histograms showing infection distributions for MeV, MuV, and HRSV. Distributions of percent infection values for siRNA treated-wells of the individual virus screens are shown. Distribution of positive (red), negative (blue) and uninfected controls (grey) are included for each screen (Anderson *et al.*, 2019)..

5.1.1.2. Comparative meta-analysis identifies common candidate proviral factors

To identify common paramyxoviral host factors, a comparative meta-analysis of the three screens using two different approaches was performed (Figure 10A). First, each screen was individually analyzed using a custom bioinformatics package that calculates statistical significance for genes and pathways by considering the distribution of all wells that belong to a specific gene or pathway by Kolmogorov-Smirnov (KS) testing. The next step was a meta-analysis combining the three screens that yielded 179 genes required for all three viruses (false discovery rate < 0.05). Analysis of the list of candidate host proviral factors for *Paramyxo-* and *Pneumoviridae* revealed enrichment in genes involved in RNA processing, mRNA translation, and proteasome-mediated degradation pathways. A complementary meta-analysis of the three data sets, using a robust Z-score imposing a stringent cutoff value of -0.8 for at least two independent siRNA pools per gene, was performed to narrow down the list of the most promising pan-paramyxovirus

host factor genes, which revealed 42 proviral genes required by all three viruses (Figure 10B). The overlap of both meta-analysis approaches yielded 24 candidates and represented the highest confidence list of candidate proviral factors broadly required by paramyxoviruses. In order to confirm these 24 hits and evaluate their importance in the *Paramyxoviridae* life cycle, a validation screen was performed with MuV, since the histogram of the initial screen showed a normal distribution of infection (Figure 10C). Since the top 24 common hits only moderately affected infection, they were not identified as top hits in the individual screens. A complementary MeV validation screen using the six top hits of the common analysis (ABCE1, COPB2, FOXP4, HSD11B2, PRR15 and RBM22), which were also identified in a HeV screen in HeLa cells using a different siRNA library (Deffrasnes *et al.*, 2016)(Figure 10D), revealed similar results (Figure 10E) (Anderson *et al.*, 2019. The protein ABCE1 was chosen for further characterization, since it was found to be a common proviral protein for MeV, MuV, HRSV, and HeV, whereas yellow fever virus (YFV) infection was not affected by ABCE1 knockdown in a screen, performed with the same siRNA library used in the paramyxovirus screens (Le Sommer *et al.*, 2012), indicating that ABCE1 may be specifically required by paramyxoviruses.

A

Analysis	Analysis of individual screens		Combined analysis of MeV, MuV, HRSV screens		Overlap: KS testing & Z-score	Overlap: 24 hits & HeV screen
	KS	Z-score	KS	Z-score		
Hits			197	42	24	6

ABCE1

B

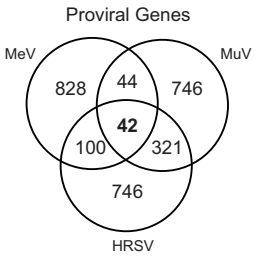

C

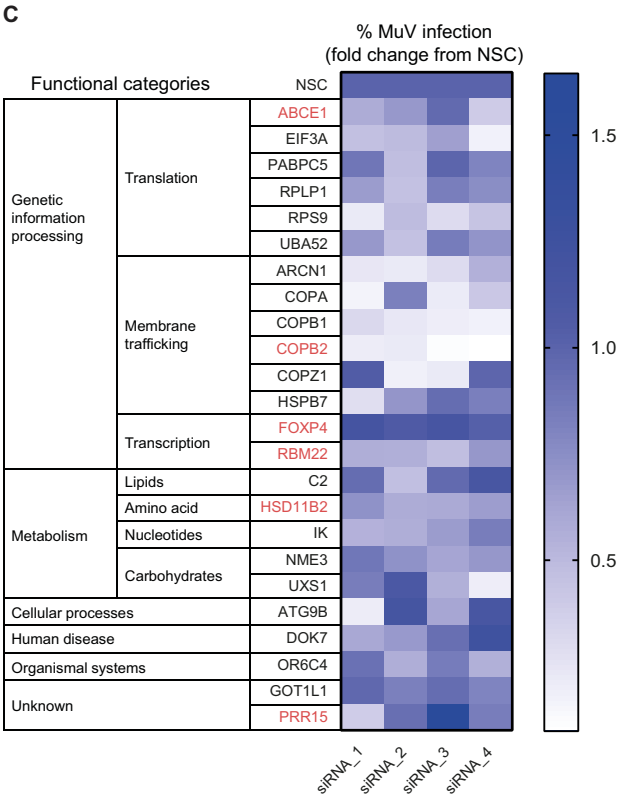

D

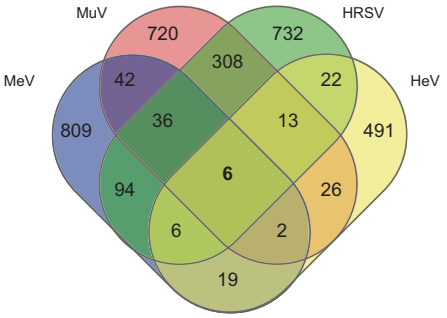

E

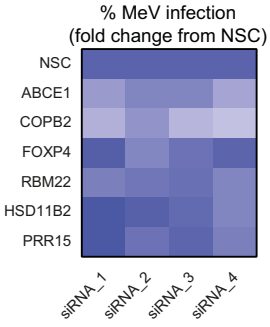

Fig. 10 | Comparative meta-analysis. **A)** Schematic overview of comparative meta-analysis. **B)** Venn diagram of common *Paramyxo-* and *Pneumoviridae* host factors. The extent of overlap among the genes required for the replication of MeV, MuV, and HRSV in both siRNA sets (robust Z score < 0.8) is shown. **C)** MuV validation screen of 24 common hits identified by both Z-score and KS analysis. At 48 h post-siRNA transfection, cells were infected with MuV at a MOI of 1 and incubated for 48 h. Percentage of infected cells was calculated and mean level of infection for NSC was set to 1. The heat map represents the fold change compared to NSC and each square depicts the average of three experiments for each individual siRNA. The genes were correlated to functional categories, as indicated beside the heat map and hits shown in red were selected for MeV validation screening. **D)** Identification of top common proviral hits. The extent of overlap among the genes required for the replication of MeV, MuV, HRSV, and HeV are shown in the Venn diagram. The six top ranking genes identified by comparative analysis of the three primary screens and the previously published HeV screen were targeted by multiple siRNAs. **E)** MeV validation screen of top 6 proviral hits. At 48 h post-siRNA transfection, cells were infected with MeV at a MOI of 0.05 and incubated for 48 h. Percentage of infected cells was calculated and mean level of infection for NSC was set to 1. The heat map represents the fold change compared to NSC and each square depicts the average of five experiments for each individual siRNA (Anderson *et al.*, 2019).

5.1.2. ABCE1 is an essential cellular host factor in the paramyxovirus and pneumovirus life cycle

5.1.2.1. Specificities of siRNAs and knockdown efficiencies were validated

In order to characterize the role of ABCE1 in the *Paramyxoviridae* life cycle, experiments to validate siRNAs and antibodies, as well as knockdown efficiency, were performed. To reliably detect ABCE1, a rabbit anti-peptide hyperimmune serum targeting the 19 C-terminal amino acid residues of human ABCE1 was generated. Specificity was confirmed by transfecting A549-hSLAM cells with an expression plasmid encoding the human ABCE1 protein with an N-terminal FLAG tag (DYKDDDDK) or left untransfected as control for protein expression. While a strong expression of FLAG-tagged ABCE1 was detected via its FLAG tag using an anti-FLAG antibody, the untransfected control does not show any ABCE1 expression (Figure 11, left panel). Using the rabbit anti-peptide hyperimmune serum, endogenous ABCE1 was observed in untransfected control cells, and an increased ABCE1 expression was detected in cells transfected with the FLAG-tagged ABCE1 plasmid (Figure 11, right panel), confirming specificity of the antisera (Anderson *et al.*, 2019).

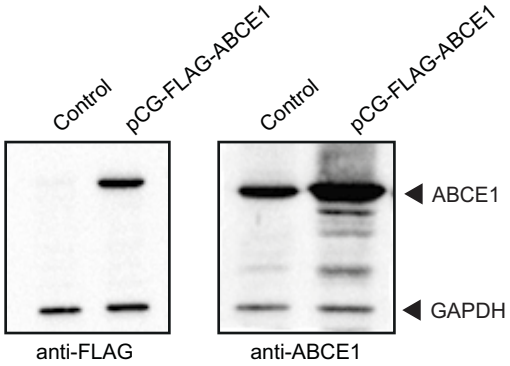

Fig. 11 | Confirmation of rabbit anti-peptide hyperimmune serum specificity. A549-hSLAM cells were transfected with an expression plasmid coding for human ABCE1 containing a FLAG tag (DYKDDDDK) at the N-terminus, or left untransfected. Either a monoclonal mouse anti-FLAG antibody (left panel) or the rabbit anti-peptide hyperimmune serum (right panel) were used in Western blot analysis (Anderson *et al.*, 2019).

To analyze the role of ABCE1 in the viral life cycle, ABCE1 levels were reduced by transient siRNA knockdown, since generation of stable ABCE1 knock out cells failed repeatedly, and prolonged ABCE1 knockdown resulted in reduced cell proliferation. The knockdown of ABCE1 mRNA and protein expression was validated using the two most effective siRNAs, ABCE1_5 and ABCE1_6. ABCE1 mRNA copy numbers were quantified by RT-qPCR 48 h after siRNA transfection and a 1000-fold reduction in mRNA levels was observed (Figure 12A). Protein expression levels 48 h, 96 h, and 120 h after siRNA transfection were reduced by more than 60%, illustrating the specificity and durability of ABCE1 knockdown (Figure 12B) (Anderson *et al.*, 2019).

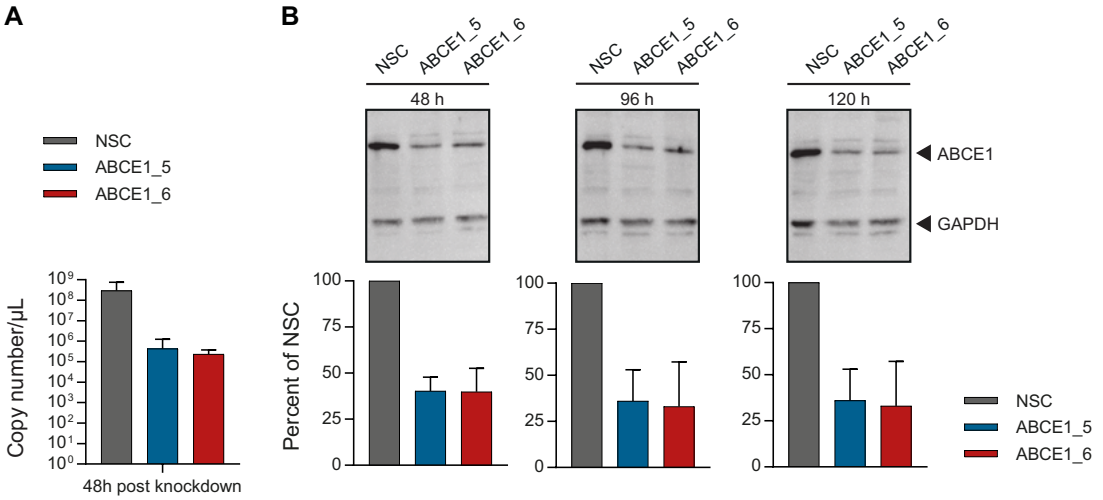

Fig. 12 | ABCE1 knockdown efficiency. A) Reduction of ABCE1 mRNA levels upon transfection with ABCE1_5 and ABCE1_6 siRNAs. At 48 h post-siRNA transfection of A549-hSLAM cells, ABCE1 mRNA copy numbers from three independent replicates were quantified by RT-qPCR. Error bars represent the standard deviation. **B)** Reduction of ABCE1 protein levels following ABCE1_5 and ABCE1_6 siRNA transfection. ABCE1 protein levels at 48 h, 96 h and 120 h post-transfection were analyzed by Western blot. ABCE1 bands from three independent replicates were quantified, normalized relative to an internal GAPDH control and are shown as percent reduction of ABCE1 expression relative to NSC. Error bars represent the standard deviation (Anderson *et al.*, 2019).

To validate the specificities of the ABCE1_5 and ABCE1_6 siRNAs, cells were transfected with a FLAG-tagged ABCE1 expression plasmid, or a derivative carrying 7-10 silent mutations in the ABCE1_5 and ABCE1_6 siRNA target sequences. After 48 h, the cells were transfected with the respective siRNAs, and ABCE1 protein levels were visualized by Western blot using a FLAG-specific antibody 48 h later. Cells transfected with a plasmid encoding a siRNA-resistant ABCE1 protein retained wild type ABCE1 levels (Figure 13A). To further validate specificity of siRNAs, ABCE1 knockdown experiments were performed with ABCE1_5 and ABCE1_6 siRNAs and their corresponding C9ll mismatch controls, where bases 9 through 11 of the siRNA were replaced with the complementary bases of the original siRNA. ABCE1 expression levels were reduced by more than 60% using ABCE1_5 and ABCE1_6, whereas ABCE1 levels for the C9ll siRNA controls remained comparable to the non-silencing control (Figure 13B, left panel). N protein levels were strongly reduced in ABCE1_5 and ABCE1_6 siRNAs transfected cells that were infected with MeV (Figure 13B, right panel). In contrast, the C9ll control siRNAs had no effect on MeV N expression, demonstrating that the ABCE1_5 and ABCE1_6 siRNAs are specific for ABCE1 and that the observed proviral effect is associated with ABCE1 expression (Anderson *et al.*, 2019).

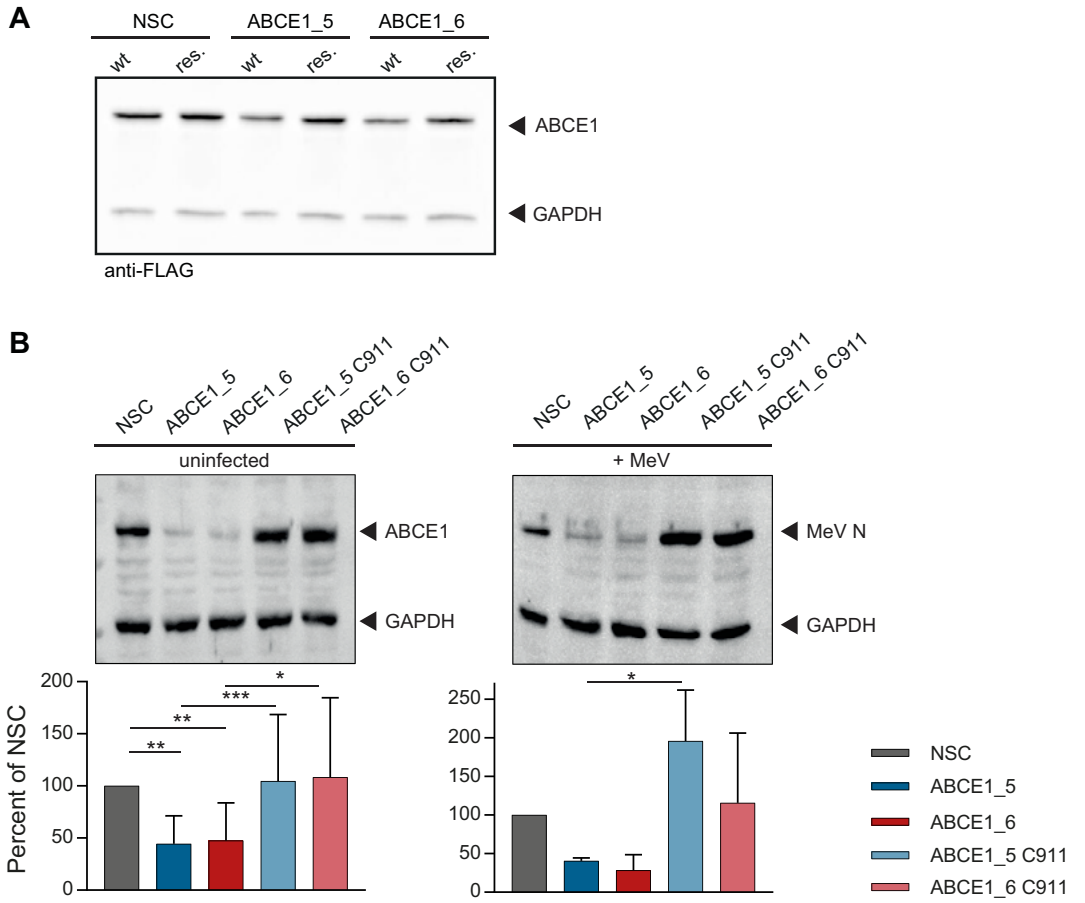

Fig. 13 | Validation of ABCE1_5 and ABCE1_6 specificity. A) Transfection of A549-hSLAM cells with an ABCE1-resistant expression plasmid. Prior to siRNA transfection, cells were transfected with the FLAG-tagged ABCE1 expression plasmid, indicated as wt, or a derivative carrying 7-10 non-coding mutations in each of the binding sites of ABCE1_5 and ABCE1_6 siRNAs, indicated as res. Protein levels were analyzed by Western blot using a monoclonal FLAG-specific antibody. **B)** Transfection of A549-hSLAM cells with siRNA and the corresponding C911 mismatch control. At 48 h post-siRNA transfection with either ABCE1-specific siRNAs or their corresponding C911 control, cells were infected with MeV at a MOI of 0.01 (right panel) or left uninfected (left panel). Protein levels from three independent replicates were quantified, NSC was set to 100%. Error bars represent the standard deviation. Groups were compared using one-way ANOVA with Sidak's multiple comparisons test. Statistical significance is indicated by * p<0.05, ** p<0.01, ***p<0.001 (Anderson *et al.*, 2019).

5.1.2.2. ABCE1 supports replication of MeV, MuV and HRSV

To evaluate the impact of ABCE1 on the viral life cycle, A549-hSLAM cells were transfected with NSC, ABCE1_5, or ABCE1_6 siRNAs. After 48 h, a multi-step growth curve was performed by infecting the cells with MeV at a MOI of 0.01. Cell-associated and released virus was quantified and viral titers were determined every 12 h for 72 h (Figure 14A). In cells transfected with ABCE1_6, production of cell-associated progeny virus was delayed by 12 h compared to NSC control, and siRNA ABCE1_5 reduced virus production more than 10-fold. Starting at 36 h post-infection, titers in cells with reduced ABCE1 levels remained around 100-fold lower than in NSC siRNA treated cells. Irrespective of ABCE1 levels, released virus was first detected after 36 h. ABCE1_6

again showed the strongest effect and resulted in a 100-fold virus reduction, whereas ABCE1_5 displayed an intermediate phenotype (Figure 14B, right panel). To analyze how ABCE1 influences the life cycles of HRSV and MuV, NSC or ABCE1_6 siRNA transfected A549-hSLAM cells were infected at a MOI of 0.01, and cell-free supernatants were harvested every 24 h for 72 h. In the absence of ABCE1, a 10-fold reduction in viral titers was observed for MuV (Figure 14C), while HRSV was almost completely inhibited (Figure 14D) (Anderson *et al.*, 2019). Taken together, these findings demonstrate that the reduction of cellular ABCE1 levels correlates with reduced MeV, MuV, and HRSV replication.

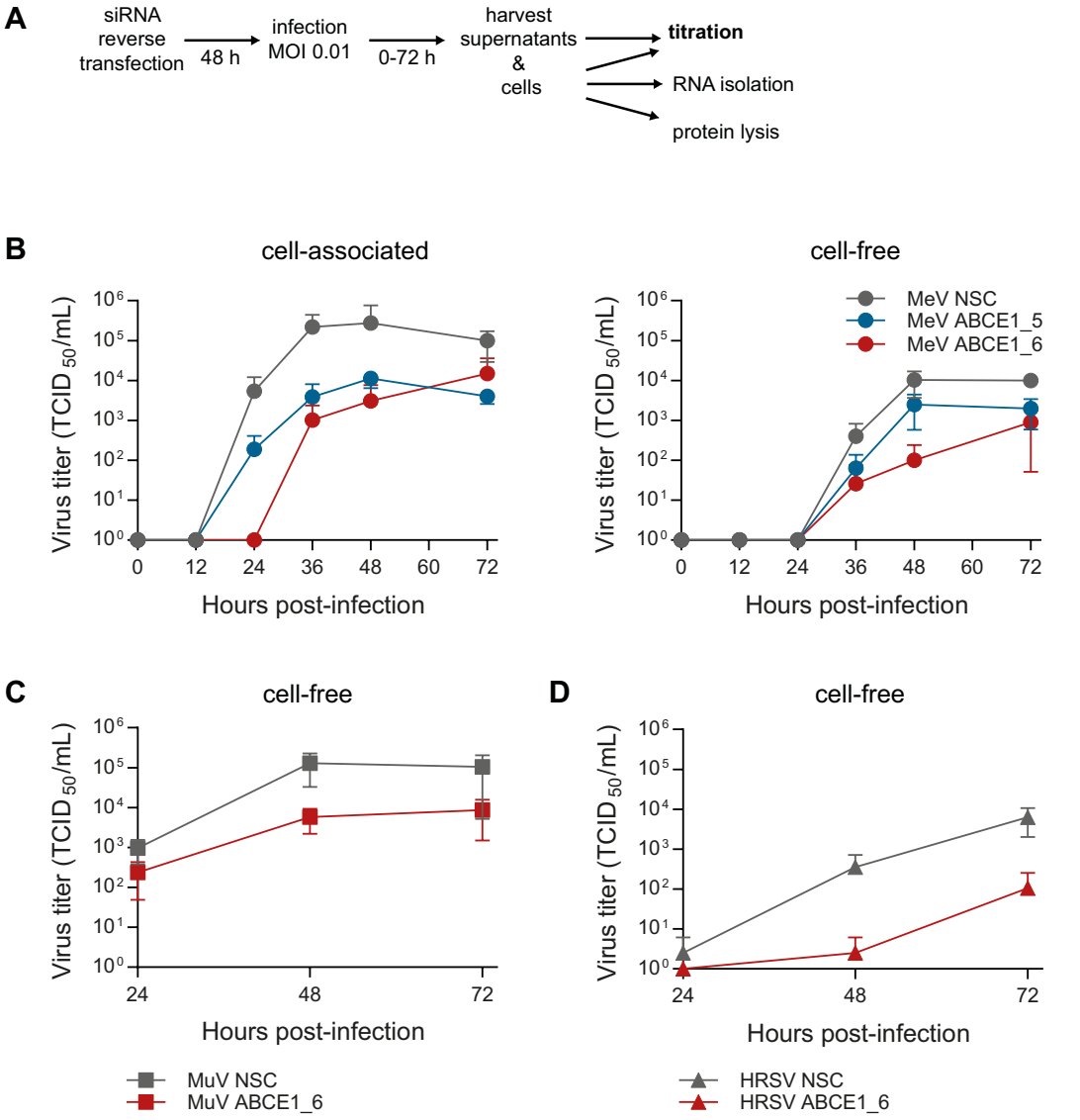

Fig. 14 | Reduction in virus replication following ABCE1 knockdown. A) Schematic overview of the experiment. **B)** Cell-associated and cell-free MeV titer reduction after ABCE1 knockdown. At 48 post-siRNA transfection with NSC, ABCE1_5 or ABCE1_6, cells were infected with MeV at a MOI of 0.01. Cells (left panel) and supernatants (right panel) were harvested at indicated time points, titrated, and viral titers were determined. **C)** and **D)** Cell-free MuV (C) and HRSV (D) titer reduction after ABCE1 knockdown. Cells were transfected with NSC, ABCE1_5 or ABCE1_6, followed by MuV (C) and HRSV (D) infection at a MOI of 0.01 at 48 h post-transfection. Each data point represents at least three replicates, and error bars indicate the standard deviation (Anderson *et al.*, 2019)

5.1.2.3. ABCE1 does not co-localize with viral proteins

The distribution of ABCE1 in uninfected and MeV-infected cells was compared and co-localization analyses of ABCE1 and viral proteins were performed. ABCE1 is known primarily for its role as a negative regulator of the IFN-induced 2-5A antiviral pathway (Bisbal *et al.*, 1995) and is also involved in the regulation of cellular protein translation (Chen *et al.*, 2006; Pisarev *et al.*, 2010. It was also found to be important for HIV capsid assembly, where ABCE1 associates with the Gag matrix protein and forms Gag-ABCE1 complexes throughout capsid formation until the start of virus maturation (Zimmerman *et al.*, 2002; Lingappa *et al.*, 2006; Dooher *et al.*, 2007), which indicates that ABCE1 may have roles in virus particle assembly and modulation of protein synthesis. Confocal microscopy analyses revealed that ABCE1 was distributed throughout the cytoplasm in non-infected cells and showed no redistribution in infected cells (Figure 15A). Furthermore, no co-localization of constituents of the viral ribonucleoprotein (RNP) complex (N) or envelope (M and H) with ABCE1 was observed (Figure 15B), suggesting that ABCE1 does not interact directly with viral proteins during viral mRNA transcription, genome replication, or virion packaging, all of which occur in close association with the viral RNP (Anderson *et al.*, 2019).

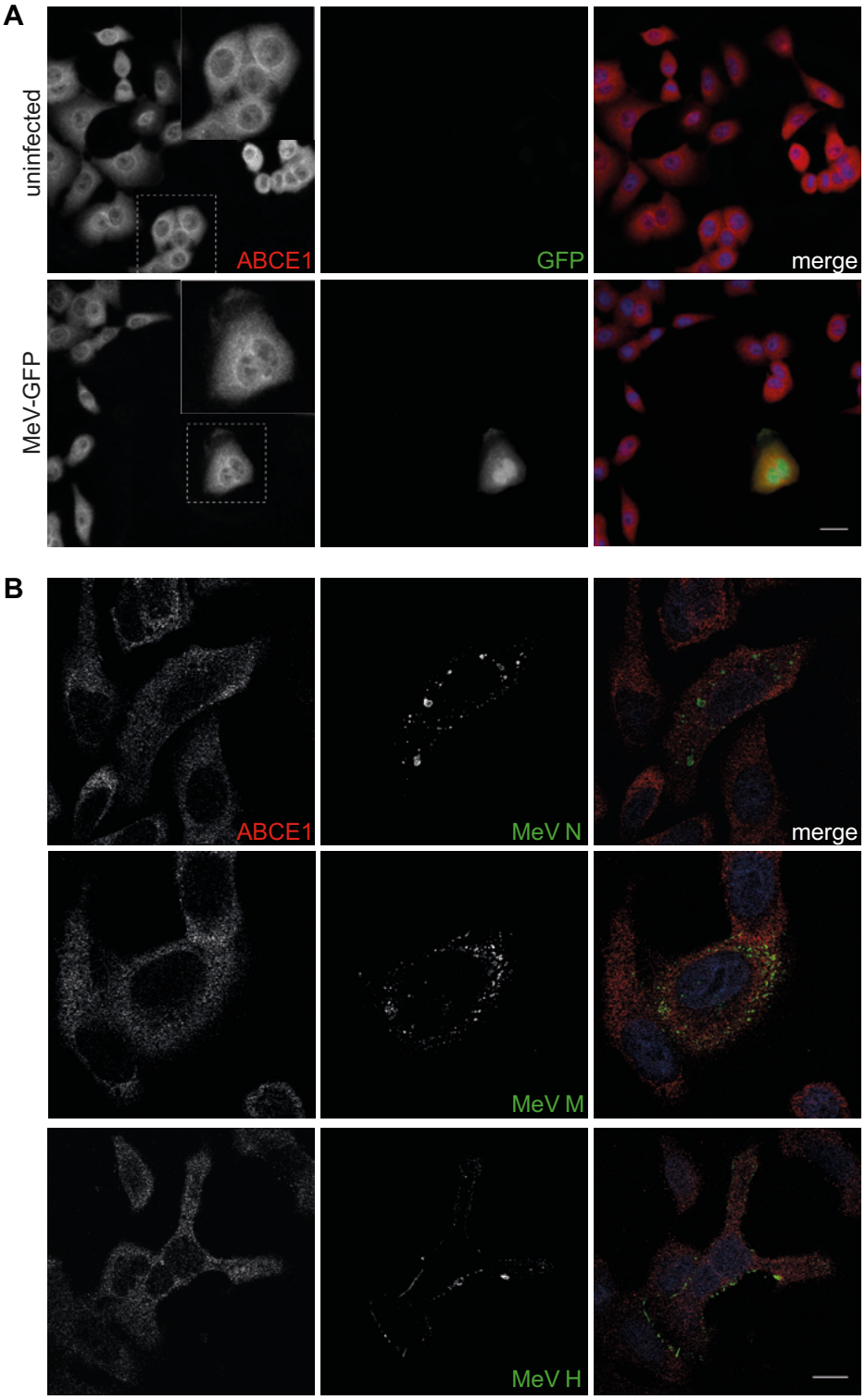

Fig. 15 | Co-staining of ABCE1 and viral proteins in MeV infected A549-hSLAM cells. A) ABCE1 distribution in uninfected and MeV infected cells. A549-hSLAM cells were infected with EGFP-expressing MeV at a MOI of 1. At 17 h post-infection, cells were fixed with 4% PFA, permeabilized, stained with rabbit anti-ABCE1 serum and Alexa Fluor 568-conjugated secondary antibody and visualized using fluorescence microscopy (magnification × 400). Scale bar, 25 µm. **B)** Co-staining of ABCE1 and MeV proteins N, M and H. A549-hSLAM cells were infected with EGFP-expressing MeV at a MOI of 1. At 24 h post-infection, cells were fixed with 4% PFA, permeabilized, stained with rabbit anti-ABCE1 serum and mouse monoclonal antibodies against either MeV N, M, or H, followed by Alexa Fluor 568-conjugated anti-rabbit and Alexa Fluor 488-conjugated anti-mouse secondary antibodies. Representative cells were chosen and analyzed via confocal microscopy (magnification × 1000). Scale bar, 10 µm (Anderson *et al.*, 2019).

5.1.2.4. ABCE1 acts at the level of protein synthesis

To investigate whether ABCE1 knockdown selectively affects viral protein synthesis, we first compared viral nucleocapsid (N) protein levels in NSC or ABCE1_6 siRNA-transfected cells, which were infected with MeV, MuV, or HRSV at a MOI of 0.01. MeV and MuV lysates were harvested after 48 and HRSV lysates were after 72 h. Compared to the levels in NSC-transfected cells, the MeV and HRSV N proteins were hardly detectable in the absence of ABCE1, and MuV N protein expression was reduced by more than 50% (Figure 16), which correlated with the impact of ABCE1 knockdown on the respective virus replication efficiency (see Figure 14) (Anderson *et al.*, 2019).

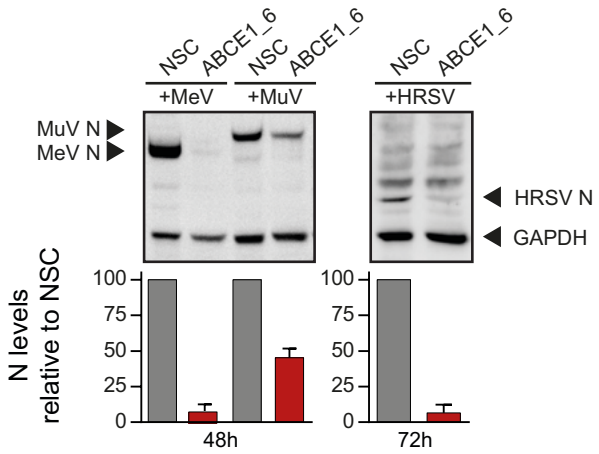

Fig. 16 | Reduction of nucleoprotein expression of MeV, MuV and HRSV infected cells following ABCE1 knockdown. At 48 h, NSC and ABCE1_6 siRNA transfected A549-hSLAM cells were infected with MeV, MuV and HRSV at a MOI of 0.01 and analyzed via Western blot at 48 h and 72 h, respectively. Protein bands from three independent replicates were quantified and normalized relative to an internal GAPDH control, and are shown as the percent reduction of viral N protein expression relative to NSC. Error bars represent the standard deviation (Anderson *et al.*, 2019).

To determine how ABCE1 affects viral protein synthesis, we assessed MeV N protein kinetics in NSC, ABCE1_5, or ABCE1_6 siRNA-transfected cells, which were infected after 48 h at a MOI of 0.01 (Figure 17A). Transfection with siRNAs ABCE1_5 and ABCE1_6 yielded a constant reduction in ABCE1 levels of 70% between 12 h and 72 h post-infection. Consistent with the MeV growth kinetics, N protein was first detected at 24 h after infection, and expression levels consistently increased in control cells. In ABCE1_6 siRNA-treated cells only basal N protein levels were detected throughout the experiment, whereas siRNA ABCE1_5 resulted in an intermediate phenotype (Figure 17B) (Anderson *et al.*, 2019).

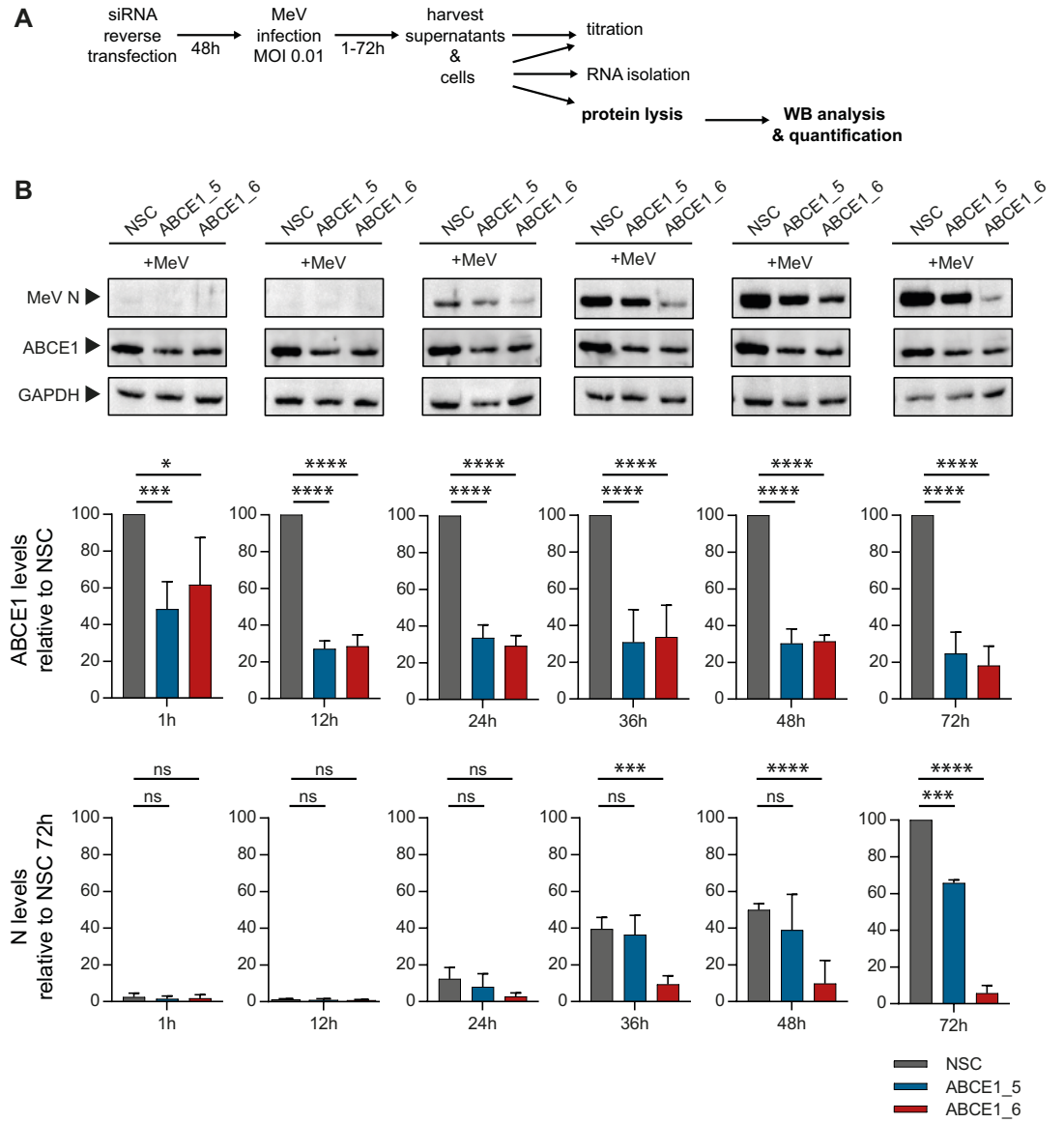

Fig. 17 | Assessment of ABCE1 knockdown on viral protein levels. A) Schematic overview of the protein kinetics experiment. **B)** ABCE1 and nucleoprotein levels in ABCE1 siRNA transfected and MeV infected cells over time. A549-hSLAM cells were transfected with NSC, ABCE1_5 and ABCE1_6, and 48 h later, infected with MeV at a MOI of 0.01. Cells were harvested at the indicated time points and protein bands from three independent replicates were quantified, normalized relative to an internal GAPDH control, and are shown as percent reduction of either ABCE1 or N expression relative to NSC. Error bars represent the standard deviation. Groups were compared using one-way ANOVA with Sidak's multiple comparisons test. Statistical significance is indicated by ns p>0.05, * p<0.01, *** p<0.001, ****p<0.0001 (Anderson *et al.*, 2019).

A complementary N protein kinetic of NSC and ABCE1 siRNA-treated A549-hSLAM cells infected with MeV at a MOI of 1 was performed to assess the influence of ABCE1 on viral protein expression in a single round of infection (Figure 18A). Low levels of N protein were first observed at 12 h post-infection, irrespective of ABCE1 levels. Strong N protein expression was detected at 24 h in NSC-treated cells, whereas cells transfected with ABCE1_5 resulted in a moderate N protein reduction, and the N protein levels in cells transfected with ABCE1_6 siRNA were reduced by approximately 50% (Figure 18B),

indicating that ABCE1 plays an important role in viral translation.

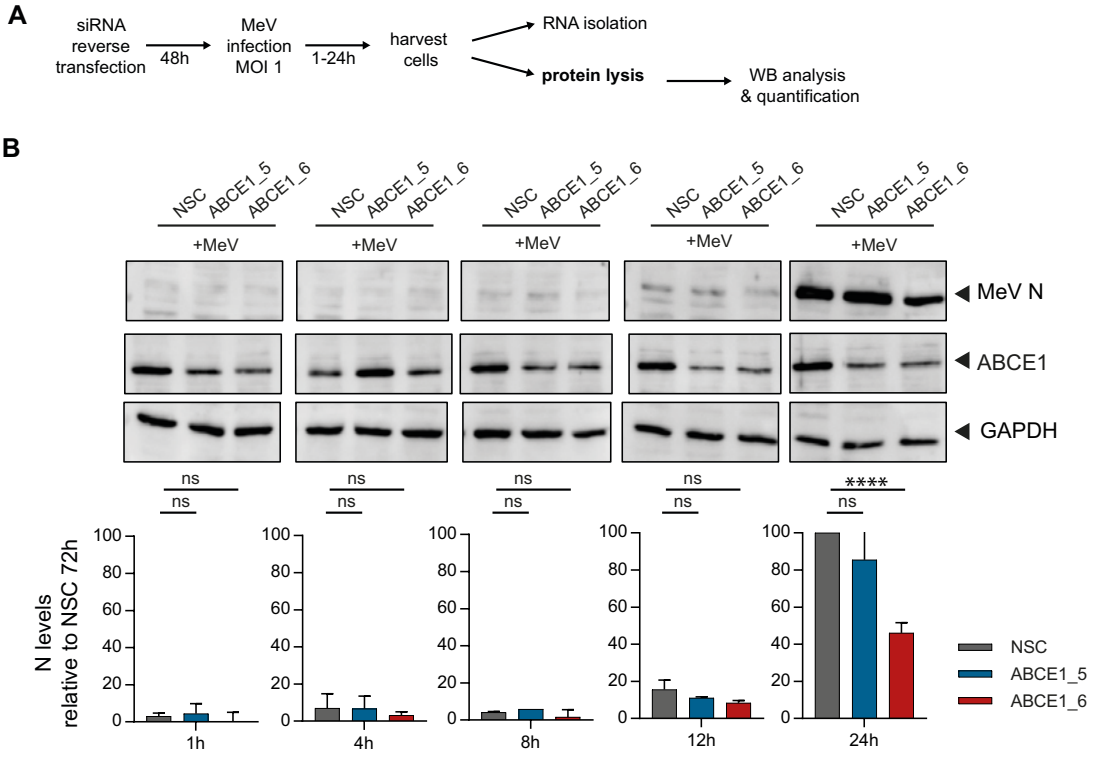

Fig. 18 | Nucleoprotein kinetics in MeV infected cells at a MOI of 1 following ABCE1 knockdown. A Schematic overview of the protein kinetics experiment. **B)** MeV N protein levels in ABCE1 siRNA transfected and MeV infected cells over time. A549-hSLAM cells were transfected with the NSC, ABCE1_5 and ABCE1_6 siRNAs, and 48 h later infected with MeV at a MOI of 1. Cells were harvested at the indicated time points and protein bands from three independent replicates were quantified, normalized relative to an internal GAPDH control and are shown as percent reduction of N protein expression relative to NSC. Error bars represent the standard deviation. Groups were compared using one-way ANOVA with Sidak's multiple comparisons test. Statistical significance is indicated by ns $p>0.05$, ****$p<0.0001$ (Anderson *et al.*, 2019).

5.1.2.5. Viral mRNA transcription is ABCE1-independent

The next step was to evaluate if the reduction in viral protein synthesis is due to a direct role of ABCE1 in translation or rather a consequence of a direct or indirect interference with viral mRNA transcription. Towards this, the kinetics of N mRNA levels was determined over the course of MeV infection at a MOI of 0.01. A549-hSLAM cells were transfected with control NSC, ABCE1_5, or ABCE1_6 siRNAs for 48 h. Cells were then infected, and samples were harvested at the indicated time points. Copy numbers of N gene mRNA were quantified from the same samples by RT-qPCR using a synthetized RNA standard (Figure 19A). N mRNA levels remained stable for the first 12 h after infection, and copy numbers then increased around 100-fold within the next 12 h irrespective of ABCE1 levels, reflecting the first round of viral replication. There was a continuous gradual increase in mRNA levels as the infection spread to new cells, which was less pronounced in ABCE1 siRNA-treated cells, resulting in statistically

significant differences beginning at 48 h after infection. MeV M mRNAs showed similar kinetics, and MeV F mRNA, which is present at lower quantities due to the viral mRNA transcriptional gradient, only increased slightly, but these differences were not statistically different from NSC-transfected cells (Figure 19B). The mRNA copy numbers of the cellular genes β-actin and PDH E1α remained stable during the infection and ABCE1 knockdown had no influence on the mRNA levels of these two cellular genes (Figure 19C) (Anderson *et al.*, 2019).

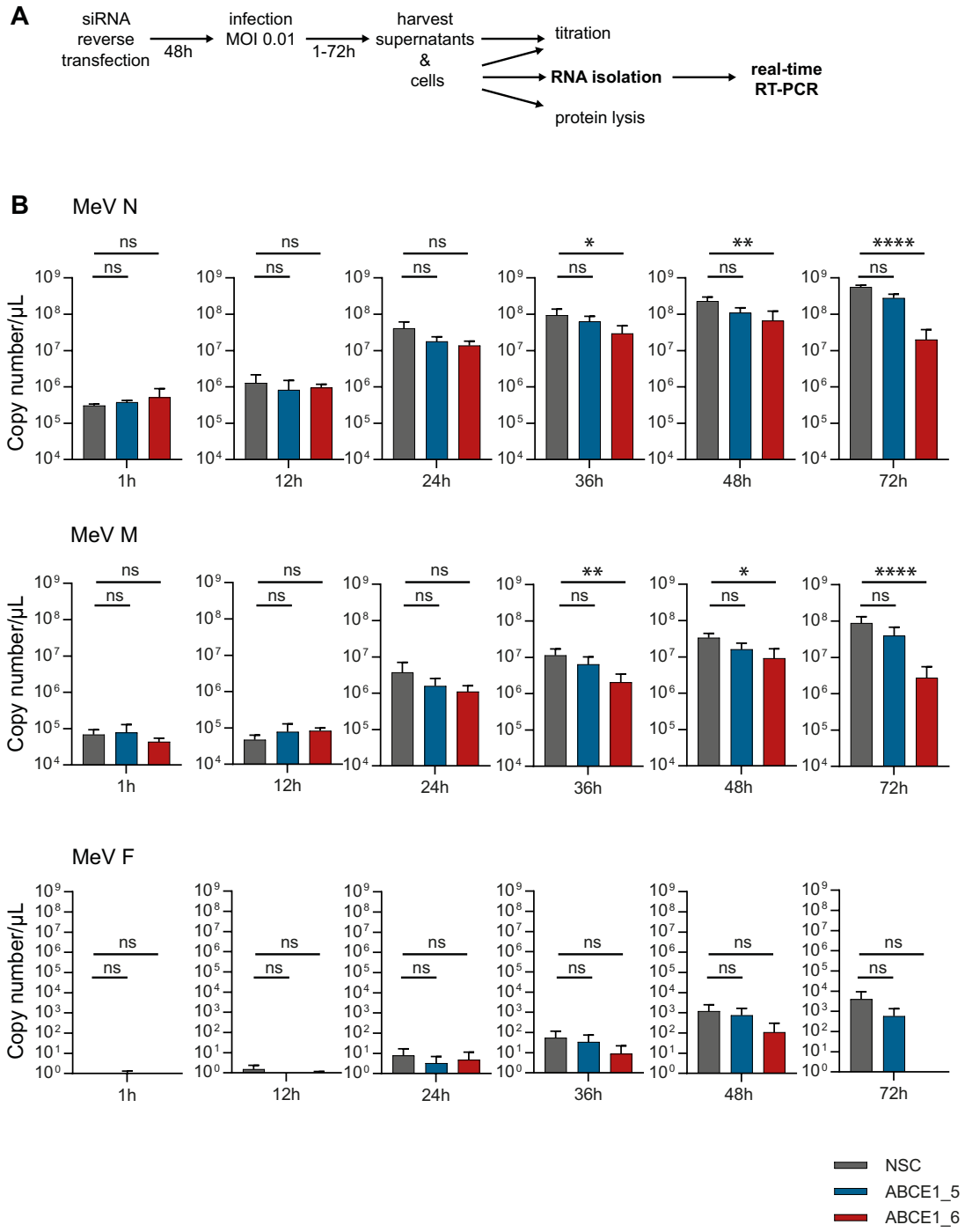

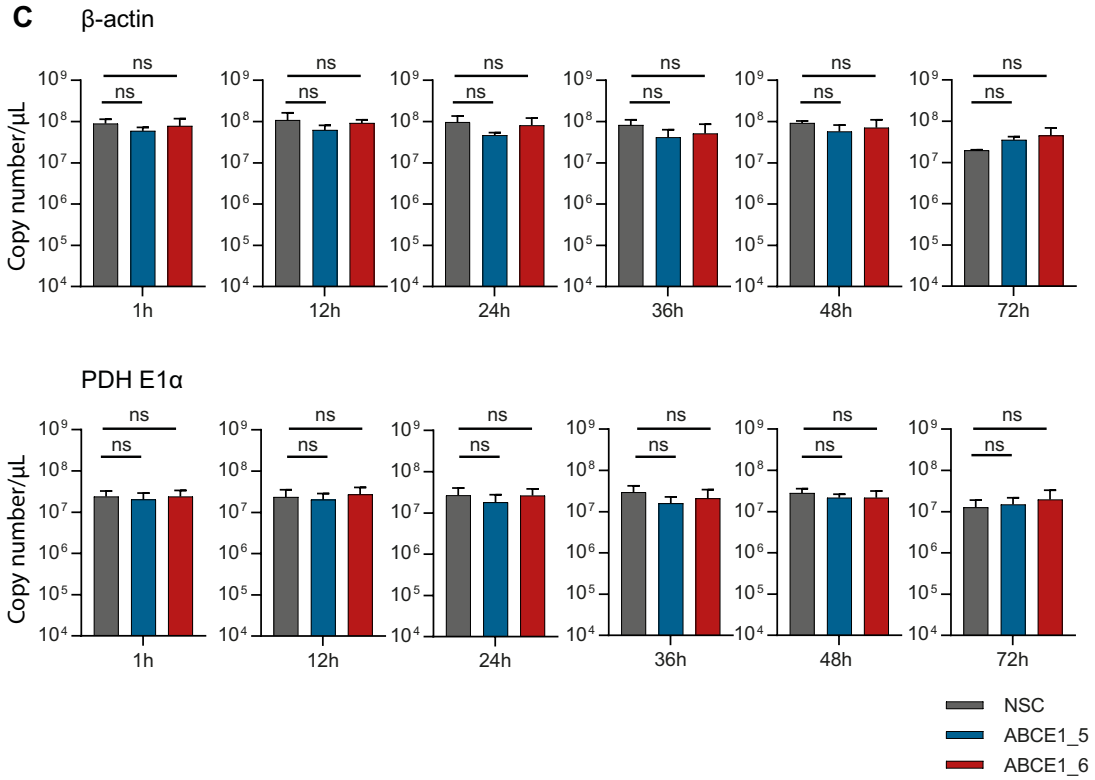

Fig. 19 | Assessment of ABCE1 knockdown on viral mRNA levels. A) Schematic overview of the mRNA kinetic experiment. **B)** Viral and **C)** cellular mRNA levels in ABCE1 siRNA-transfected and MeV-infected cells over time. A549-hSLAM cells were transfected with the NSC, ABCE1_5 and ABCE1_6 siRNAs, and 48 h later infected with MeV at a MOI of 0.01 and RNA was isolated at the indicated time points. mRNA copy numbers of viral MeV N, M, and F, and cellular β-actin and PDH E1α from three independent replicates each were quantified by RT-qPCR. Error bars represent the standard deviation. Log_2-transformed groups were compared using one-way ANOVA with Sidak's multiple comparisons test. Statistical significance is indicated by ns $p>0.05$, * $p<0.05$, ** $p<0.01$, ****$p<0.0001$ (Anderson *et al.*, 2019).

The mRNA kinetics were also determined in NSC and ABCE1 siRNA-transfected A549-hSLAM cells infected with MeV at a MOI of 1 (Figure 20A). N mRNA levels remained stable for the first 8 h after infection. At 12 h post-infection, a minimal increase in copy numbers was observed, and at 24 h post-infection a 10-100-fold increase in N mRNA levels was detected independent of ABCE1 levels (Figure 20B). The viral M and F mRNAs followed similar kinetics, but the overall copy numbers were lower due to the transcriptional gradient. As with the cellular mRNA kinetics at a lower MOI, cellular copy numbers in cells infected with MeV at a MOI of 1 remained stable and ABCE1 did not affect the mRNA levels (Figure 20C), demonstrating that ABCE1 does not directly influence viral mRNA synthesis.

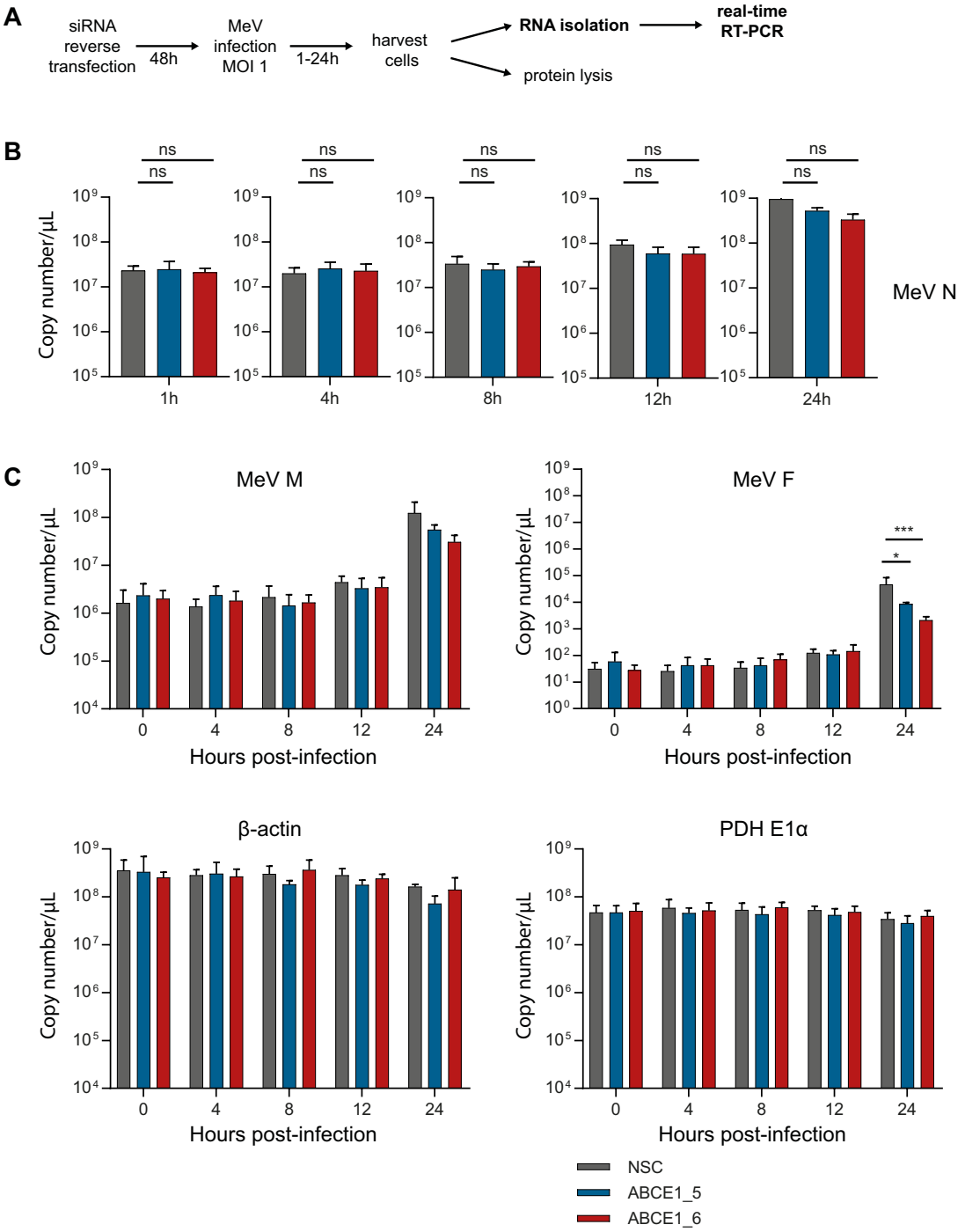

Fig. 20 | Viral and cellular mRNA kinetics in MeV infected cells at a MOI of 1 following ABCE1 knockdown. A) Schematic overview of the mRNA kinetic experiment. **B)** MeV N mRNA copy numbers and **C)** copy numbers of MeV M and F viral mRNAs, and copy numbers of β-actin and PDH E1α cellular mRNAs in ABCE1 siRNA-transfected and MeV-infected cells. A549-hSLAM cells were transfected with NSC, ABCE1_5 and ABCE1_6, and 48 h later infected with MeV at a MOI of 1, and RNA was isolated at indicated time points. mRNA copy numbers from three independent replicates were quantified by RT-qPCR. Error bars represent the standard deviation. Log_2-transformed groups were compared using one-way ANOVA with Sidak's multiple comparisons test. Statistical significance is indicated by ns $p>0.05$, * $p<0.05$, *** $p<0.001$.

5.1.2.6. ABCE1 does not influence primary transcription

Following cell entry, primary transcription of mRNAs templated by the viral genomic RNA is initiated, and viral proteins are then translated by the host cell machinery. During replication, the newly synthesized genomic RNA is tightly associated with the N protein to provide a helical template for viral secondary transcription and replication. To further evaluate the reason for the observed reduction in viral protein synthesis, we investigated whether primary transcription is affected by ABCE1 knockdown by measuring MeV N mRNA levels in A549-hSLAM cells exposed to the protein synthesis inhibitor CHX. A549-hSLAM cells were transfected either with control NSC or ABCE1_6 siRNAs for 48 h, infected with MeV at a MOI of 1, and treated with 100 µg/mL CHX, which blocks *de novo* protein synthesis, or left untreated, starting 30 min before infection. Copy numbers of MeV N and β-actin mRNA levels were quantified at different times after infection by RT-qPCR using a synthetized RNA standard (Figure 21A). A general gradual increase in MeV N copy numbers over time in the absence of CHX irrespective of ABCE1 levels can be observed, whereas N mRNA levels remained stable during CHX-treatment. For the first 12 h after infection, no differences between copy numbers of MeV N mRNA in the presence or absence of CHX was observed, which is expected for the initial phase of viral mRNA transcription in infected cells driven by the viral polymerase complex from incoming virions. Consistent with the kinetics at a MOI of 0.01, mRNA levels increased more than 10-fold in the absence of CHX at the 24 h time point, irrespective of cellular ABCE1 levels (Figure 21B). Neither CHX treatment nor ABCE1 knockdown had an effect on β-actin mRNA levels (Figure 21C). These data demonstrate that ABCE1 does not directly influence viral transcription (Anderson *et al.*, 2019).

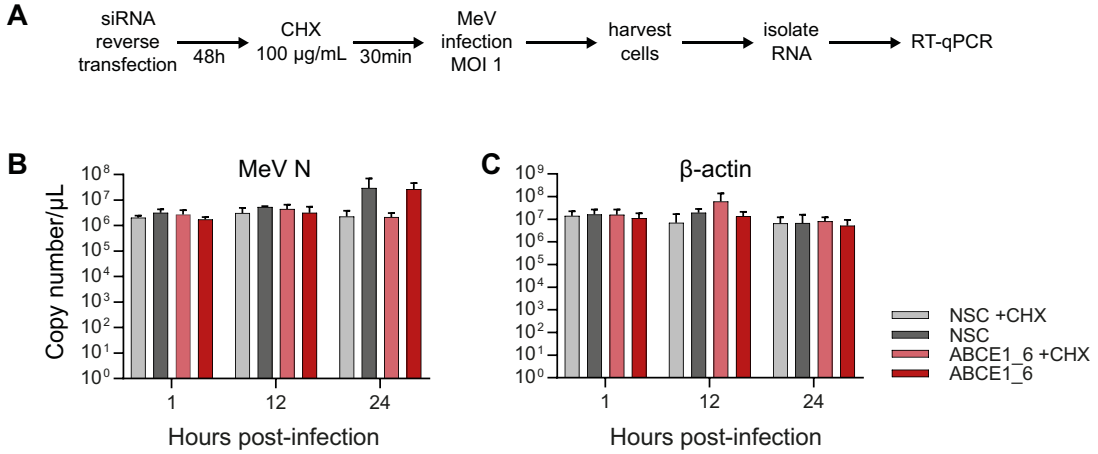

Fig. 21 | Assessment of ABCE1 knockdown on viral primary transcription. A) Schematic overview of the experimental workflow. **B)** Analysis of *de novo* mRNA synthesis. A549-hSLAM cells were transfected with either NSC or ABCE1_6 siRNAs for 48 h, followed by infection with either MeV at a MOI of 1. Cells were treated with 100 µg/mL CHX or left untreated 30 min prior to infection and RNA was isolated at indicated time points. mRNA copy numbers from three independent replicates were quantified by RT-qPCR. Error bars represent the standard deviation (Anderson *et al.*, 2019).

5.1.2.7. Type I IFN treatment does not affect MeV replication in the absence of ABCE1

ABCE1 can form a heterodimer with RNase L and inhibits its function as effector of the IFN-dependend 2-5A/RNase L pathway, which naturally results in RNase L-mediated mRNA degradation of single stranded viral (Baglioni, Benedetti and Williams, 1984; Li, Blackford and Hassel, 1998), messenger (Bisbal *et al.*, 2000; Li *et al.*, 2000; Khabar *et al.*, 2003; Chandrasekaran *et al.*, 2004), and ribosomal RNAs (Bisbal *et al.*, 1995). However, RNase L protein levels in A549-hSLAM cells were not reliably detectable and determination of knockdown efficiency was not possible. We therefore decided to analyze the indirect effect of RNase L on viral replication by investigating either MeV replication efficiency in the presence of type I IFN treatment, or the extent of innate immune activation. Towards this, A549-hSLAM cells were transfected with either NSC, ABCE1_5, or ABCE1_6 siRNAs for 24 h and were then pre-treated with IFN-α (5 U/mL) or left untreated. After a further 24 h, cells were infected with MeV at a MOI of 1, and cell lysates were harvested 24 h after infection (Figure 22A). Type I IFN treatment had a small, but not statistically significant effect on MeV N protein levels in the presence or absence of ABCE1 (Figure 22A and B), indicating that virus replication is not affected (Anderson *et al.*, 2019).

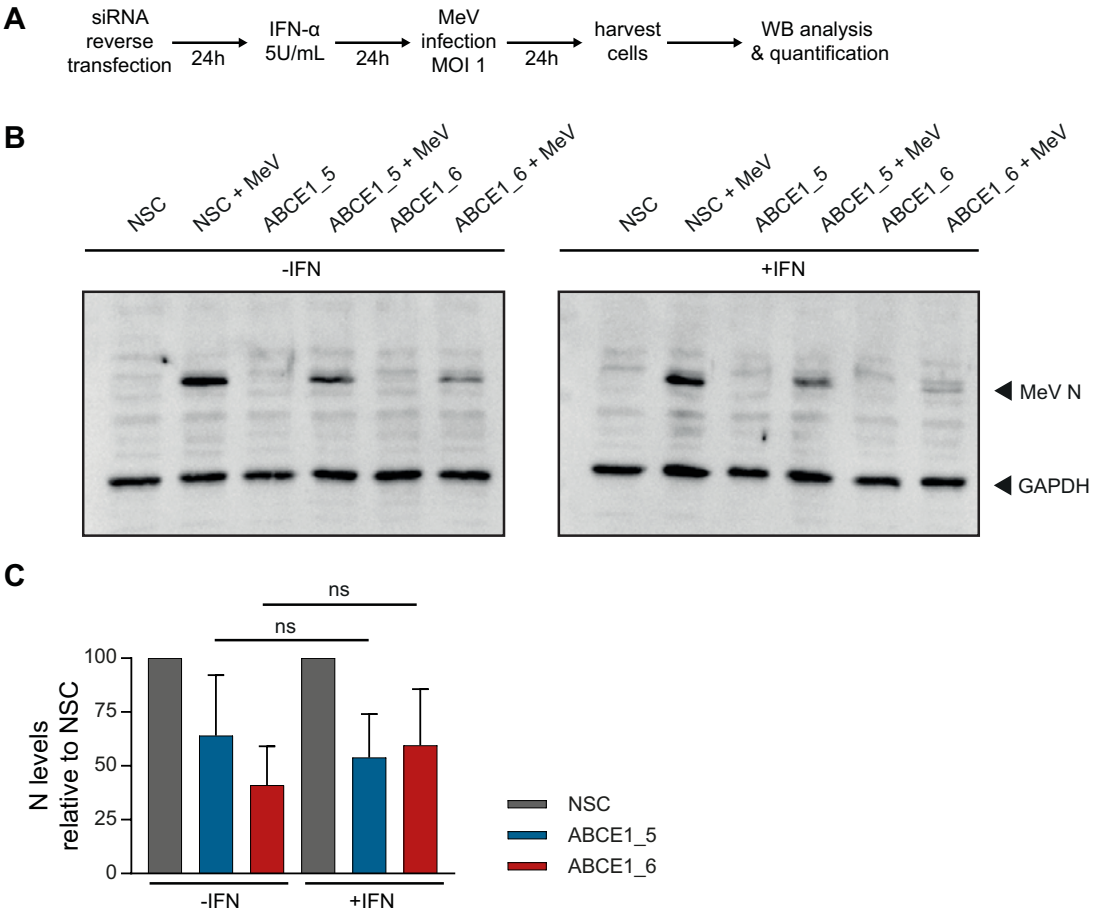

Fig. 22 | Type I IFN treatment does not affect MeV replication in the absence of ABCE1. A) Schematic overview of the experimental workflow. **B)** and **C)** Nucleoprotein expression in the absence and presence of type I IFN in ABCE1 knockdown cells. A549-hSLAM cells were transfected with the NSC, ABCE1_5 and ABCE1_6 siRNAs for 24 h, pre-treated with IFN-α (5 U/mL), or left untreated, and then infected with MeV at a MOI of 1 for a further 24 h. At 24 h post-infection, cells were harvested and analyzed by Western blot (B) and protein bands from three independent replicates were quantified (C), normalized relative to an internal GAPDH control and are shown as percent reduction of N levels relative to NSC. Error bars represent the standard deviation. Statistical significance is indicated by ns p>0.05 (Anderson *et al.*, 2019).

5.1.2.8. Proviral effect of ABCE1 is not due to a modulation of global innate immune activation

Innate immune response activation was assessed by quantifying relative mRNA levels of four different immune modulators: 2′-5′-oligoadenylate synthetase 3 (OAS3), an enzyme induced by IFNs which synthesizes 2′, 5′ adenosine (2-5A) oligomers that bind and activate RNase L (Hassel *et al.*, 1993; Bisbal *et al.*, 1995); the cytokine interferon beta (IFNβ), which is released as part of the innate immune response to defend against viral infections (Binder and Griffin, 2001, 2003; Patterson *et al.*, 2002); the IFN-induced dynamin-like GTPase Mx1, which antagonizes the replication of several different RNA and DNA viruses (Staeheli *et al.*, 1988; Li *et al.*, 2012); and ribonuclease L (RNase L), a component of the IFN-regulated 2-5A system (Bisbal *et al.*, 1995). Towards this,

A549-hSLAM cells were transfected with NSC, ABCE1_5, or ABCE1_6 siRNAs for 48 h, infected with MeV at a MOI of 1, and harvested at the indicated time points. Relative changes in mRNA levels from three independent experiments were quantified by RT-qPCR using the ΔΔCt method (Livak and Schmittgen, 2001) with β-actin as standard (Figure 23A). Quantification of relative mRNA induction over the first 24 h showed a gradual increase of OAS3, IFNβ, and Mx1, which mirrored the increase in MeV N mRNA levels over the same period. While there was some variability, there was no correlation with ABCE1 levels. RNase L mRNA copy numbers were also not affected by ABCE1 levels and remained largely stable, with a slight increase at the 24 h time point (Figure 23B) (Anderson *et al.*, 2019). Taken together, these results indicate that viral mRNA transcription is ABCE1-independent and that the proviral effect of ABCE1 is not due to a modulation of global innate immune activation.

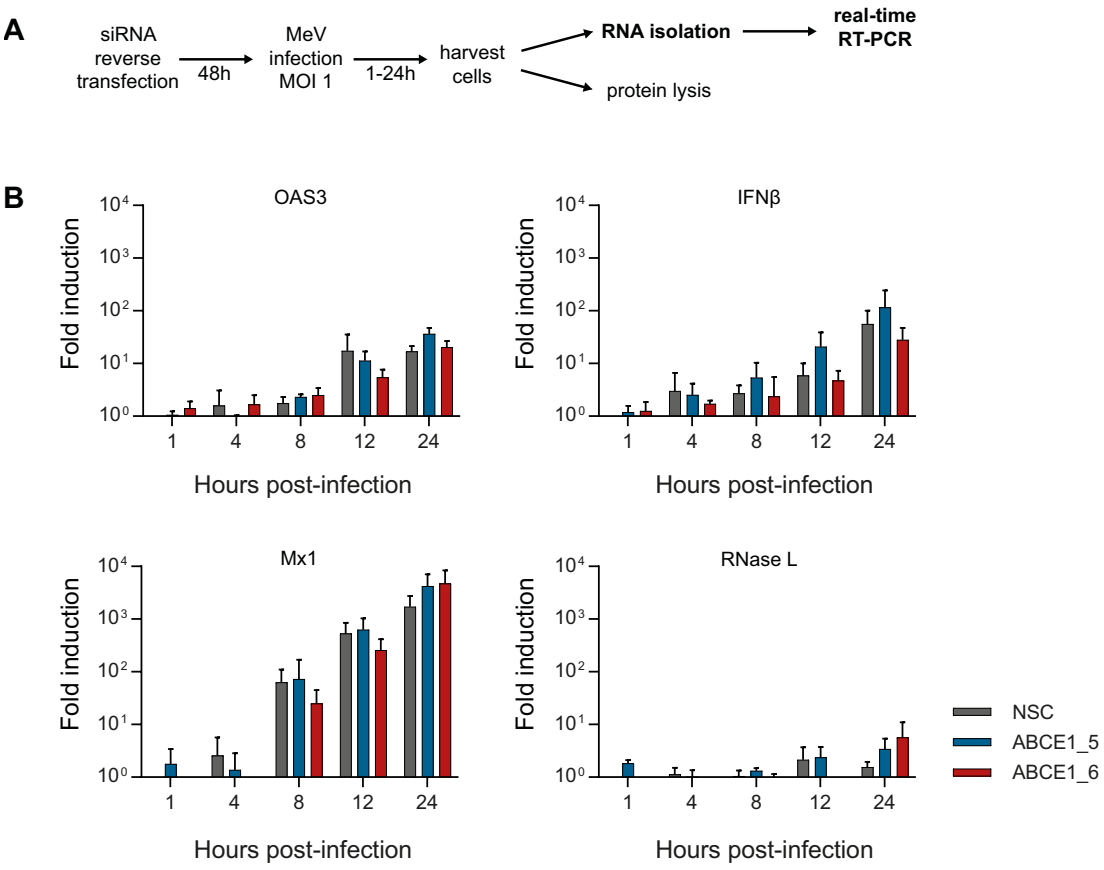

Fig. 23 | Role of ABCE1 in innate immune response. A) Schematic overview of the mRNA kinetic experiment. **B)** mRNA levels of immune modulators OAS3, IFNβ, Mx1 and RNase L in ABCE1 knockdown cells. A549-hSLAM cells were transfected with NSC, ABCE1_5 and ABCE1_6 for 48 h, infected with MeV at a MOI of 1. Cells were harvested, RNA was isolated at indicated time points and relative changes in mRNA levels from three independent experiments were quantified by RT-qPCR using the ΔΔCt method with β-actin as standard. Error bars indicate the standard deviation, and none of the differences seen reached statistical significance (ns p>0.05) (Anderson *et al.*, 2019).

5.1.2.9. Efficient viral protein synthesis is ABCE1-dependent

Based on the observed effect of ABCE1 on viral protein synthesis and its role in translation and ribosome recycling, we next evaluated the relative importance of ABCE1 on total *de novo* cellular protein synthesis using catalyzed fluorescent labeling of proteins in cells treated with O-propargyl-puromycin (OPP) at different times after infection. The protein synthesis inhibitor OPP disrupts peptide transfer on ribosomes causing non-specific premature chain termination during translation. At 48 h after infection with MeV, MuV, or HRSV, siRNA-transfected cells were treated with OPP for the indicated times, and the incorporated OPP was coupled to Alexa Fluor 594 via click reaction. The fluorescence signal was quantified by flow cytometry (Figure 24A). siRNA-mediated knockdown of ABCE1 resulted in a modest reduction of global cellular *de novo* protein synthesis in non-infected and infected cells (Figure 24B). In the context of infection, this reduction reached statistical significance at longer labeling times, indicating a cumulative effect (Anderson *et al.*, 2019).

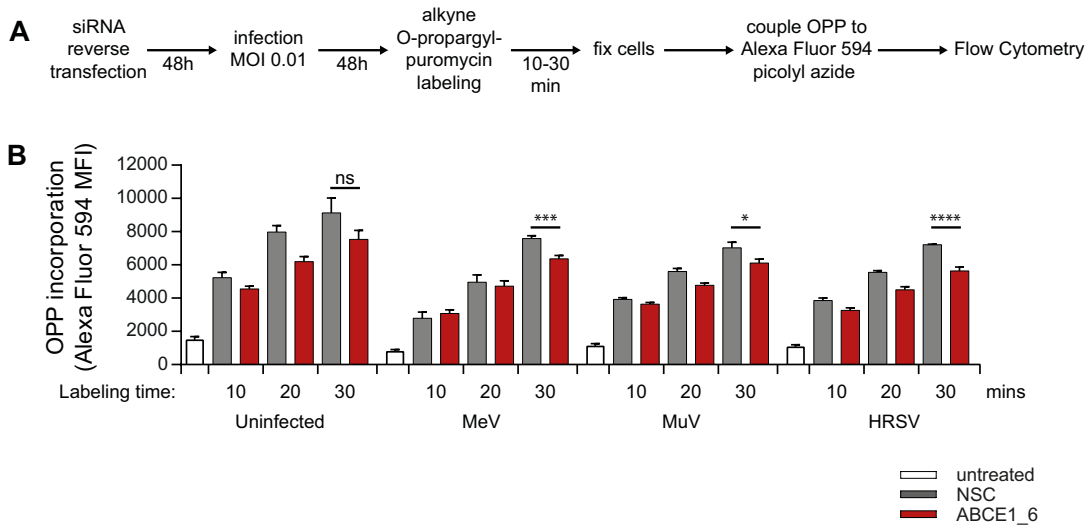

Fig. 24 | Quantification of global cellular *de novo* protein synthesis. A) Schematic overview of the OPP-labeling experiment. **B)** Quantification of total cellular de novo translation by incorporation of O-propargyl-puromycin (OPP). siRNA-transfected and MeV, MuV, and HRSV-infected A549-hSLAM cells were treated at 48 h post-infection with OPP for 10, 20 and 30 min. Incorporated OPP was coupled to Alexa Fluor 594, and the fluorescence signal was quantified by flow cytometry. Error bars represent the standard error of the mean. Statistical significance was determined by one-tailed t tests and is indicated by ns $p>0.05$, * $p<0.05$, *** $p<0.001$, ****$p<0.0001$ (Anderson *et al.*, 2019).

To determine if viral and cellular protein synthesis was affected differently, we compared the amount of newly synthetized protein over time using ^{35}S pulse labeling. At 48 h incubation, NSC or ABCE1_6 siRNA-transfected A549-hSLAM cells were infected with MeV at a MOI of 0.1 and labeled with ^{35}S-Met/Cys 24 h later. The cellular proteins β-actin and PDH E1α, and the MeV M and F proteins from infected cells were immunoprecipitated, and the dried gels were visualized by exposure to phosphor

screens (Figure 25A). Knockdown of ABCE1 had no effect on protein synthesis of β-actin and PDH E1α, two cellular proteins with moderate and high turnover rates, respectively, whereas viral protein synthesis represented by the MeV M and F proteins was reduced by 30-50% compared to the expression levels achieved in the presence of ABCE1 at the respective time points (Figure 25B). Especially for the MeV F protein, which is present at lower quantities due to the transcriptional gradient, the difference in the amount of newly synthetized protein increased over time. Copy numbers of the respective mRNAs corresponding to the ^{35}S pulse labeling were quantified by RT-qPCR using a synthetized RNA standard for each gene and there were no significant differences in the cellular or viral mRNA levels at that time point (Figure 25C), confirming that ABCE1 exerts its effect at the translational level. Comparison of cellular and viral protein expression levels in samples from ABCE1_6 siRNA-transfected cells relative to NSC-treated cells at the 30-min time point showed around 60% reduction for MeV M and 40% for MeV F, which was significantly different compared to the cellular proteins (Figure 25D), indicating that ABCE1 is important for viral translation (Anderson *et al.*, 2019).

.

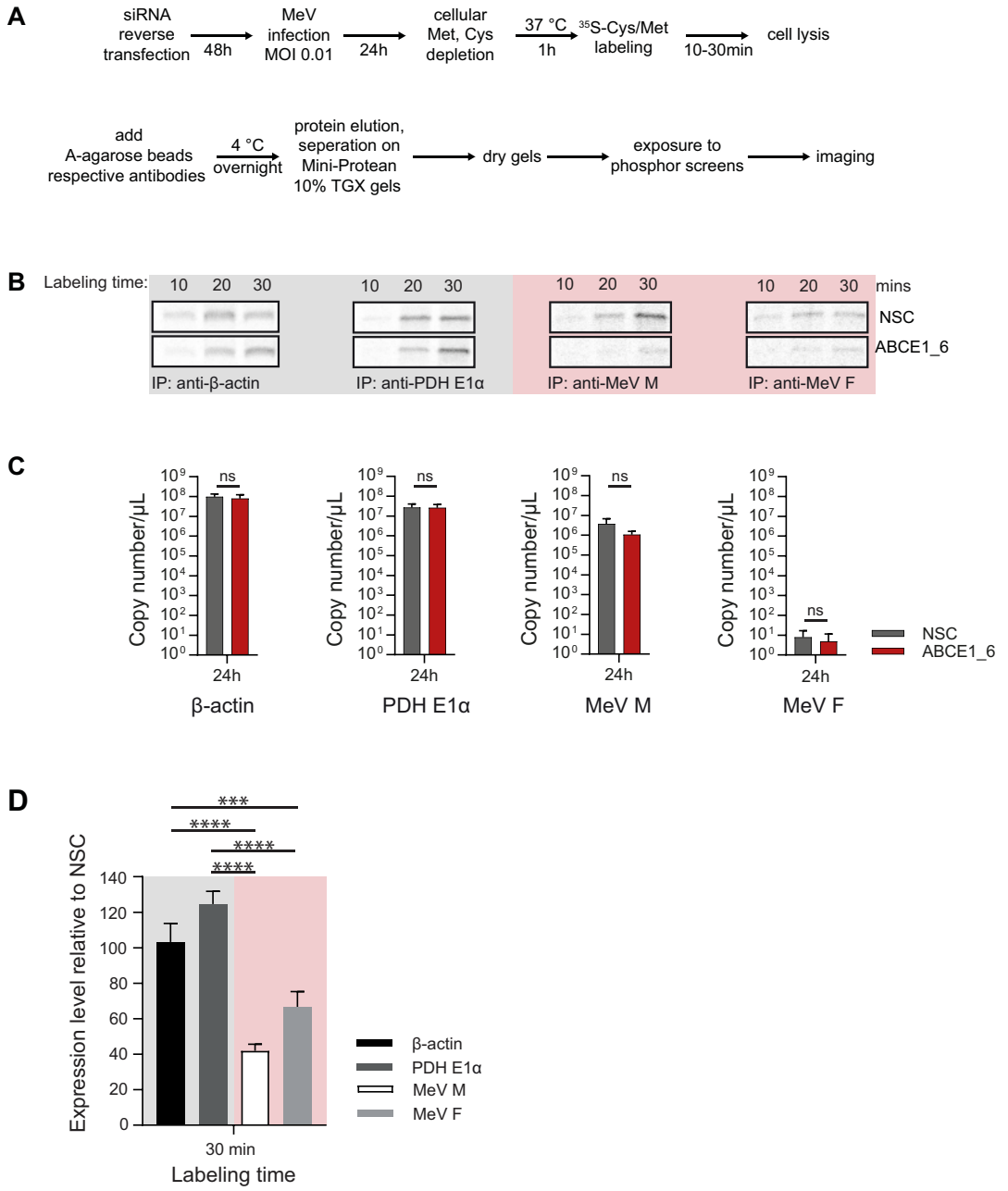

Fig. 25 | ABCE1 effect on *de novo* viral protein translation. A) Schematic overview of the ^{35}S pulse labeling. **B-D)** Analysis of protein translation by ^{35}S pulse labeling and quantification of the corresponding mRNA levels. A549-hSLAM cells were transfected with NSC or ABCE1_6 siRNAs for 48 h, followed by MeV infection at a MOI of 0.1 and labeled with ^{35}S-Met/Cys 24 h later. **B)** Immunoprecipitated cellular proteins β-actin and PDH E1α, and MeV M and F proteins from infected cells were visualized by exposure to phosphor screens. Representative phosphor screen images are shown. **C)** Copy numbers of the respective mRNAs from three independent experiments corresponding to the ^{35}S pulse labeling were quantified by RT-qPCR using a synthetized RNA standard for each gene. **D)** Quantification of ^{35}S pulse label incorporation. The expression levels in samples shown in (B) from ABCE1_6 siRNA-treated cells relative to NSC-treated cells were calculated for each protein. The average from three independent experiments for the 30 min time point is shown. Statistical significance in is indicated by ns $p>0.05$, *** $p<0.001$, **** $p<0.0001$ (Anderson *et al.*, 2019).

We next investigated the importance of ABCE1 on *de novo Paramyxoviridae* and *Pneumoviridae* protein translation by performing CHX chase experiments. A549-hSLAM cells were transfected with control NSC or ABCE1_6 siRNAs for 48 h and then treated with 100 µg/mL CHX starting 30 min before infection with MeV, MuV, or HRSV at a MOI of 1. After 24 h, CHX was removed and samples were harvested after an additional incubation of 24 h (Figure 26A). Reduction of ABCE1 levels resulted in a significant inhibition of *de novo* synthesis of all viral nucleoproteins. MeV and MuV *de novo* N protein syntheses were reduced by approximately 30%, whereas *de novo* translation of HRSV was reduced by 80% in the absence of ABCE1 (Figure 26B), demonstrating a specific role of ABCE1 in translation of *Paramyxo-* and *Pneumoviridae* mRNAs (Anderson *et al.*, 2019).

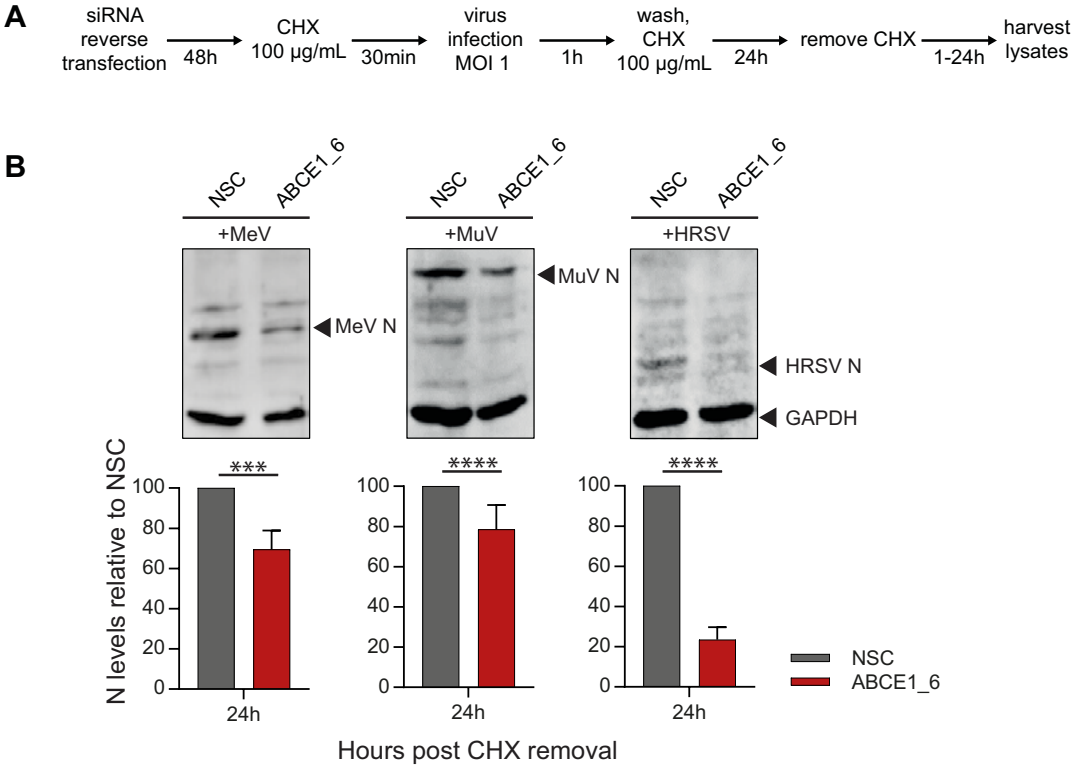

Fig. 26 | Influence of ABCE1 on *de novo* protein synthesis of MeV, MuV and HRSV. A) Schematic overview of the cycloheximide (CHX) chase experiment. **B)** Analysis of de novo translation of MeV, MuV and HRSV in the absence of ABCE1 performing a CHX chase. A549-hSLAM cells were transfected with NSC or ABCE1_6 siRNAs for 48 h, infected with MeV at a MOI of 1, and treated with 100 µg/mL CHX or left untreated starting 30 min before infection. After 24 h, CHX was removed and samples were harvested after additional 24 h incubation. MeV, MuV, and HRSV N protein bands were quantified and normalized relative to an internal GAPDH control. Each graph shows the average from three independent experiments, and error bars represent the standard deviation. Statistical significance is indicated by *** p<0.001, ****p<0.0001 (Anderson *et al.*, 2019).

5.1.2.10. The ABCE1 proviral effect requires viral gene expression in the context of infection

To further analyze the role of ABCE1 in the translation of viral proteins, the influence of ABCE1 on nucleoprotein expression in cells either infected with MeV or transfected with a N-FLAG expressing plasmid was compared. A549-hSLAM cells were transfected with NSC or ABCE1_6 siRNAs for 24 h and were then transfected with either a control empty vector plasmid or a plasmid expressing MeV N containing an N-terminal FLAG tag. After another 24 h, cells were either infected with MeV at a MOI of 0.1 or left uninfected and were harvested 24 h later (Figure 27A). In contrast to the reduction of MeV N protein levels in infected ABCE1 knockdown cells, there was no effect on MeV N protein levels in cells transfected with a eukaryotic MeV N expression plasmid (Figure 27B) (Anderson *et al.*, 2019).

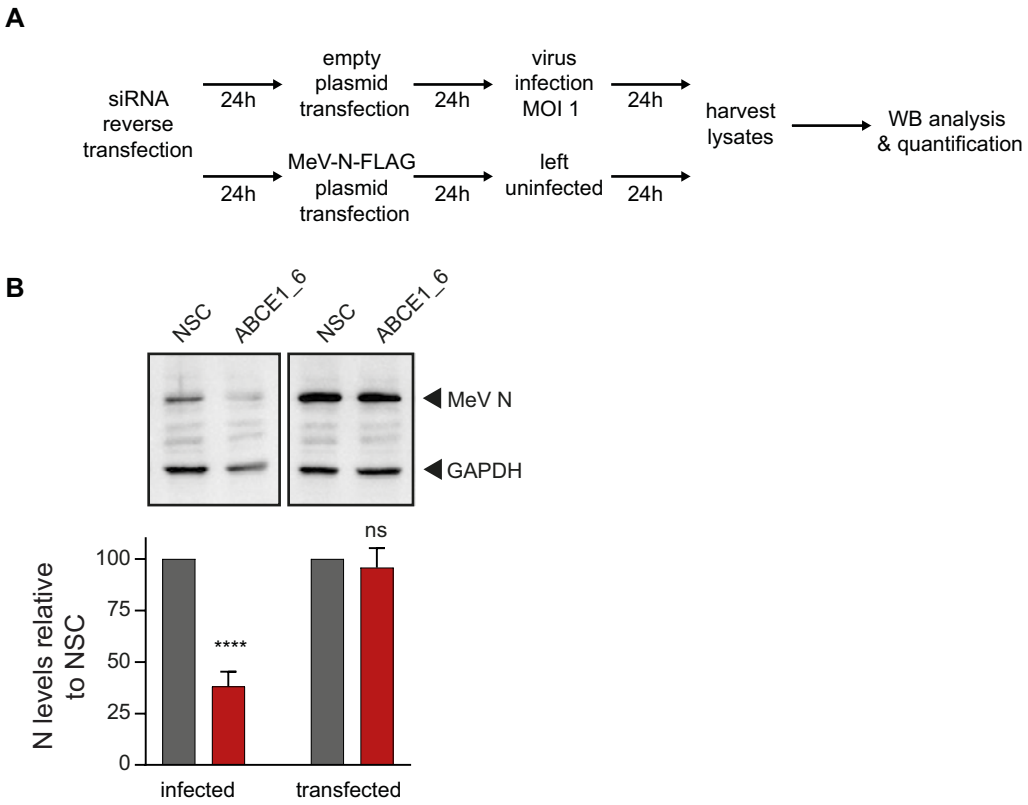

Fig. 27 | Plasmid-expressed MeV N is not sensitive to ABCE1 knockdown. A) Schematic overview of the experiment. **B)** Effect of ABCE1 knockdown on nucleoprotein expression in MeV infected and MeV N-FLAG transfected cells. At 24 h, siRNA-treated A549-hSLAM cells were transfected with either a control empty vector plasmid or a MeV-N-FLAG expressing plasmid for 24 h, followed by either MeV infection at a MOI of 0.1 or left uninfected, respectively. MeV N levels were quantified and NSC was set to 100%. Data are representative of four independent experiments. Error bars represent standard deviations. Statistical significance is indicated by ns $p>0.05$, **** $p<0.0001$ (Anderson *et al.*, 2019).

Next, we evaluated MeV N expression in the absence of ABCE1 and eIF3A, another hit of the top 24 common proviral factors, which plays a role in translation initiation and is known to associate with ABCE1 (Dong *et al.*, 2004). Towards this, A549-hSLAM cells

were reverse transfected with ABCE1 and eIF3A siRNA combinations for 48 h , followed by MeV infection with a MOI of 0.01. At 48 h post-infection, cells were harvested, and MeV N expression was analyzed by Western blot (Figure 28A). Comparison of the proviral activity of ABCE1 with eIF3A revealed a similar reduction in MeV protein levels, and there was no additive effect when both genes were targeted simultaneously (Figure 28B), highlighting the dependence of *Paramyxo*- and *Pneumoviridae* on specific translation factors (Anderson *et al.*, 2019).

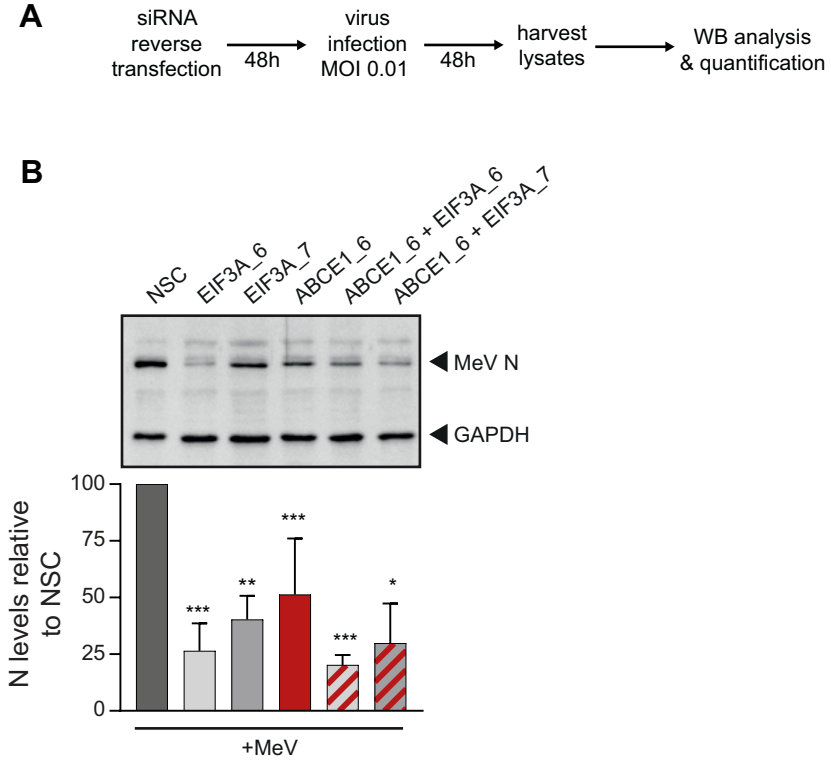

Fig. 28 | ABCE1 and eIF3A have similar effects on MeV replication. A) Schematic overview of ABCE1 and EIF3A knockdown experiment. **B)** Nucleoprotein expression in the absence of ABCE1 and eIF3A. A549-hSLAM cells were transfected with ABCE1 and eIF3A siRNAs, followed by MeV infection at a MOI of 0.01. At 48 h post-infection, cells were harvested. MeV N protein levels were quantified and NSC was set to 100%. Data are representative of three independent replicates. Statistical significance is indicated by ns p>0.05, * p<0.05, ** p<0.01, *** p<0.001 (Anderson *et al.*, 2019).

The 5′ untranslated regions (UTRs) of paramyxovirus mRNAs play an important role in translation of viral proteins, and the 5′-UTRs of paramyxo- and pneumoviral mRNAs can vary in length depending on the gene and virus (Fields, Knipe and Howley, 2007). We thus assessed whether viral 5′-UTRs differentially affect protein translation in the presence or absence of ABCE1 knockdown. Towards this, the 5′-UTRs of the MeV N, M, and F genes, as well as those from the MuV, HRSV, and HeV N and F genes were introduced upstream of a firefly luciferase (ffLuc) reporter gene followed by a HCV internal ribosomal entry site (IRES) that mediates translation of a *Renilla* luciferase (RenLuc) reporter gene for normalization (Figure 29B) (Müller *et al.*, 2018). Hep G2 cells were transfected with NSC, ABCE1_5, and ABCE1_6 siRNAs in 96-well plates

along with the dual-luciferase reporter plasmids. Luciferase values were read 48 h after transfection (Figure 29A), and ffLuc signals for each well were normalized to the RenLuc signal. While ABCE1 knockdown resulted in an overall increase in ffLuc luciferase expression from all the tested plasmids independent of the 5′-UTR inserted (Figure 29C top panels), the relative expression levels remained stable (Figure 29C, bottom panels), demonstrating that viral 5′-UTRs were not sufficient to confer sensitivity to ABCE1 knockdown (Anderson *et al.*, 2019).

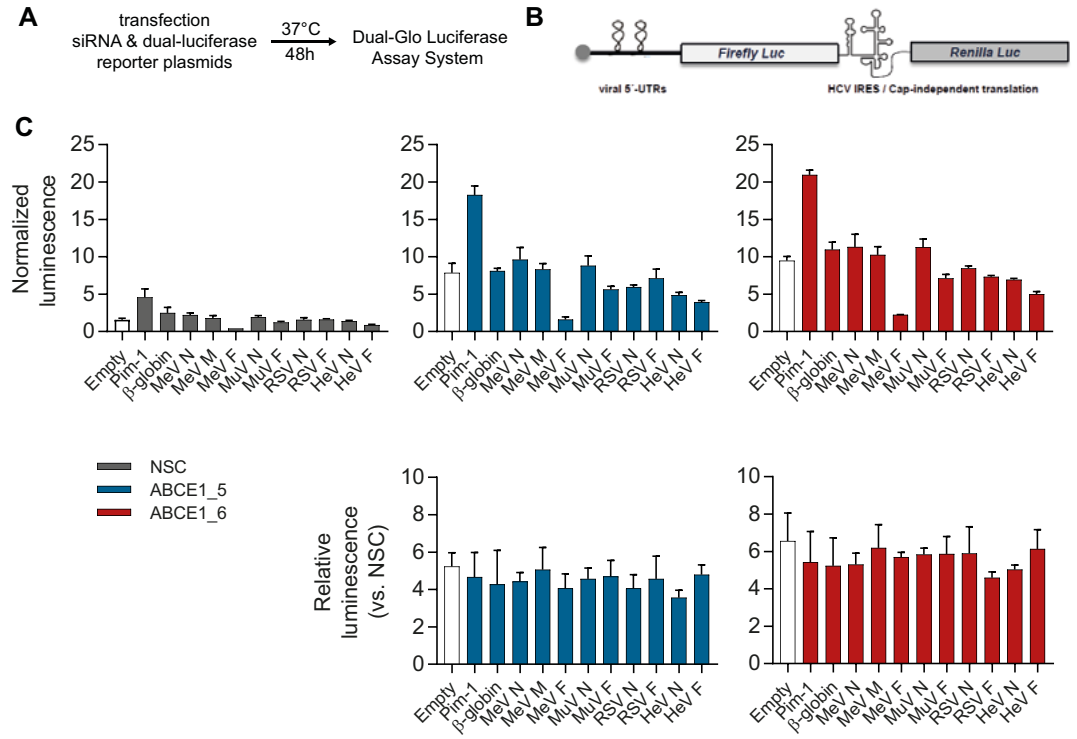

Fig. 29 | Effect of viral 5′ untranslated regions (UTRs) on reporter gene translation. A) Schematic overview of the experiment. **B)** Schematic presentation of the dual luciferase reporter vector (Müller *et al.*, 2018). Reprinted from Antiviral Research, Volume 150, Müller et al., Pages 123-129, © 2018, with permission from Elsevier. **C)** Influence of ABCE1 on viral 5' UTRs. Hep G2 cells were transfected with NSC, ABCE1_5 and ABCE1_6 along with dual-luciferase reporter plasmids in 96 well plates and luciferase values were read 48 h post-transfection. Translation of firefly luciferase (ffLuc) is mediated by upstream cellular or viral UTRs, translation of the downstream Renilla luciferase (RenLuc) is driven by the hepatitis C virus (HCV) internal ribosomal entry site (IRES). ffLuc signals for each well were normalized to the RenLuc signal. Transfections in each replicate were performed in triplicate, and all experiments were performed three times (Anderson *et al.*, 2019).

5.2. Assessment of the antiviral efficacy of the compound ERDRP-0519 against MeV *in vivo*

5.2.1. Inhibitor treatment reduces severity of clinical signs of MeV disease

Even though the MeV vaccine is safe and efficacious, ongoing vaccination campaigns over the last decades have not been sufficient to eradicate the virus. An antiviral drug that reduces disease severity and virus shedding could make an important contribution to this effort. The compound ERDRP-0519 is a small-molecule viral polymerase inhibitor that reduces the activity of the MeV L protein, likely by binding to the catalytic domain responsible for phosphodiester bond formation. Starting with the lead compound AS-136a, identified in a high throughput screen, ERDRP-0519 was optimized to improve water solubility and to increase oral bioavailability in a rat pharmacokinetic model (Yoon *et al.*, 2009). Here, the efficacy of ERDRP-0519 was tested in the squirrel monkey model of MeV infection and disease. A single-dose oral pharmacokinetic study in three animals prior to the main study revealed that the oral dosing regimen resulted in therapeutically-relevant plasma concentrations of the inhibitor. Based on these findings, the efficacy study was designed. Groups of five animals were either left untreated or treated twice daily by intragastric administration. Treatment was initiated 12 h before or 3 or 7 days after infection and continued for 14 days. Clinical assessment and weight and temperature measurements were performed under anesthesia every morning to evaluate severity of disease, MeV-induced fever, and weight loss. The body temperature of healthy squirrel monkeys ranges between 38.5-39.5 °C, and low temperatures at the first day are due to the body temperature-depressing effect of the injection anesthesia used for infection. Rectal temperatures of the untreated animals and the D7 group increased above 39.5 °C between days 3 and 7 after infection, while body temperature of -12 h and D3 groups remained within the normal range (Figure 30A). However, the -12 h and D3 groups developed fever around 3-4 days after cessation of the inhibitor treatment (Figure 30A). The body weight of the untreated, -12 h, and D7 groups remained stable over the course of infection, while some weight loss was observed for the D3 group (Figure 30B). In this group, one animal continually lost weight and eventually died on day 15 from causes unrelated to infection. The two co-housed animals experienced stress-induced weight-loss during this period, but quickly recovered after the death of the sick monkey.

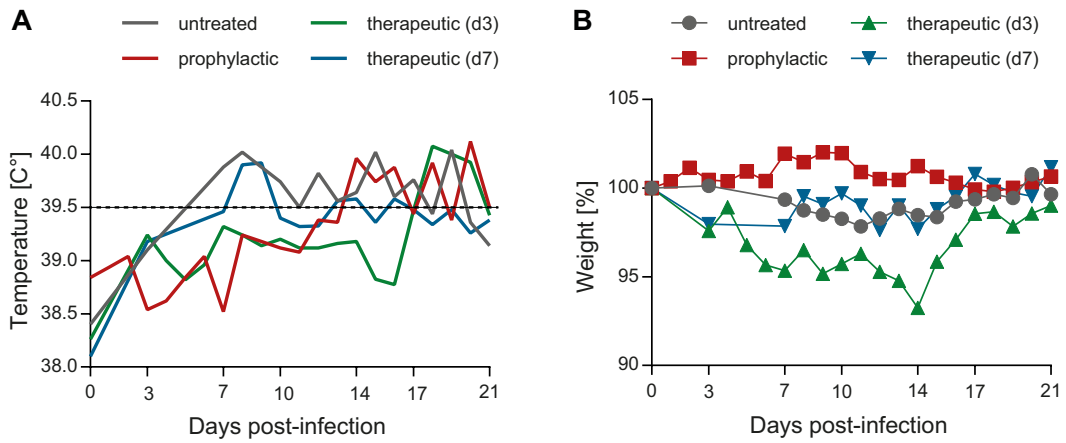

Fig. 30 | Body temperature and body weight of MeV-infected squirrel monkeys. A) Rectal temperature was measured during anesthesia every morning to evaluate fever related to MeV infection. Lines represent the mean of the respective group (n=5). The dotted line indicates the body temperature threshold for fever. The average of the three treated groups was calculated and set as the average temperature for the untreated group on day 0. **B)** Body weight was measured during anesthesia every morning to evaluate weight-loss related to MeV infection. Lines indicate the average of the whole group (n=5), except for therapeutically treated group (d3) from day 15 onwards (n=4). Average group weight on day 0 was set to 100%; measurements of the following days were normalized to that value and are expressed as the percentage of initial weight.

All animals in the untreated group developed isolated spots 7-9 days post-infection, and rash severity increased in two of the five animals during the following week, leading to generalized rash and crusts around the nose and eyes (Figure 31B and D). The remaining animals showed only isolated spots until day 12. In contrast, none of the animals treated with ERDRP-0519 developed a generalized rash and squirrel monkeys in the prophylactically treated group remained free of all clinical signs during the study (Figure 31A and C). Three animals of the D3 group showed clinical signs, with two of these animals developing sporadic red spots for one to two days, while one animal had red spots in several isolated areas which lasted from day 7 to 13 post-infection. All animals of the D7 group developed clinical signs ranging from isolated spots to mild rash, but the severity was markedly reduced compared to the untreated group. On day 12, at the peak of clinical disease, three animals showed a mild rash, while only isolated spots were observed in two animals. Clinical signs of all groups are summarized in Figure 31E. Taken together, these data demonstrate that prophylactic treatment prevents clinical disease, and treatment initiation in early infection stages reduces disease severity.

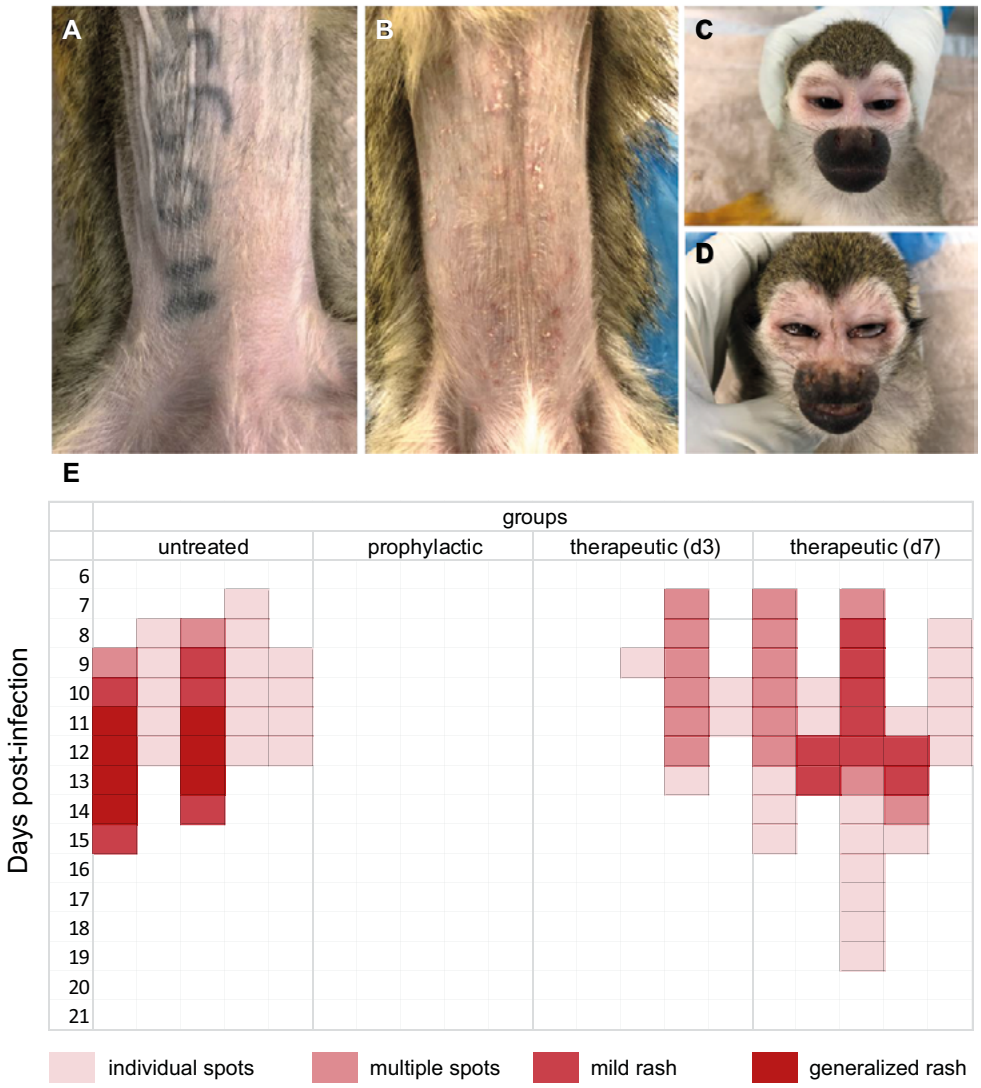

Fig. 31 | Clinical signs after MeV infection and drug treatment. A-D) Comparison of rash in prophylactically and untreated squirrel monkeys at 13 days post-infection. Abdomen (A, B) and face (C, D) of representative prophylactically treated or untreated monkeys, respectively. **E)** Overview of clinical signs. Each column and row represent one individual animal and the day post-infection, respectively. Colors of boxes indicate the severity of rash.

5.2.2. ERDRP-0519 drug treatment strongly reduced viral replication

To evaluate the efficacy of ERDRP-0519 treatment and its effect on MeV replication, blood samples were taken at different time points to assess cell-associated viremia and neutralizing antibody responses (not shown). Virus titers in PBMCs of untreated and D7 groups peaked between day 7 and 10, and decreased during the following two weeks until the infection was cleared on day 21. In contrast, animals of the D3 treated group showed almost no detectable viral load in PBMCs and cleared the infection by 17 days post-infection, and prophylactically treated animals had no detectable virus throughout the treatment, with the exception of one animal that developed a mild viremia once the drug treatment was stopped (Figure 32A). Overall, the reduction of viremia corresponded to the onset of ERDRP-0519 treatment.

To evaluate MeV shedding in the upper respiratory tract, throat swabs were collected. In the untreated group, virus was detected on days 7 and 10, correlating with the peak of clinical disease. In contrast, viral titers of the D3 group were 10-100-fold reduced compared to the untreated group, and no virus was detected in the prophylactically treated group. D7 group had viral titers similar to the untreated group on day 7, but viral shedding was rapidly and strongly reduced by approximately 100-fold within 3 days after the start of drug treatment (Figure 32B), illustrating that antiviral treatment at the beginning of clinical disease reduced viral load in the upper respiratory tract and may prevent transmission.

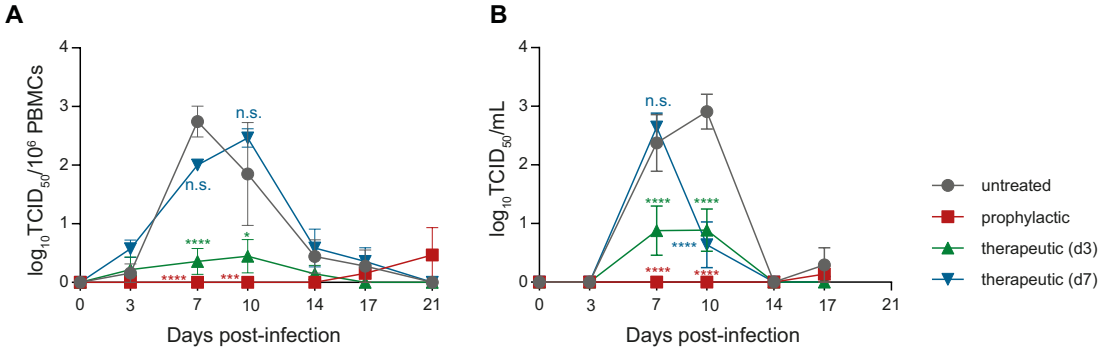

Fig. 32 | ERDRP-0519 treatment strongly reduced viral loads. A) PBMC titration and **B)** Throat swab titration expressed as $\log_{10}$ $TCID_{50}$ per 10^6 cells or mL, respectively. Lines indicate group averages (n=5). Error bars represent standard error of the mean. Statistical analysis was performed using two-way ANOVA with Tukey post-test and the untreated group was used as a reference. Statistical significance is indicated by ns p>0.05, *** p<0.001, **** p<0.0001.

5.2.3. ERDRP-0519 drug treatment reduced MeV-induced immunosuppression

For the assessment of MeV-induced immunosuppression, total white blood cell counts were determined. Leucocyte counts in untreated animals decreased as low as 2×10^3 cells/µL blood on day 10 after infection and then recovered gradually over the course of the study, but did not recover to pre-infection levels. In contrast, leucocyte counts of the prophylactically treated group remained stable over the course of the study, indicating that the drug treatment prevents immunosuppression. Animals of the D3 and D7 groups showed a decrease in leucocyte counts between days 3 and 7 post-infection, but a rapid stabilization and recovery of leucocyte counts was observed after treatment initiation (Figure 33), suggesting that ERDRP-0519 drug treatment reduces severity of MeV-induced immunosuppression, even after its onset.

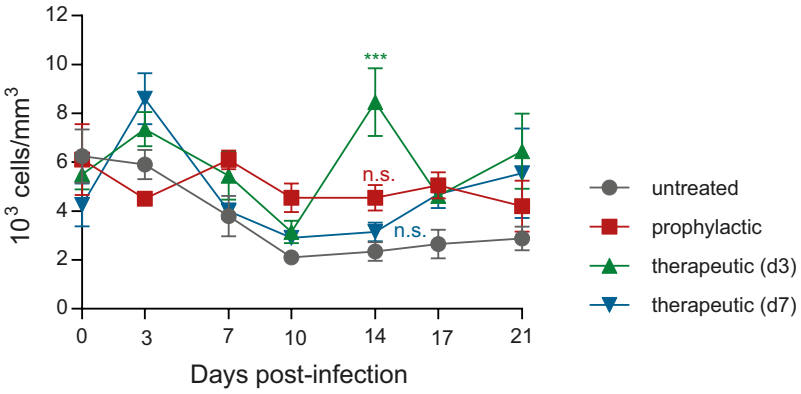

Fig. 33 | ERDRP-0519 treatment alleviated MeV-induced immunosuppression. Total white blood cell counts were measured and are expressed as 10^3 cells/mm^3 blood. Lines indicate the group average (n=5). Statistical analysis was performed using Two-way ANOVA with Tukey post-test and the untreated group as a reference. Statistical significance is indicated by ns $p>0.05$, *** $p<0.001$.

6. DISCUSSION

MeV, MuV, and HRSV are representatives of the *Paramyxoviridae* and *Pneumoviridae* families and have high clinical relevance. While the MeV and MuV vaccines are among the most successful vaccines available today (Croghan, 1966; Hilleman, 1992; Njeumi *et al.*, 2012; Middleton *et al.*, 2014; Broder, Weir and Reid, 2016), an approved vaccine for HRSV remains an important unmet medical need. With the exception of a prophylactic monoclonal antibody-based treatment against HRSV, no approved therapeutics are available (Anderson *et al.*, 2013). As obligate intracellular parasites, viruses exploit the host translational machinery and other host factors during infection to mediate viral protein synthesis and to replicate their genomes. Based on their inhibitory mechanisms, antiviral reagents can be divided into two groups, inhibitors that target the virus itself or inhibitors that target host cell factors. Antivirals directed against viral targets are primarily specific for viral enzymes or block viral entry or the formation of the viral replication machinery. Host-targeting antivirals interfere with cellular factors that are involved in the viral life cycle, by regulating the function of the immune system or other cellular processes in host cells (Müller and Kräusslich, 2009; Lou, Sun and Rao, 2014). Host-targeting antivirals are promising because since they are unlikely to induce mutations in these host genes, and are therefore less prone to the development of drug resistance.

The availability of genome-scale loss-of-function screens has enabled unbiased investigation of the role of cellular proteins in diverse processes (Mohr *et al.*, 2014; Shalem, Sanjana and Zhang, 2015). We used genome-scale siRNA screens with wild-type MeV, MuV, and HRSV in A549 cells to identify common host factors involved in the *Paramyxo*- and *Pneumoviridae* life cycles. These screens not only provided insights in the biology of these viruses, but also constitute a basis for rationally-designed therapeutics. By performing a comparative meta-analysis of two independent comparative analyses of the three siRNA screens, we were able to identify 24 common proviral factors, which were then subsequently confirmed by validation screens. Six of these genes, ABCE1, COPB2, RBM22, FOXP4, HSD11B2, and PRR15 were also hits in a recently published HeV screen (Deffrasnes *et al.*, 2016), further strengthening the confidence of our analysis. ABCE1 is a multifunctional protein involved in inhibition of RNase L-mediated signaling, HIV particle assembly, and ribosome recycling (Tian, Han and Tian, 2012). We found that it plays a critical role in paramyxovirus and pneumovirus protein synthesis by decreasing MeV, MuV, and HRSV nucleoprotein expression in ABCE1 knockdown cells. While only modestly affecting global cellular protein synthesis, ABCE1 knockdown strongly inhibited *de novo* synthesis of MeV proteins, indicating that paramyxo- and pneumoviral mRNAs may exploit specific translation mechanisms.

In a separate study we investigated the antiviral efficacy of the small molecule MeV polymerase inhibitor ERDRP-0519 in squirrel monkeys. Since the prevalence of chronic viral infections, the emergence and re-emergence of viral infections, and resistance to currently used antiviral drugs have led to increased demand for new antivirals, both strategies, targeting highly conserved viral enzymes such as the MeV polymerase and the host factor ABCE1 are thus promising approaches that warrant further investigation.

6.1. Targeting host cell factors as an antiviral strategy

6.1.1. What is the role of RNase L in viral infections?

ABCE1 was first identified as an inhibitor of RNase L in the IFN-inducible pathway. RNase L plays a central role in the antiviral and antiproliferative activities of IFN and contributes to innate immunity and cell metabolism. During viral infections, IFN induces the transcription of several 2-5A synthetases and after activation by dsRNA structures produced during the replication of many viruses, 2-5A OAS produces 5′-triphosphorylated, 2′,5′-oligoadenylates (2–5A) from ATP. 2-5A binds and activates RNase L to degrade viral and cellular RNAs (Bisbal *et al.*, 1995). The 2-5A/RNase L pathway is a critical part of the innate immune response against a number of viruses, including vaccinia virus, reovirus, and encephalomyocarditis virus (EMCV) (Nilsen, Maroney and Baglioni, 1982; Díaz-Guerra, Rivas and Esteban, 1997; Ghosh, Sarkar and Sen, 2000). ABCE1 acts as a negative regulator of RNase L by forming a heterodimer, thereby preventing the binding of 2–5A to RNase L in a noncompetitive manner. As a consequence, ABCE1 supports the replication of RNA viruses such as EMCV and HIV by inhibiting the IFN-induced activation of the 2-5A/RNase L pathway (Martinand *et al.*, 1998, 1999). A 2-5A homolog showed enhanced antiviral activity in cell culture and induced the cleavage of HRSV genomic RNA in an RNase L- and virus sequence-specific manner in African green monkeys (Leaman *et al.*, 2002), illustrating the potential of RNase L activating drugs to inhibit paramyxovirus infections. The importance of this pathway for the control of virus replication has been confirmed by other small molecule activators of RNase L identified in high throughput FRET screens, which demonstrated broad antiviral activity against Sendai virus and human parainfluenza virus 3 (Thakur *et al.*, 2007). In our experimental system, reduction of ABCE1 expression did not result in increased RNase L activity as measured by MeV mRNAs levels. The kinetics of cytokine induction that would normally be associated with increased RNase L activity were also unaffected by inhibition of ABCE1. This supports the notion that the 2-5A/RNase L pathway is not responsible for the decreased viral replication that we observed. However, the RNase L inhibitory activity of ABCE1 may still contribute to the proviral effect on *Paramyxo*- and *Pneumoviridae* replication we observed.

6.1.2. Viral strategies to manipulate translation

Eukaryotic translation is a complex process that can generally be divided into four steps: initiation, elongation, termination, and recycling. ABCE1 has a crucial role in ribosome recycling, which links the translational termination and initiation processes. Viruses rely on the host machinery for the translation of viral proteins. During infection, viral mRNAs must compete with host mRNAs for access to ribosomes and a limited pool of cellular translation factors to ensure that they are preferentially translated. Viruses have developed a variety of strategies either to repress or even shut off host cell protein synthesis to recruit ribosomes so that viral mRNAs out-compete cellular mRNAs and are preferentially translated, or to use strategies that favor alternative translation initiation (Jaafar and Kieft, 2019). Some viruses have evolved mechanism of interacting with the host translational machinery to shutoff host gene expression. Global inhibition of cellular protein synthesis enhances viral gene expression and counteracts the antiviral response (Au and Jan, 2014). The first step is to interrupt the formation of the multisubunit translation initiation complex eIF4F and the 43S pre-initiation complex via proteolytic cleavage, modulation of eIFs, or by sequestration (Jaafar and Kieft, 2019). During poliovirus infection, cleavage of the eukaryotic initiation factor eIF4G1, PABP, and eIF5B inhibits the cap-dependent translation, which results in a strong decrease in host cell protein synthesis (Gradi *et al.*, 1998; de Breyne *et al.*, 2008; Rivera and Lloyd, 2008) and an increase in IRES-mediated translation of picornavirus mRNA (Belsham and Sonenberg, 1996). In contrast, influenza virus mRNA translation is cap-dependent (Katze and Krug, 1990), and viral protein synthesis is enhanced via virus-mediated endonucleolytic cleavage of host mRNA m^7G caps and transfer to viral transcripts ("cap-snatching"). Cellular mRNAs are subsequently destabilized, eIF4E is dephosphorylated, and host factors are recruited to the 5′ leader sequence of the influenza virus mRNAs (Park and Katze, 1995; Park, Wilusz and Katze, 1999). VSV infection induces the dephosphorylation of eIF4E and disassembly of the eIF4F complex by eIF4E-binding protein 4E-BP1, which contributes to the blocking of host but not viral protein translation (Connor and Lyles, 2002).

While all these viruses induce host cell shut off by interfering with cellular mRNA or protein synthesis, replication of the *Paramyxo-* and *Pneumoviridae* seems to require ongoing cellular protein synthesis. In the case of parainfluenza virus 5, the P and V proteins actively prevent shutdown of translation by limiting the activation of PKR (Gainey *et al.*, 2008). Impairment of PKR activation has also been reported for the MeV C protein (Pfaller *et al.*, 2014), and although PKR is activated during HRSV infection, there is no complete inhibition of protein translation. Instead, HRSV sequesters PKR by binding to the viral N protein, thereby limiting phosphorylation of eIF2α and

maintaining cellular and viral protein translation (Groskreutz *et al.*, 2010). Our data show that MeV, MuV, and HRSV infections lead to a modest decrease in global protein synthesis, and that ABCE1 knockdown resulted in a modest reduction in overall protein synthesis. However, viral protein synthesis was dramatically affected under the same conditions, demonstrating that this process is critically dependent on ABCE1. Taken together, our results demonstrate that paramyxovirus and pneumovirus mRNAs are disproportionally sensitive to the loss of ABCE1 function. Perturbations in ABCE1 levels are tolerated by the cell but have a dramatic effect on the viral life cycle (Figure 34).

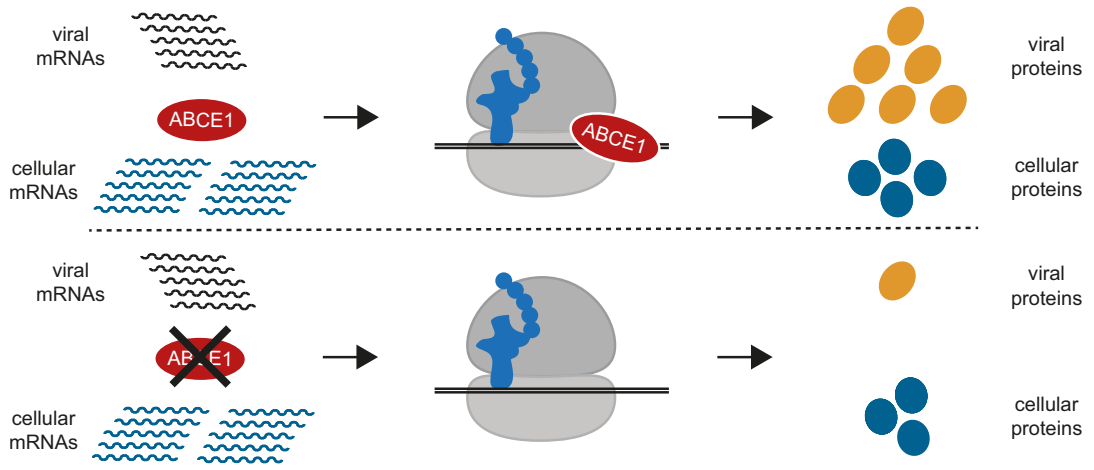

Fig. 34 | Model for the differential effects of ABCE1 knockdown on viral and cellular protein translation. In cells with normal ABCE1 levels, viral proteins are preferentially translated over cellular proteins resulting in proportionately higher levels of viral protein expression (top). In cells with reduced ABCE1 levels, viral protein translation is drastically reduced, while translation of cellular proteins is only moderately affected (bottom) (Anderson *et al.*, 2019).

6.1.3. Do specialized ribosomes preferentially translate certain mRNAs?

It is interesting to note that ABCE1 is known to form a stable complex with the small ribosomal subunit during the recycling of terminated or stalled ribosomes and that 30 proteins of the small ribosomal subunit were among the top 100 proviral genes identified by the KS analysis in our work, while only 5 large ribosomal subunit proteins scored in the same group. While we observed a disproportionate dependence of paramyxoviruses and pneumoviruses on small ribosomal subunit proteins, screens for flavivirus host factors identified large ribosomal subunit proteins at the top of the list (Le Sommer *et al.*, 2012). Recently, a cryo-EM structure of the yeast 40S–ABCE1 post-splitting complex at 3.9-Å resolution was published. The FeS cluster domain of ABCE1 interacts with the rRNA helices h5, h44, and the ribosomal protein uS12, and the HLH and hinge domains of ABCE1 form contacts to rRNA helices h5–h15 and h8–h14 and to the ribosomal protein eS24 (Heuer *et al.*, 2017). ABCE1 has been shown to interact with initiation factors eIF2, eIF5, and eIF3 in *Drosophila melanogaster* and *S.*

cerevisiae (Dong *et al.*, 2004; Hinnebusch, 2006; Andersen and Leevers, 2007; Skabkin *et al.*, 2013). The structure of the native post-splitting complex reveals ABCE1 to be a component of the 43S pre-initiation complex including the initiation factors eIF1a, eIF2, eIF3 and the initiator tRNA (Heuer *et al.*, 2017). In our work, both the KS and robust Z score analyses identified eIF3A as a top proviral factor and suggested that other eIF3 subunits were likely involved, implying that the eIF3 complex may be exquisitely required for at least some paramyxovirus mRNA translation. Another common hit for MeV, MuV, and HRSV was RPLP1, which has recently been implicated in ABCE1-dependent ribosome recycling. Our data revealed that ABCE1 knockdown affects the translation of viral mRNAs strongly, while cellular protein synthesis is only modestly affected.

Why are *Paramyxo-* and *Pneumoviridae* mRNAs so sensitive to ABCE1? The human 80S ribosome has a molecular weight of 4.3 MDa. The 60S subunit consists of the 28S, 5S and 5.8S rRNAs and 47 other proteins, while the 40S subunit is composed of a single 18S rRNA chain and 33 other proteins (Khatter *et al.*, 2015). The ribosome has previously been viewed as a passive, invariant, and indiscriminate machine, where ribosome recruitment is seen as the end-point of regulation. However, recent developments have confirmed the existence of specialized ribosomes that are generated due to heterogeneous ribosomal proteins composition, post-translational modifications of ribosomal proteins subsets, variations in ribosomal RNA sequences, or binding to distinct ribosome-associated factors, all of which point to ribosome activity being highly regulated (Xue and Barna, 2012). Translating ribosomes are heterogeneous in their ribosomal protein composition and can preferentially translate specific subpools of mRNAs (Shi and Barna, 2015; Genuth and Barna, 2018; Guo, 2018). The ribosomal protein L38 (RPL38) promotes selective translational control of Hox mRNAs mediated by two *cis*-regulatory elements, translation inhibitory element and IRES element, present in their 5′ UTRs to impede cap-dependent translation and independently recruit ribosomes carrying RPL38 to initiate translation. In RPL38 mutant embryos, total protein synthesis was unaffected, while translation of a subset of Hox mRNAs was impaired (Kondrashov *et al.*, 2011; Xue *et al.*, 2015). Heterogeneous compositions of actively translating ribosomes within mouse embryonic cells were also identified by quantitative mass spectrometry. Affinity purification and ribosome profiling revealed that ribosomes containing RPS25/eS25 or RPL10/uL1 preferentially translate specific subsets of transcripts, including those regulating metabolism, the cell cycle, and development. IRES elements in the mRNAs' 5′ UTRs contribute to the unique translational regulation by RPL10A (Shi *et al.*, 2017). In addition to variation of RP composition, heterogeneous ribosomes can also emerge from ribosome-associated

factors. The scaffold protein RACK1 was recently found to be important for efficient translation of mRNAs with short open reading frames (Thompson *et al.*, 2016). The ribosome-associated factor FMRP binds directly to ribosomes and blocks the binding of eEF1A•GTP•aminoacyl-tRNA ternary complex and eEF2 to the 80S ribosome to inhibit the transit of the ribosomes on the target mRNAs (Darnell *et al.*, 2011; Chen *et al.*, 2014).

Viruses also use specialized ribosomes for viral IRES-mediated translation. The ribosomal protein RPS25 is specifically required for IRES-mediated translation initiation of cricket-paralysis virus (CrPV) and HCV (Landry, Hertz and Thompson, 2009). Translation initiation by the 40S ribosomal subunit from the CrPV intergenic IRES and the HCV IRES was blocked when RPS25 was not present. Interestingly, regulation of viral translation by specialized ribosomes is not restricted to IRES-mediated translation, but can also occur for cap-dependent translation. VSV translation depends specifically on the ribosomal protein rpL40, which is required for 80S ribosome association with VSV mRNAs via a *cis*-regulatory element (Lee, Burdeinick-Kerr and Whelan, 2013). Intriguingly, rpL40 is not essential for bulk cellular or cap-independent translation, but, with the exception of VSV, is necessary for members of the order *Mononegavirales*, including MeV and rabies virus.

The discovery that heterogeneous ribosomes translate distinct mRNAs is quite recent, and there are many outstanding questions regarding the functional impact of specialized ribosomes and the mechanisms by which they preferentially translate mRNAs. ABCE1 may act as a ribosome-associated factor mediating selective mRNA translation and that paramyxo- and pneumoviruses exploit this strategy to recruit ribosomes for efficient viral translation. It must be emphasized that not all paramyxo- and pneumovirus mRNAs likely require ABCE1 to the same extent, since these mRNAs vary in their structures and most likely in their dependence on other host factors. The long 3′ UTR of the M mRNA increases M protein production and promotes virus replication, while the long 5′ UTR of the F mRNA decreases F protein production, which inhibits virus replication and reduces cytopathic effect (Takeda *et al.*, 2005). MeV N mRNA translation is enhanced by La autoantigen (SSB) overexpression, and this is thought to be mediated by an interaction between SSB and the short 5′ UTR of MeV N mRNA (Inoue *et al.*, 2011). Since the 5′ UTR of paramyxo- and pneumoviral mRNAs can vary in length depending on the gene and virus, we tested the sensitivity to ABCE1 knockdown using dual-luciferase reporter gene assays. The viral 5′ UTRs mediated translation to varying extents, but ABCE1 knockdown had no specific effect on any of the viral UTRs. However, it is also conceivable that 3′ UTRs of viral mRNAs may recruit ABCE1 to selectively enhance viral translation. Techniques such as ribosome profiling, the deep-sequencing of ribosome-protected mRNA fragments, is a valuable

and versatile tool to profile and monitor global translation. Towards this, we plan to perform translatome profiling experiments to determine if ABCE1 exerts its influence on viral translation via this route. Comparative studies of translation in paramyxo- and pneumovirus-infected cells in the presence and absence of ABCE1 will provide more insight in protein synthesis and the mechanisms of translational control.

6.2. Direct targeting of the virus life cycle

Targeting steps in viral replication that rely on cellular proteins is challenging, since detailed knowledge on the virus-host-interaction is necessary and adverse effects on the host organism have to be considered. In contrast, virus-encoded enzymes such as the polymerase are ideal targets for the development of antiviral therapeutics. The small-molecule inhibitor ERDRP-0519 binds to the MeV polymerase domain that catalyzes phosphodiester bond formation, thereby reducing the activity of the MeV polymerase. Antiviral drugs targeting viral polymerases of a wide range of viruses have already been developed, including cytomegalovirus (CMV) (Andrei, De Clercq and Snoeck, 2009), herpes simplex virus (HSV) (Billich, 2001) and HBV (Palumbo, 2008). Nucleoside analogs such as acyclovir and ganciclovir are in fact the most commonly used drugs to treat herpes infections (Strasfeld and Chou, 2010). Antiviral agents against HBV are also nucleoside (lamivudine, entecavir) or nucleotide (adefovir) analogs which selectively target the HBV DNA polymerase (Strasfeld and Chou, 2010). However, emergence of drug resistance after ongoing viral replication and prolonged drug exposure is a major challenge. The development of drug resistance has been seen for many viruses including HBV as well as the herpesviruses CMV, HSV, and varicella-zoster virus (Strasfeld and Chou, 2010).

For influenza treatment, M2 ion channel inhibitors (amantadine and rimantadine) and neuraminidase (NA) inhibitors (oseltamivir, zanamivir, peramivir, and laninamivir), have been licensed, and more recently, the first generation of polymerase inhibitors (baloxavir) was approved by the FDA (FDA, 2018). However, emergence of antiviral drug resistance in influenza virus infections is also a major problem (Hussain *et al.*, 2017), with virtually all circulating strains being resistant to M2 ion channel inhibitors, and the prevalence of NA inhibitor resistance is increasing. Despite decreasing HIV death rates in regions of the world that have full access to antiretroviral drugs, there is concern about the emergence and transmission of drug-resistant HIV strains. HIV drug resistance occurs with all antiretroviral agents (Kozal, 2009). Since resistance to all commonly used reverse transcriptase inhibitors (evirapine, efavirenz, delavirdine, etravirine, and rilpivirine) have been found, several new antiretroviral classes that inhibit other aspects of the viral life cycle have been developed, including protease

inhibitors, fusion inhibitors, CCR5 antagonists, and integrase inhibitors (Kozal, 2009). As a consequence, a combined drug therapy targeting different viral functions simultaneously is currently the standard regimen to treat HIV infections.

To evaluate the risk for the emergence of ERDRP-0519-resistant MeV mutants in treated individuals, known resistance hotspots for mutations in CR II (residue 589), CR III (residues 768 and 776), and CR IV (residues 1170, 1233, and 1239) (Yoon *et al.*, 2009) of virus isolates from all MeV-positive squirrel monkeys were screened (data not shown in the dissertation). These hotspot mutations were identified in previous resistance studies after *in vitro* drug treatment using MeV and CDV (Yoon *et al.*, 2009; Krumm *et al.*, 2014). Sequencing of viruses isolated from treated and untreated animals revealed no signature drug resistance mutations in these hotspots, which is promising for its potential use in clinical settings. The drug most effectively reduces or prevents MeV disease if administered before infection or early after infection. The inhibitor could therefore be useful in MeV outbreak scenarios where it would be given either prophylactically or therapeutically to unvaccinated contacts to reduce disease severity and prevent the spread of disease. Indeed, ERDRP-0519 treatment reduced virus shedding into the upper respiratory tract in prophylactically and therapeutically (D3) treated animals. Disruption of the virus transmission cycle is a key component of the global MeV eradication campaign. This is especially important given the high MeV reproduction rate which necessitates the correspondingly high vaccination coverage rates that are often not achieved, but are required to maintain herd immunity (WHO, 2018c).

7. REFERENCES

Andersen, D. S. and Leevers, S. J. (2007) 'The essential drosophila ATP-binding cassette domain protein, pixie, binds the 40 S ribosome in an ATP-dependent manner and is required for translation initiation', Journal of Biological Chemistry, 282(20), pp. 14752–14760. doi: 10.1074/jbc.M701361200.

Anderson, D. E. et al. (2019) 'Comparative loss-of-function screens reveal ABCE1 as an essential cellular host factor for efficient translation of Paramyxoviridae and Pneumoviridae', mBio, 10. doi: 10.1128/mBio.00826-19.

Anderson, L. J. et al. (2013) 'Strategic priorities for respiratory syncytial virus (RSV) vaccine development.', Vaccine, 31 Suppl 2, pp. B209-15. doi: 10.1016/j.vaccine.2012.11.106.

Andrei, G., De Clercq, E. and Snoeck, R. (2009) 'Drug targets in cytomegalovirus infection.', Infectious disorders drug targets, 9(2), pp. 201–22. doi: 10.2174/187152609787847758.

Andrejeva, J. et al. (2004) 'The V proteins of paramyxoviruses bind the IFN-inducible RNA helicase, mda-5, and inhibit its activation of the IFN-beta promoter.', Proceedings of the National Academy of Sciences of the United States of America, 101(49), pp. 17264–9. doi: 10.1073/pnas.0407639101.

Arneborn, P. and Biberfeld, G. (1983) 'T-lymphocyte subpopulations in relation to immunosuppression in measles and varicella.', Infection and immunity, 39(1), pp. 29–37. PMID: 6600445.

Ashiru, O., Howe, J. D. and Butters, T. D. (2014) 'Nitazoxanide, an antiviral thiazolide, depletes ATP-sensitive intracellular Ca2+ stores', Virology, 462–463, pp. 135–148. doi: 10.1016/j.virol.2014.05.015.

Au, H. H. and Jan, E. (2014) 'Novel viral translation strategies', Wiley Interdisciplinary Reviews: RNA, 5(6), pp. 779–801. doi: 10.1002/wrna.1246.

Bachmann, M. F. et al. (1996) 'Dendritic cells process exogenous viral proteins and virus-like particles for class I presentation to CD8+ cytotoxic T lymphocytes', European Journal of Immunology, 26(11), pp. 2595–2600. doi: 10.1002/eji.1830261109.

Baglioni, C., Benedetti, A. De and Williams, G. J. (1984) 'Cleavage of nascent reovirus mRNA by localized activation of the 2'-5'-oligoadenylate-dependent endoribonuclease', J Virol, 52(3), pp. 865–71. PMID: 6208382.

Bangor-Jones, R. D. et al. (2009) 'A prolonged mumps outbreak among highly vaccinated Aboriginal people in the Kimberley region of Western Australia.', The Medical journal of Australia, 191(7), pp. 398–401. PMID: 19807634.

Bankamp, B. et al. (1996) 'Domains of the measles virus N protein required for binding to P protein and self-assembly.', Virology, 216(1), pp. 272–7. doi: 10.1006/viro.1996.0060.

Bankamp, B. et al. (2005) 'Identification of naturally occurring amino acid variations that affect the ability of the measles virus C protein to regulate genome replication and transcription.', Virology, 336(1), pp. 120–9. doi: 10.1016/j.virol.2005.03.009.

Barthelme, D. et al. (2007) 'Structural Organization of Essential Iron-Sulfur Clusters in the Evolutionarily Highly Conserved ATP-binding Cassette Protein ABCE1', Journal of Biological Chemistry, 282(19), pp. 14598–14607. doi: 10.1074/jbc.M700825200.

Bauer, J. A. et al. (2010) 'RNA interference (RNAi) screening approach identifies agents that enhance paclitaxel activity in breast cancer cells.', Breast cancer research : BCR, 12(3), p. R41. doi: 10.1186/bcr2595.

Becker, T. et al. (2012) 'Structural basis of highly conserved ribosome recycling in eukaryotes and archaea', Nature, 482(7386), pp. 501–506. doi: 10.1038/nature10829.

Behera, A. K. et al. (2001) 'Blocking Intercellular Adhesion Molecule-1 on Human Epithelial Cells Decreases Respiratory Syncytial Virus Infection', Biochemical and Biophysical Research Communications, 280(1), pp. 188–195. doi: 10.1006/bbrc.2000.4093.

Bellini, W. J. et al. (1985) 'Measles virus P gene codes for two proteins', J Virol, 53(3), pp. 908–919. doi: 10.1113/jphysiol.2011.224741.

Belsham, G. J. and Sonenberg, N. (1996) 'RNA-protein interactions in regulation of picornavirus RNA translation.', Microbiological reviews, 60(3), pp. 499–511. PMID: 8840784.

Bernstein, E. et al. (2001) 'Role for a bidentate ribonuclease in the initiation step of RNA interference', Nature, 409(6818), pp. 363–366. doi: 10.1038/35053110.

Billich, A. (2001) 'Entecavir (Bristol-Myers Squibb).', Current opinion in investigational drugs (London, England : 2000), 2(5), pp. 617–21. PMID: 11569933.

Binder, G. K. and Griffin, D. E. (2001) 'Interferon-gamma-mediated site-specific clearance of alphavirus from CNS neurons.', Science (New York, N.Y.). American Association for the Advancement of Science, 293(5528), pp. 303–6. doi: 10.1126/science.1059742.

Binder, G. K. and Griffin, D. E. (2003) 'Immune-mediated clearance of virus from the central nervous system.', Microbes and infection, 5(5), pp. 439–48. doi: 10.1016/S1286-4579(03)00047-9

Birmingham, A. et al. (2006) '3' UTR seed matches, but not overall identity, are associated with RNAi off-targets.', Nature methods, 3(3), pp. 199–204. doi: 10.1038/nmeth854.

Bisbal, C. et al. (1995) 'Cloning and characterization of a RNAse L inhibitor. A new component of the interferon-regulated 2-5A pathway.', The Journal of biological chemistry, 270(22), pp. 13308–17. doi: 10.1074/jbc.270.22.13308.

Bisbal, C. et al. (2000) 'The 2'-5' oligoadenylate/RNase L/RNase L inhibitor pathway regulates both MyoD mRNA stability and muscle cell differentiation.', Molecular and cellular biology, 20(14), pp. 4959–69. doi: 10.1128/MCB.20.14.4959-4969.2000.

Boettcher, M. and Hoheisel, J. D. (2010) 'Pooled RNAi Screens - Technical and Biological Aspects.', Current genomics, 11(3), pp. 162–7. doi: 10.2174/138920210791110988.

Bonaparte, M. I. et al. (2005) 'Ephrin-B2 ligand is a functional receptor for Hendra virus and Nipah virus', Proceedings of the National Academy of Sciences, 102(30), pp. 10652–10657. doi: 10.1073/pnas.0504887102.

Booker, M. et al. (2011) 'False negative rates in Drosophila cell-based RNAi screens: a case study.', BMC genomics, 12(1), p. 50. doi: 10.1186/1471-2164-12-50.

Borchers, A. T. et al. (2013) 'Respiratory syncytial virus - A comprehensive review', Clinical Reviews in Allergy and Immunology, 45(3), pp. 331–379. doi: 10.1007/s12016-013-8368-9.

Bourhis, J.-M. et al. (2004) 'The C-terminal domain of measles virus nucleoprotein belongs to the class of intrinsically disordered proteins that fold upon binding to their physiological partner.', Virus research, 99(2), pp. 157–67. doi: 10.1016/j.virusres.2003.11.007.

Boutros, M. and Ahringer, J. (2008) 'The art and design of genetic screens: RNA interference.', Nature reviews. Genetics, 9(7), pp. 554–66. doi: 10.1038/nrg2364.

Boxall, N. et al. (2008) 'An increase in the number of mumps cases in the Czech Republic, 2005-2006.', Euro surveillance : bulletin Europeen sur les maladies transmissibles = European communicable disease bulletin, 13(16).

Brass, A. L. et al. (2008) 'Identification of host proteins required for HIV infection through a functional genomic screen.', Science (New York, N.Y.), 319(5865), pp. 921–6. doi: 10.1126/science.1152725.

de Breyne, S. et al. (2008) 'Cleavage of eukaryotic initiation factor eIF5B by enterovirus 3C proteases', Virology, 378(1), pp. 118–122. doi: 10.1016/j.virol.2008.05.019.

Broder, C. C., Weir, D. L. and Reid, P. A. (2016) 'Hendra virus and Nipah virus animal vaccines', Vaccine, 34(30), pp. 3525–3534. doi: 10.1016/j.vaccine.2016.03.075.

Brown, A. et al. (2015) 'Structural basis for stop codon recognition in eukaryotes', Nature, 524(7566), pp. 493–496. doi: 10.1038/nature14896.

Brunell, P. A. et al. (1968) 'Ineffectiveness of isolation of patients as a method of preventing the spread of mumps. Failure of the mumps skin-test antigen to predict immune status.', The New England journal of medicine, 279(25), pp. 1357–61. doi: 10.1056/NEJM196812192792502.

Buehler, E., Chen, Y.-C. and Martin, S. (2012) 'C911: A Bench-Level Control for Sequence Specific siRNA Off-Target Effects', PLoS ONE. Edited by S. Semsey. Public Library of Science, 7(12), p. e51942. doi: 10.1371/journal.pone.0051942.

Cathomen, T. et al. (1998) 'A matrix-less measles virus is infectious and elicits extensive cell fusion: consequences for propagation in the brain.', The EMBO journal, 17(14), pp. 3899–908. doi: 10.1093/emboj/17.14.3899.

Cathomen, T., Naim, H. Y. and Cattaneo, R. (1998) 'Measles viruses with altered envelope protein cytoplasmic tails gain cell fusion competence.', Journal of virology, 72(2), pp. 1224–34. PMID: 9445022.

Cattaneo, R. et al. (1987) 'Altered transcription of a defective measles virus genome derived from a diseased human brain.', The EMBO journal, 6(3), pp. 681–8. PMID: 3582370.

Cattaneo, R. et al. (1989) 'Measles virus editing provides an additional cysteine-rich protein.', Cell, 56(5), pp. 759–64. PMID: 2924348.

Centers for Disease Control and Prevention (CDC) (1986) 'Mumps--United States, 1984-1985.', MMWR. Morbidity and mortality weekly report, 35(13), pp. 216–9.

Centers for Disease Control and Prevention (CDC) (2006) 'Brief report: update: mumps activity--United States, January 1-October 7, 2006.', MMWR. Morbidity and mortality weekly report, 55(42), pp. 1152–3.

Centers for Disease Control and Prevention (CDC) (2010) 'Update: mumps outbreak - New York and New Jersey, June 2009-January 2010.', MMWR. Morbidity and mortality weekly report, 59(5), pp. 125–9.

Cevik, B. et al. (2004) 'The phosphoprotein (P) and L binding sites reside in the N-terminus of the L subunit of the measles virus RNA polymerase', Virology, 327(2), pp. 297–306. doi: 10.1016/j.virol.2004.07.002.

Chandrasekaran, K. et al. (2004) 'RNase-L regulates the stability of mitochondrial DNA-encoded mRNAs in mouse embryo fibroblasts', Biochemical and Biophysical Research Communications, 325(1), pp. 18–23. doi: 10.1016/j.bbrc.2004.10.016.

Chattopadhyay, A. and Shaila, M. S. (2004) 'Rinderpest virus RNA polymerase subunits: Mapping of mutual interacting domains on the large protein L and phosphoprotein P', Virus Genes, 28(2), pp. 169–178. doi: 10.1023/B:VIRU.0000016855.25662.95.

Chen, E. et al. (2014) 'Fragile X Mental Retardation Protein Regulates Translation by Binding Directly to the Ribosome', Molecular Cell, 54(3), pp. 407–417. doi: 10.1016/j.molcel.2014.03.023.

Chen, Z.-Q. et al. (2006) 'The essential vertebrate ABCE1 protein interacts with eukaryotic initiation factors.', The Journal of biological chemistry, 281(11), pp. 7452–7. doi: 10.1074/jbc.M510603200.

Chua, K. B. (2000) 'Nipah Virus: A Recently Emergent Deadly Paramyxovirus', Science, 288(5470), pp. 1432–1435. doi: 10.1126/science.288.5470.1432.

Colf, L. A., Juo, Z. S. and Garcia, K. C. (2007) 'Structure of the measles virus hemagglutinin.', Nature structural & molecular biology, 14(12), pp. 1227–8. doi: 10.1038/nsmb1342.

Collins, P. L. and Graham, B. S. (2008) 'Viral and Host Factors in Human Respiratory Syncytial Virus Pathogenesis', Journal of Virology, 82(5), pp. 2040–2055. doi: 10.1128/JVI.01625-07.

Collins, P. L. and Karron, R. A. (2013) 'Respiratory Syncytial Virus and Metapneumovirus', in Fields Virology. Lippincott, Williams, and Wilkins, pp. 1086–1123. doi: 9781451105636.

Collins, P. L. and Melero, J. A. (2011) 'Progress in understanding and controlling respiratory syncytial virus: Still crazy after all these years', Virus Research, 162(1–2), pp. 80–99. doi: 10.1016/j.virusres.2011.09.020.

Connor, J. H. and Lyles, D. S. (2002) 'Vesicular stomatitis virus infection alters the eIF4F translation initiation complex and causes dephosphorylation of the eIF4E binding protein 4E-BP1.', Journal of virology. American Society for Microbiology (ASM), 76(20), pp. 10177–87. doi: 10.1128/JVI.76.20.10177-10187.2002.

Cooney, M. K., Fox, J. P. and Hall, C. E. (1975) 'The Seattle Virus Watch. VI. Observations of infections with and illness due to parainfluenza, mumps and respiratory syncytial viruses and Mycoplasma pneumoniae.', American journal of epidemiology, 101(6), pp. 532–51. doi: 10.1093/oxfordjournals.aje.a112125

Cortese, M. M. et al. (2008) 'Mumps Vaccine Performance among University Students during a Mumps Outbreak', Clinical Infectious Diseases, 46(8), pp. 1172–1180. doi: 10.1086/529141.

Creagh, E. M. and O'Neill, L. A. J. (2006) 'TLRs, NLRs and RLRs: a trinity of pathogen sensors that co-operate in innate immunity.', Trends in immunology, 27(8), pp. 352–7. doi: 10.1016/j.it.2006.06.003.

Croghan, D. L. (1966) 'Attenuated live-virus canine distemper vaccines.', Journal of the American Veterinary Medical Association, 149(5), pp. 662–5. PMID: 6008148.

Curran, J. et al. (1995) 'Paramyxovirus Phosphoproteins Form Homotrimers as Determined by an Epitope Dilution Assay, via Predicted Coiled Coils', Virology, 214(1), pp. 139–149. doi: 10.1006/viro.1995.9946.

Currier, M. G. et al. (2016) 'EGFR Interacts with the Fusion Protein of Respiratory Syncytial Virus Strain 2-20 and Mediates Infection and Mucin Expression', PLOS Pathogens. Edited by M. T. Heise. Public Library of Science, 12(5), p. e1005622. doi: 10.1371/journal.ppat.1005622.

Darnell, J. C. et al. (2011) 'FMRP Stalls Ribosomal Translocation on mRNAs Linked to Synaptic Function and Autism', Cell, 146(2), pp. 247–261. doi: 10.1016/j.cell.2011.06.013.

Deffrasnes, C. et al. (2016) 'Genome-wide siRNA Screening at Biosafety Level 4 Reveals a Crucial Role for Fibrillarin in Henipavirus Infection', PLOS Pathogens. Edited by B. Lee. Public Library of Science, 12(3), p. e1005478. doi: 10.1371/journal.ppat.1005478.

Delpeut, S. et al. (2017) 'Nectin-4 Interactions Govern Measles Virus Virulence in a New Model of Pathogenesis, the Squirrel Monkey (Saimiri sciureus).', Journal of virology. Edited by T. S. Dermody, 91(11), pp. e02490-16. doi: 10.1128/JVI.02490-16.

Desfosses, A. et al. (2011) 'Nucleoprotein-RNA Orientation in the Measles Virus Nucleocapsid by Three-Dimensional Electron Microscopy', Journal of Virology, 85(3), pp. 1391–1395. doi: 10.1128/JVI.01459-10.

Diamond, M. S. and Farzan, M. (2013) 'The broad-spectrum antiviral functions of IFIT and IFITM proteins', Nature Reviews Immunology, 13(1), pp. 46–57. doi: 10.1038/nri3344.

Díaz-Guerra, M., Rivas, C. and Esteban, M. (1997) 'Inducible Expression of the 2-5A Synthetase/RNase L System Results in Inhibition of Vaccinia Virus Replication', Virology, 227(1), pp. 220–228. doi: 10.1006/viro.1996.8294.

Dietzel, E., Kolesnikova, L. and Maisner, A. (2013) 'Actin filaments disruption and stabilization affect measles virus maturation by different mechanisms.', Virology journal. BioMed Central, 10, p. 249. doi: 10.1186/1743-422X-10-249.

Domachowske, J. B. and Rosenberg, H. F. (1999) 'Respiratory syncytial virus infection: Immune response, immunopathogenesis, and treatment', Clinical Microbiology Reviews, 12(2), pp. 298–309. PMID: 10194461.

Dong, J. et al. (2004) 'The essential ATP-binding cassette protein RLI1 functions in translation by promoting preinitiation complex assembly.', The Journal of biological

chemistry. American Society for Biochemistry and Molecular Biology, 279(40), pp. 42157–68. doi: 10.1074/jbc.M404502200.

Dooher, J. E. et al. (2007) 'Host ABCE1 is at plasma membrane HIV assembly sites and its dissociation from Gag is linked to subsequent events of virus production.', Traffic (Copenhagen, Denmark), 8(3), pp. 195–211. doi: 10.1111/j.1600-0854.2006.00524.x.

Drysdale, S. B., Green, C. A. and Sande, C. J. (2016) 'Best practice in the prevention and management of paediatric respiratory syncytial virus infection', Therapeutic Advances in Infectious Disease, 3(2), pp. 63–71. doi: 10.1177/2049936116630243.

Duprex, W. P., Collins, F. M. and Rima, B. K. (2002) 'Modulating the function of the measles virus RNA-dependent RNA polymerase by insertion of green fluorescent protein into the open reading frame', J.Virol., 76(14), pp. 7322–7328. doi: Doi 10.1128/Jvi.76.14.7322-7328.2002.

Echeverri, C. J. et al. (2006) 'Minimizing the risk of reporting false positives in large-scale RNAi screens.', Nature methods, 3(10), pp. 777–9. doi: 10.1038/nmeth1006-777.

Echeverri, C. J. and Perrimon, N. (2006) 'High-throughput RNAi screening in cultured cells: a user's guide.', Nature reviews. Genetics, 7(5), pp. 373–84. doi: 10.1038/nrg1836.

Eisenhut, M. (2006) 'Extrapulmonary manifestations of severe respiratory syncytial virus infection - A systematic review', Critical Care, 10(4), p. R107. doi: 10.1186/cc4984.

Eisenhut, M. (2007) 'Cerebral involvement in respiratory syncytial virus disease', Brain and Development, 29(7), p. 454. doi: 10.1016/j.braindev.2006.11.007.

Elango, N. et al. (1989) 'mRNA sequence and deduced amino acid sequence of the mumps virus small hydrophobic protein gene.', Journal of virology, 63(3), pp. 1413–5. PMID: 2915385.

Evans, D. R. and Guy, H. I. (2004) 'Mammalian Pyrimidine Biosynthesis: Fresh Insights into an Ancient Pathway', Journal of Biological Chemistry, 279(32), pp. 33035–33038. doi: 10.1074/jbc.R400007200.

Falschlehner, C. et al. (2010) 'High-throughput RNAi screening to dissect cellular pathways: a how-to guide.', Biotechnology journal, 5(4), pp. 368–76. doi: 10.1002/biot.200900277.

FDA (2018) Press Announcements - FDA approves new drug to treat influenza. Office of the Commissioner. Available at: https://www.fda.gov/NewsEvents/Newsroom/PressAnnouncements/ucm624226.htm (Accessed: 4 April 2019).

Fields, B. N., Knipe, D. M. (David M. and Howley, P. M. (2007) Fields virology. 5th ed. Philadelphia: Wolters Kluwer Health/Lippincott Williams & Wilkins.

Fields, B. N., Knipe, D. M. (David M. and Howley, P. M. (2013) Fields virology. 6th ed. Philadelphia: Kluwer Health/Lippincott Williams & Wilkins.

Fire, A. et al. (1998) 'Potent and specific genetic interference by double-stranded RNA in Caenorhabditis elegans', Nature, 391(6669), pp. 806–811. doi: 10.1038/35888.

Floyd-Smith, G., Slattery, E. and Lengyel, P. (1981) 'Interferon action: RNA cleavage pattern of a (2'-5')oligoadenylate--dependent endonuclease.', Science (New York, N.Y.), 212(4498), pp. 1030–2. PMID: 6165080.

Franz, S. et al. (2017) 'Mumps Virus SH Protein Inhibits NF-κB Activation by Interacting with Tumor Necrosis Factor Receptor 1, Interleukin-1 Receptor 1, and Toll-Like Receptor 3 Complexes', Journal of Virology. Edited by S. López, 91(18), pp. e01037-17. doi: 10.1128/JVI.01037-17.

Gainey, M. D. et al. (2008) 'Paramyxovirus-induced shutoff of host and viral protein synthesis: role of the P and V proteins in limiting PKR activation.', Journal of virology, 82(2), pp. 828–39. doi: 10.1128/JVI.02023-07.

Genuth, N. R. and Barna, M. (2018) 'The Discovery of Ribosome Heterogeneity and Its Implications for Gene Regulation and Organismal Life', Molecular Cell, 71(3), pp. 364–374. doi: 10.1016/j.molcel.2018.07.018.

Ghosh, A., Sarkar, S. N. and Sen, G. C. (2000) 'Cell growth regulatory and antiviral effects of the P69 isozyme of 2-5 (A) synthetase', Virology, 266(2), pp. 319–328. doi: 10.1006/viro.1999.0085.

Gonsalves, F. C. et al. (2011) 'An RNAi-based chemical genetic screen identifies three small-molecule inhibitors of the Wnt/wingless signaling pathway.', Proceedings of the National Academy of Sciences of the United States of America, 108(15), pp. 5954–63. doi: 10.1073/pnas.1017496108.

Goulet, M.-L. et al. (2013) 'Systems Analysis of a RIG-I Agonist Inducing Broad Spectrum Inhibition of Virus Infectivity', PLoS Pathogens. Edited by G. C. Sen, 9(4), p. e1003298. doi: 10.1371/journal.ppat.1003298.

Gradi, A. et al. (1998) 'Proteolysis of human eukaryotic translation initiation factor eIF4GII, but not eIF4GI, coincides with the shutoff of host protein synthesis after poliovirus infection.', Proceedings of the National Academy of Sciences of the United States of America, 95(19), pp. 11089–94. doi: 10.1073/pnas.95.19.11089.

Griffin, D. E. (2013) 'Measles virus', in Fields Virology. Lippincott, Williams, and Wilkins, pp. 1042–1069.

Griffiths, C., Drews, S. J. and Marchant, D. J. (2017) 'Respiratory Syncytial Virus: Infection, Detection, and New Options for Prevention and Treatment.', Clinical microbiology reviews. American Society for Microbiology Journals, 30(1), pp. 277–319. doi: 10.1128/CMR.00010-16.

Groskreutz, D. J. et al. (2010) 'Respiratory syncytial virus limits alpha subunit of eukaryotic translation initiation factor 2 (eIF2alpha) phosphorylation to maintain translation and viral replication.', The Journal of biological chemistry. American Society for Biochemistry and Molecular Biology, 285(31), pp. 24023–31. doi: 10.1074/jbc.M109.077321.

Guo, H. (2018) 'Specialized ribosomes and the control of translation', Biochemical Society Transactions, 46(4), pp. 855–869. doi: 10.1042/BST20160426.

Hacking, D. and Hull, J. (2002) 'Respiratory syncytial virus - Viral biology and the host response', Journal of Infection, 45(1), pp. 18–24. doi: 10.1053/jinf.2002.1015.

Hall, C. B. et al. (1981) 'Infectivity of respiratory syncytial virus by various routes of inoculation', Infection and Immunity, 33(3), pp. 779–783. PMID: 7287181.

Hall, C. B., Simoes, E. A. F. and Anderson, L. J. (2013) 'Clinical and epidemiologic features of respiratory syncytial virus', Current Topics in Microbiology and Immunology, 372, pp. 39–57. doi: 10.1007/978-3-642-38919-1-2.

Hall, W. C. et al. (1971) 'Pathology of measles in rhesus monkeys.', Veterinary pathology, 8(4), pp. 307–319. doi: 10.1177/030098587100800403.

Hammond, S. M. et al. (2000) 'An RNA-directed nuclease mediates post-transcriptional gene silencing in Drosophila cells', Nature, 404(6775), pp. 293–296. doi: 10.1038/35005107.

Harcourt, J. et al. (2006) 'Respiratory syncytial virus G protein and G protein CX3C motif adversely affect CX3CR1+ T cell responses.', Journal of immunology (Baltimore, Md. : 1950), 176(3), pp. 1600–8. doi: 10.4049/jimmunol.176.3.1600.

Harrison, M. S., Sakaguchi, T. and Schmitt, A. P. (2010) 'Paramyxovirus assembly and budding: Building particles that transmit infections', The International Journal of Biochemistry & Cell Biology, 42(9), pp. 1416–1429. doi: 10.1016/j.biocel.2010.04.005.

Hassel, B. A. et al. (1993) 'A dominant negative mutant of 2-5A-dependent RNase suppresses antiproliferative and antiviral effects of interferon.', The EMBO journal, 12(8), pp. 3297–304. PMID: 7688298.

Hedlund, M. et al. (2010) 'Sialidase-Based Anti–Influenza Virus Therapy Protects against Secondary Pneumococcal Infection', The Journal of Infectious Diseases, 201(7), pp. 1007–1015. doi: 10.1086/651170.

Heuer, A. et al. (2017) 'Structure of the 40S-ABCE1 post-splitting complex in ribosome recycling and translation initiation.', Nature structural & molecular biology, 24(5), pp. 453–460. doi: 10.1038/nsmb.3396.

Hilleman, M. R. (1992) 'Past, present, and future of measles, mumps, and rubella virus vaccines.', Pediatrics, 90(1 Pt 2), pp. 149–53. PMID: 1603640.

Hinnebusch, A. G. (2006) 'eIF3: a versatile scaffold for translation initiation complexes', Trends in Biochemical Sciences, 31(10), pp. 553–562. doi: 10.1016/j.tibs.2006.08.005.

Hoffmann, H.-H. et al. (2011) 'Broad-spectrum antiviral that interferes with de novo pyrimidine biosynthesis.', Proceedings of the National Academy of Sciences of the United States of America, 108(14), pp. 5777–82. doi: 10.1073/pnas.1101143108.

Hoffmann, H.-H., Palese, P. and Shaw, M. (2008) 'Modulation of influenza virus replication by alteration of sodium ion transport and protein kinase C activity', Antiviral Research, 80(2), pp. 124–134. doi: 10.1016/j.antiviral.2008.05.008.

Holguera, J., Villar, E. and Muñoz-Barroso, I. (2014) 'Identification of cellular proteins that interact with Newcastle Disease Virus and human Respiratory Syncytial Virus by a two-dimensional virus overlay protein binding assay (VOPBA).', Virus research, 191, pp. 138–42. doi: 10.1016/j.virusres.2014.07.031.

Horikami, S. M. et al. (1994) 'An amino-proximal domain of the L protein binds to the P protein in the measles virus RNA polymerase complex', Virology, 205(2), pp. 540–545. doi: 10.1080/13621718.2017.1389837.

Huang, I.-C. et al. (2011) 'Distinct Patterns of IFITM-Mediated Restriction of Filoviruses, SARS Coronavirus, and Influenza A Virus', PLoS Pathogens. Public Library of Science, 7(1), p. e1001258. doi: 10.1371/JOURNAL.PPAT.1001258.

Huber, M. et al. (1991) 'Measles virus phosphoprotein retains the nucleocapsid protein in the cytoplasm.', Virology, 185(1), pp. 299–308. doi: 10.1016/0042-6822(91)90777-9.

Hui, D. J. et al. (2003) 'Viral Stress-inducible Protein p56 Inhibits Translation by Blocking the Interaction of eIF3 with the Ternary Complex eIF2·GTP·Met-tRNA $_{i}$', Journal of Biological Chemistry, 278(41), pp. 39477–39482. doi: 10.1074/jbc.M305038200.

Hussain, M. et al. (2017) 'Drug resistance in influenza A virus: the epidemiology and management.', Infection and drug resistance. Dove Press, 10, pp. 121–134. doi: 10.2147/IDR.S105473.

ICTV (2019) International Committee on Taxonomy of Viruses (ICTV). Available at: https://talk.ictvonline.org/taxonomy/ (Accessed: 11 March 2019).

Inoue, Y. et al. (2011) 'Selective translation of the measles virus nucleocapsid mRNA by la protein.', Frontiers in microbiology, 2, p. 173. doi: 10.3389/fmicb.2011.00173.

Ito, M. et al. (2013) 'Measles virus nonstructural C protein modulates viral RNA polymerase activity by interacting with host protein SHCBP1.', Journal of virology, 87(17), pp. 9633–42. doi: 10.1128/JVI.00714-13.

Iwasaki, M. et al. (2009) 'The matrix protein of measles virus regulates viral RNA synthesis and assembly by interacting with the nucleocapsid protein.', Journal of virology. American Society for Microbiology (ASM), 83(20), pp. 10374–83. doi: 10.1128/JVI.01056-09.

Jaafar, Z. A. and Kieft, J. S. (2019) 'Viral RNA structure-based strategies to manipulate translation', Nature Reviews Microbiology. Nature Publishing Group, 17(2), pp. 110–123. doi: 10.1038/s41579-018-0117-x.

Jack, P. J. M. et al. (2005) 'The complete genome sequence of J virus reveals a unique genome structure in the family Paramyxoviridae.', Journal of virology, 79(16), pp. 10690–700. doi: 10.1128/JVI.79.16.10690-10700.2005.

Jeong, K.-I. et al. (2015) 'CX3CR1 Is Expressed in Differentiated Human Ciliated Airway Cells and Co-Localizes with Respiratory Syncytial Virus on Cilia in a G Protein-Dependent Manner', PLOS ONE. Edited by J. S. Tregoning, 10(6), p. e0130517. doi: 10.1371/journal.pone.0130517.

Johnson, S. M. et al. (2015) 'Respiratory Syncytial Virus Uses CX3CR1 as a Receptor on Primary Human Airway Epithelial Cultures', PLOS Pathogens. Edited by M. T. Heise, 11(12), p. e1005318. doi: 10.1371/journal.ppat.1005318.

Kaplow, I. M. et al. (2009) 'RNAiCut: automated detection of significant genes from functional genomic screens.', Nature methods, 6(7), pp. 476–7. doi: 10.1038/nmeth0709-476.

Karcher, A., Schele, A. and Hopfner, K.-P. (2008) 'X-ray Structure of the Complete ABC Enzyme ABCE1 from Pyrococcus abyssi', Journal of Biological Chemistry, 283(12), pp. 7962–7971. doi: 10.1074/jbc.M707347200.

Kato, H. et al. (2006) 'Differential roles of MDA5 and RIG-I helicases in the recognition of RNA viruses.', Nature, 441(7089), pp. 101–5. doi: 10.1038/nature04734.

Katze, M. G. and Krug, R. M. (1990) 'Translational control in influenza virus-infected cells.', Enzyme, 44(1–4), pp. 265–77. PMID: 2133654.

Kawai, T. and Akira, S. (2010) 'The role of pattern-recognition receptors in innate immunity: update on Toll-like receptors.', Nature immunology, 11(5), pp. 373–84. doi: 10.1038/ni.1863.

Kerr, I. D. (2004) 'Sequence analysis of twin ATP binding cassette proteins involved in translational control, antibiotic resistance, and ribonuclease L inhibition', Biochemical and Biophysical Research Communications, 315(1), pp. 166–173. doi: 10.1016/j.bbrc.2004.01.044.

Khabar, K. S. A. et al. (2003) 'RNase L mediates transient control of the interferon response through modulation of the double-stranded RNA-dependent protein kinase PKR.', The Journal of biological chemistry, 278(22), pp. 20124–32. doi: 10.1074/jbc.M208766200.

Khatter, H. et al. (2015) 'Structure of the human 80S ribosome', Nature. Nature Publishing Group, 520(7549), pp. 640–645. doi: 10.1038/nature14427.

Kinch, M. S. et al. (2009) 'FGI-104: a broad-spectrum small molecule inhibitor of viral infection.', American journal of translational research, 1(1), pp. 87–98. Available at: http://www.ncbi.nlm.nih.gov/pubmed/19966942 (Accessed: 5 February 2019).doi: 10.1016/j.antiviral.2009.02.082.

Kingston, R. L., Baase, W. A. and Gay, L. S. (2004) 'Characterization of Nucleocapsid Binding by the Measles Virus and Mumps Virus Phosphoproteins', Journal of Virology, 78(16), pp. 8630–8640. doi: 10.1128/JVI.78.16.8630-8640.2004.

Kobune, F. et al. (1996) 'Nonhuman primate models of measles.', Laboratory animal science, 46(3), pp. 315–20. PMID: 8799939.

Koethe, S., Avota, E. and Schneider-Schaulies, S. (2012) 'Measles Virus Transmission from Dendritic Cells to T Cells: Formation of Synapse-Like Interfaces Concentrating Viral and Cellular Components', Journal of Virology, 86(18), pp. 9773–81. doi: 10.1128/JVI.00458-12.

Kondrashov, N. et al. (2011) 'Ribosome-mediated specificity in Hox mRNA translation and vertebrate tissue patterning.', Cell, 145(3), pp. 383–397. doi: 10.1016/j.cell.2011.03.028.

König, R. et al. (2008) 'Global analysis of host-pathogen interactions that regulate early-stage HIV-1 replication.', Cell, 135(1), pp. 49–60. doi: 10.1016/j.cell.2008.07.032.

König, R. et al. (2010) 'Human host factors required for influenza virus replication', Nature. Nature Publishing Group, 463(7282), pp. 813–817. doi: 10.1038/nature08699.

Kozal, M. J. (2009) 'Drug-resistant human immunodefiency virus', Clinical Microbiology and Infection, 15, pp. 69–73. doi: 10.1111/j.1469-0691.2008.02687.x.

Krishnan, M. N. et al. (2008) 'RNA interference screen for human genes associated with West Nile virus infection', Nature, 455(7210), pp. 242–245. doi: 10.1038/nature07207.

Krumm, S. A. et al. (2014) 'An orally available, small-molecule polymerase inhibitor shows efficacy against a lethal morbillivirus infection in a large animal model.', Science translational medicine. NIH Public Access, 6(232), p. 232ra52. doi: 10.1126/scitranslmed.3008517.

Krusat, T. and Streckert, H. J. (1997) 'Heparin-dependent attachment of respiratory syncytial virus (RSV) to host cells.', Archives of virology, 142(6), pp. 1247–54. PMID: 9229012.

Krzyzaniak, M. A. et al. (2013) 'Host Cell Entry of Respiratory Syncytial Virus Involves Macropinocytosis Followed by Proteolytic Activation of the F Protein', PLoS Pathogens. Edited by A. Pekosz. Public Library of Science, 9(4), p. e1003309. doi: 10.1371/journal.ppat.1003309.

Kurt-Jones, E. A. et al. (2000) 'Pattern recognition receptors TLR4 and CD14 mediate response to respiratory syncytial virus', Nature Immunology, 1(5), pp. 398–401. doi: 10.1038/80833.

Lamb, R. A. and Parks, G. D. (2013) 'Paramyxoviridae: the viruses and their replication', in Fields Virology. Lippincott, Williams, and Wilkins, pp. 957–995.

Landry, D. M., Hertz, M. I. and Thompson, S. R. (2009) 'RPS25 is essential for translation initiation by the Dicistroviridae and hepatitis C viral IRESs', Genes & Development, 23(23), pp. 2753–2764. doi: 10.1101/gad.1832209.

Lassus, P., Rodriguez, J. and Lazebnik, Y. (2002) 'Confirming Specificity of RNAi in Mammalian Cells', Science Signaling, 2002(147), pp. pl13–pl13. doi: 10.1126/stke.2002.147.pl13.

Leaman, D. W. et al. (2002) 'Targeted Therapy of Respiratory Syncytial Virus in African Green Monkeys by Intranasally Administered 2-5A Antisense', Virology, 292(1), pp. 70–77. doi: 10.1006/viro.2001.1213.

Lee, A. S.-Y., Burdeinick-Kerr, R. and Whelan, S. P. J. (2013) 'A ribosome-specialized translation initiation pathway is required for cap-dependent translation of vesicular stomatitis virus mRNAs', Proceedings of the National Academy of Sciences, 110(1), pp. 324–329. doi: 10.1073/pnas.1216454109.

Lee, A. S.-Y., Burdeinick-Kerr, R. and Whelan, S. P. J. (2014) 'A genome-wide small interfering RNA screen identifies host factors required for vesicular stomatitis virus infection.', Journal of virology. American Society for Microbiology (ASM), 88(15), pp. 8355–60. doi: 10.1128/JVI.00642-14.

Lee, Y. et al. (2006) 'The role of PACT in the RNA silencing pathway', The EMBO Journal, 25(3), pp. 522–532. doi: 10.1038/sj.emboj.7600942.

Li, N. et al. (2012) 'MxA inhibits hepatitis B virus replication by interaction with hepatitis B core antigen', Hepatology, 56(3), pp. 803–811. doi: 10.1002/hep.25608.

Li, Q. et al. (2009) 'A genome-wide genetic screen for host factors required for hepatitis C virus propagation.', Proceedings of the National Academy of Sciences of the United States of America, 106(38), pp. 16410–5. doi: 10.1073/pnas.0907439106.

Li, X. L. et al. (2000) 'RNase-L-dependent destabilization of interferon-induced mRNAs. A role for the 2-5A system in attenuation of the interferon response.', The Journal of biological chemistry, 275(12), pp. 8880–8. doi: 10.1074/jbc.275.12.8880.

Li, X. L., Blackford, J. A. and Hassel, B. A. (1998) 'RNase L mediates the antiviral effect of interferon through a selective reduction in viral RNA during encephalomyocarditis virus infection.', Journal of virology, 72(4), pp. 2752–9. PMID: 9525594.

Li, Z. et al. (2011) 'Function of the small hydrophobic protein of J paramyxovirus.', Journal of virology, 85(1), pp. 32–42. doi: 10.1128/JVI.01673-10.

Li, Z. et al. (2015) 'Type II integral membrane protein, TM of J paramyxovirus promotes cell-to-cell fusion.', Proceedings of the National Academy of Sciences of the United States of America. National Academy of Sciences, 112(40), pp. 12504–9. doi: 10.1073/pnas.1509476112.

Lingappa, J. R. et al. (2006) 'Basic residues in the nucleocapsid domain of Gag are required for interaction of HIV-1 gag with ABCE1 (HP68), a cellular protein important for HIV-1 capsid assembly.', The Journal of biological chemistry, 281(7), pp. 3773–84. doi: 10.1074/jbc.M507255200.

Liu, J. et al. (2004) 'Argonaute2 Is the Catalytic Engine of Mammalian RNAi', Science, 305(5689), pp. 1437–1441. doi: 10.1126/science.1102513.

Livak, K. J. and Schmittgen, T. D. (2001) 'Analysis of Relative Gene Expression Data Using Real-Time Quantitative PCR and the 2−ΔΔCT Method', Methods, 25(4), pp. 402–408. doi: 10.1006/meth.2001.1262.

Lo, M. S., Brazas, R. M. and Holtzman, M. J. (2005) 'Respiratory Syncytial Virus Nonstructural Proteins NS1 and NS2 Mediate Inhibition of Stat2 Expression and Alpha/Beta Interferon Responsiveness', Journal of Virology, 79(14), pp. 9315–9319. doi: 10.1128/JVI.79.14.9315-9319.2005.

Lou, Z., Sun, Y. and Rao, Z. (2014) 'Current progress in antiviral strategies', Trends in Pharmacological Sciences, 35(2), pp. 86–102. doi: 10.1016/j.tips.2013.11.006.

Ludlow, M. et al. (2015) 'Pathological consequences of systemic measles virus infection', Journal of Pathology, 235(2), pp. 253–65. doi: 10.1002/path.4457.

Ludlow, M., Allen, I. and Schneider-Schaulies, J. (2009) 'Systemic spread of measles virus: Overcoming the epithelial and endothelial barriers', Thrombosis and Haemostasis, 102(6), pp. 1050–6. doi: 10.1160/TH09-03-0202.

Luyet, P.-P. et al. (2008) 'The ESCRT-I Subunit TSG101 Controls Endosome-to-Cytosol Release of Viral RNA', Traffic, 9(12), pp. 2279–2290. doi: 10.1111/j.1600-0854.2008.00820.x.

Malhotra, R. et al. (2003) 'Isolation and characterisation of potential respiratory syncytial virus receptor(s) on epithelial cells.', Microbes and infection, 5(2), pp. 123–33. PMID: 12650770.

Marchant, D. et al. (2010) 'Toll-Like Receptor 4-Mediated Activation of p38 Mitogen-Activated Protein Kinase Is a Determinant of Respiratory Virus Entry and Tropism', Journal of Virology. American Society for Microbiology Journals, 84(21), pp. 11359–11373. doi: 10.1128/JVI.00804-10.

Marin, M. et al. (2008) 'Mumps vaccination coverage and vaccine effectiveness in a large outbreak among college students—Iowa, 2006', Vaccine, 26(29–30), pp. 3601–3607. doi: 10.1016/j.vaccine.2008.04.075.

Marr, N. and Turvey, S. E. (2012) 'Role of human TLR4 in respiratory syncytial virus-induced NF-κB activation, viral entry and replication', Innate Immunity, 18(6), pp. 856–865. doi: 10.1177/1753425912444479.

Martinand, C. et al. (1998) 'RNase L inhibitor (RLI) antisense constructions block partially the down regulation of the 2-5A/RNase L pathway in encephalomyocarditis-virus-(EMCV)-infected cells.', European journal of biochemistry, 254(2), pp. 248–55. PMID: 9660177.

Martinand, C. et al. (1999) 'RNase L inhibitor is induced during human immunodeficiency virus type 1 infection and down regulates the 2-5A/RNase L pathway in human T cells.', Journal of virology, 73(1), pp. 290–6. PMID: 9847332

Mateo, M. et al. (2015) 'Connections matter - how viruses use cell-cell adhesion components', Journal of Cell Science, 128(3), pp. 431–9. doi: 10.1242/jcs.159400.

Matrosovich, M., Herrler, G. and Klenk, H. D. (2013) 'Sialic Acid Receptors of Viruses', in Topics in current chemistry, pp. 1–28. doi: 10.1007/128_2013_466.

McChesney, M. B. et al. (1997) 'Experimental measles: I. Pathogenesis in the normal and the immunized host', Virology, 233(1), pp. 74–84. doi: 10.1006/viro.1997.8576.

McNabb, S. J. N. et al. (2007) 'Summary of notifiable diseases --- United States, 2005.', MMWR. Morbidity and mortality weekly report, 54(53), pp. 1–92. PMID: 17392681

Meister, G. et al. (2004) 'Human Argonaute2 Mediates RNA Cleavage Targeted by miRNAs and siRNAs', Molecular Cell, 15(2), pp. 185–197. doi: 10.1016/j.molcel.2004.07.007.

Mejías, A. et al. (2005) 'Respiratory syncytial virus infections: Old challenges and new opportunities', Pediatric Infectious Disease Journal, 24, pp. 189–197. doi: 10.1097/01.inf.0000188196.87969.9a.

Meng, J. et al. (2016) 'Respiratory Syncytial Virus Attachment Glycoprotein Contribution to Infection Depends on the Specific Fusion Protein', Journal of Virology. Edited by D. S. Lyles, 90(1), pp. 245–253. doi: 10.1128/JVI.02140-15.

Middleton, D. et al. (2014) 'Hendra virus vaccine, a one health approach to protecting horse, human, and environmental health.', Emerging infectious diseases, 20(3), pp. 372–9. doi: 10.3201/eid2003.131159.

Mohr, S., Bakal, C. and Perrimon, N. (2010) 'Genomic screening with RNAi: results and challenges.', Annual review of biochemistry, 79(1), pp. 37–64. doi: 10.1146/annurev-biochem-060408-092949.

Mohr, S. E. et al. (2014) 'RNAi screening comes of age: improved techniques and complementary approaches.', Nature reviews. Molecular cell biology, 15(9), pp. 591–600. doi: 10.1038/nrm3860.

Mortimer, P. P. (1978) 'Mumps prophylaxis in the light of a new test for antibody.', British medical journal, 2(6151), pp. 1523–4. doi: 10.1136/bmj.2.6151.1523.

Moss, W. J. and Griffin, D. E. (2006) 'Global measles elimination', Nature Reviews Microbiology. Nature Publishing Group, 4(12), pp. 900–908. doi: 10.1038/nrmicro1550.

Mühlebach, M. D. et al. (2011) 'Adherens junction protein nectin-4 is the epithelial receptor for measles virus', Nature, 480(7378), pp. 530–533. doi: 10.1038/nature10639.

Müller, B. and Kräusslich, H.-G. (2009) 'Antiviral Strategies', in Antiviral Strategies. Berlin, Heidelberg: Springer Berlin Heidelberg, pp. 1–24. doi: 10.1007/978-3-540-79086-0_1.

Müller, C. et al. (2018) 'Broad-spectrum antiviral activity of the eIF4A inhibitor silvestrol against corona- and picornaviruses', Antiviral Research. Elsevier, 150, pp. 123–129. doi: 10.1016/J.ANTIVIRAL.2017.12.010.

Naik, G. S. and Tyagi, M. G. (2012) 'A Pharmacological Profile of Ribavirin and Monitoring of its Plasma Concentration in Chronic Hepatitis C Infection', Journal of Clinical and Experimental Hepatology, 2(1), pp. 42–54. doi: 10.1016/S0973-6883(12)60090-5.

Naim, H. Y. (2015) 'Live Attenuated Measles Mumps and Rubella Vaccines: An Over View', International Journal of Vaccines & Vaccination. MedCrave Online, 1(1), pp. 1–0. doi: 10.15406/ijvv.2015.01.00005.

Nair, H. et al. (2010) 'Global burden of acute lower respiratory infections due to respiratory syncytial virus in young children: a systematic review and meta-analysis', The Lancet, 375(9725), pp. 1545–1555. doi: 10.1016/S0140-6736(10)60206-1.

Negrete, O. A. et al. (2005) 'EphrinB2 is the entry receptor for Nipah virus, an emergent deadly paramyxovirus', Nature, 436(7049), pp. 401–405. doi: 10.1038/nature03838.

Neumann, G. (2000) 'Influenza A virus NS2 protein mediates vRNP nuclear export through NES-independent interaction with hCRM1', The EMBO Journal, 19(24), pp. 6751–6758. doi: 10.1093/emboj/19.24.6751.

Nicholls, J. M., Moss, R. B. and Haslam, S. M. (2013) 'The use of sialidase therapy for respiratory viral infections.', Antiviral research, 98(3), pp. 401–9. doi: 10.1016/j.antiviral.2013.04.012.

Nilsen, T. W., Maroney, P. A. and Baglioni, C. (1982) 'Synthesis of (2'-5')oligoadenylate and activation of an endoribonuclease in interferon-treated HeLa cells infected with reovirus.', Journal of virology, 42(3), pp. 1039–45. PMID: 6178844

Njeumi, F. et al. (2012) 'The long journey: a brief review of the eradication of rinderpest.', Revue scientifique et technique (International Office of Epizootics), 31(3), pp. 729–46. PMID: 23520729

Noyce, R. S. and Richardson, C. D. (2012) 'Nectin 4 is the epithelial cell receptor for measles virus', Trends in Microbiology, 20(9), pp. 429–39. doi: 10.1016/j.tim.2012.05.006.

Nürenberg-Goloub, E. et al. (2018) 'Ribosome recycling is coordinated by processive events in two asymmetric ATP sites of ABCE1', Life Science Alliance, 1(3), p. e201800095. doi: 10.26508/lsa.201800095.

Nürenberg, E. and Tampé, R. (2013) 'Tying up loose ends: Ribosome recycling in eukaryotes and archaea', Trends in Biochemical Sciences, 38(2), pp. 64–74. doi: 10.1016/j.tibs.2012.11.003.

Ogino, T. et al. (2005) 'Sendai virus RNA-dependent RNA polymerase L protein catalyzes cap methylation of virus-specific mRNA.', The Journal of biological chemistry, 280(6), pp. 4429–35. doi: 10.1074/jbc.M411167200.

Olagnier, D. et al. (2014) 'Inhibition of Dengue and Chikungunya Virus Infections by RIG-I-Mediated Type I Interferon-Independent Stimulation of the Innate Antiviral Response', Journal of Virology, 88(8), pp. 4180–4194. doi: 10.1128/JVI.03114-13.

Palumbo, E. (2008) 'New drugs for chronic hepatitis B: a review.', American journal of therapeutics, 15(2), pp. 167–72. doi: 10.1097/MJT.0b013e318155a191.

Park, D. W. et al. (2007) 'Mumps outbreak in a highly vaccinated school population: Assessment of secondary vaccine failure using IgG avidity measurements', Vaccine, 25(24), pp. 4665–4670. doi: 10.1016/j.vaccine.2007.04.013.

Park, Y. W. and Katze, M. G. (1995) 'Translational control by influenza virus. Identification of cis-acting sequences and trans-acting factors which may regulate selective viral mRNA translation.', The Journal of biological chemistry, 270(47), pp. 28433–9. doi: 10.1074/jbc.270.47.28433

Park, Y. W., Wilusz, J. and Katze, M. G. (1999) 'Regulation of eukaryotic protein synthesis: selective influenza viral mRNA translation is mediated by the cellular RNA-binding protein GRSF-1.', Proceedings of the National Academy of Sciences of the United States of America, 96(12), pp. 6694–9. doi: 10.1073/pnas.96.12.6694

Parker, W. B. (2005) 'Metabolism and antiviral activity of ribavirin', Virus Research. Elsevier, 107(2), pp. 165–171. doi: 10.1016/J.VIRUSRES.2004.11.006.

Patterson, C. E. et al. (2002) 'Immune-mediated protection from measles virus-induced central nervous system disease is noncytolytic and gamma interferon dependent.', Journal of virology. American Society for Microbiology Journals, 76(9), pp. 4497–506. doi: 10.1128/JVI.76.9.4497-4506.2002.

Permar, S. R. et al. (2003) 'Role of CD8+ lymphocytes in control and clearance of measles virus infection of rhesus monkeys.', Journal of Virology, 77(7), pp. 4396–400. doi: Doi 10.1128/Jvi.77.7.4396-4400.2003.

Perwitasari, O. et al. (2014) 'Verdinexor, a Novel Selective Inhibitor of Nuclear Export, Reduces Influenza A Virus Replication In Vitro and In Vivo', Journal of Virology, 88(17), pp. 10228–10243. doi: 10.1128/JVI.01774-14.

Pfaller, C. K. et al. (2014) 'Measles Virus C Protein Impairs Production of Defective Copyback Double-Stranded Viral RNA and Activation of Protein Kinase R', Journal of Virology, 88(1), pp. 456–68. doi: 10.1128/JVI.02572-13.

Pfaller, C. K. and Conzelmann, K.-K. (2008) 'Measles virus V protein is a decoy substrate for IkappaB kinase alpha and prevents Toll-like receptor 7/9-mediated interferon induction.', Journal of virology, 82(24), pp. 12365–73. doi: 10.1128/JVI.01321-08.

Philip, R. N., Reinhard, K. R. and Lackman, D. B. (1959) 'Observations on a mumps epidemic in a virgin population.', American journal of hygiene, 69(2), pp. 91–111. PMID:13626949.

Pichlmair, A. et al. (2011) 'IFIT1 is an antiviral protein that recognizes 5′-triphosphate RNA', Nature Immunology, 12(7), pp. 624–630. doi: 10.1038/ni.2048.

Pisarev, A. V et al. (2010) 'The role of ABCE1 in eukaryotic posttermination ribosomal recycling.', Molecular cell, 37(2), pp. 196–210. doi: 10.1016/j.molcel.2009.12.034.

Pisareva, V. P. et al. (2011) 'Dissociation by Pelota, Hbs1 and ABCE1 of mammalian vacant 80S ribosomes and stalled elongation complexes.', The EMBO journal, 30(9), pp. 1804–17. doi: 10.1038/emboj.2011.93.

Plattet, P. et al. (2016) 'Measles Virus Fusion Protein: Structure, Function and Inhibition', Viruses, 8(4), p. 112. doi: 10.3390/v8040112.

Plemper, R. K. and Compans, R. W. (2003) 'Mutations in the putative HR-C region of the measles virus F2 glycoprotein modulate syncytium formation', Journal of Virology, 77(7), pp. 4181–90. doi: 10.1128/JVI.77.7.4181.

Plemper, R. K., Hammond, A. L. and Cattaneo, R. (2000) 'Characterization of a region of the measles virus hemagglutinin sufficient for its dimerization', J.Virol., 74(14), pp. 6485–93. doi: 10.1128/JVI.74.14.6485-6493.2000.

Plumet, S., Duprex, W. P. and Gerlier, D. (2005) 'Dynamics of Viral RNA Synthesis during Measles Virus Infection', Journal of Virology, 79(11), pp. 6900–6908. doi: 10.1128/JVI.79.11.6900-6908.2005.

Poch, O. et al. (1990) 'Sequence comparison of five polymerases (L proteins) of unsegmented negative-strand RNA viruses: theoretical assignment of functional domains', Journal of General Virology, 71, pp. 1153–62. doi: 10.1099/0022-1317-71-5-1153.

Postovit, V. A. (1983) '[Epidemic parotitis in adults].', Voenno-meditsinskii zhurnal, (3), pp. 38–41. PMID: 6868421.

Preis, A. et al. (2014) 'Cryoelectron Microscopic Structures of Eukaryotic Translation Termination Complexes Containing eRF1-eRF3 or eRF1-ABCE1', Cell Reports, 8(1), pp. 59–65. doi: 10.1016/j.celrep.2014.04.058.

Ramaswamy, M. et al. (2004) 'Specific inhibition of type I interferon signal transduction by respiratory syncytial virus.', American journal of respiratory cell and molecular biology, 30(6), pp. 893–900. doi: 10.1165/rcmb.2003-0410OC.

Raveh, A. et al. (2013) 'Discovery of Potent Broad Spectrum Antivirals Derived from Marine Actinobacteria', PLoS ONE. Edited by A. Ianora, 8(12), p. e82318. doi: 10.1371/journal.pone.0082318.

Rennick, L. J. et al. (2015) 'Live-Attenuated Measles Virus Vaccine Targets Dendritic Cells and Macrophages in Muscle of Nonhuman Primates', Journal of Virology. Edited by D. S. Lyles, 89(4), pp. 2192–2200. doi: 10.1128/JVI.02924-14.

Reutter, G. L. et al. (2001) 'Mutations in the Measles Virus C Protein That Up Regulate Viral RNA Synthesis', Virology, 285(1), pp. 100–109. doi: 10.1006/viro.2001.0962.

Rivera, C. I. and Lloyd, R. E. (2008) 'Modulation of enteroviral proteinase cleavage of poly(A)-binding protein (PABP) by conformation and PABP-associated factors', Virology, 375(1), pp. 59–72. doi: 10.1016/j.virol.2008.02.002.

RKI (2013) RKI - RKI-Ratgeber - Mumps. Available at: https://www.rki.de/DE/Content/Infekt/EpidBull/Merkblaetter/Ratgeber_Mumps.html. (Accessed: 14 March 2019).

RKI (2015) RKI - RKI-Ratgeber - Respiratorische Synzytial-Virus-Infektionen (RSV). Available at: https://www.rki.de/DE/Content/Infekt/EpidBull/Merkblaetter/Ratgeber_RSV.html (Accessed: 14 March 2019).

Roberts, C. et al. (2009) 'Mumps outbreak on the island of Anglesey, North Wales, December 2008-January 2009.', Euro surveillance : bulletin Europeen sur les maladies transmissibles = European communicable disease bulletin, 14(5). PMID: 19215718.

Rodriguez, K. R. and Horvath, C. M. (2014) 'Paramyxovirus V Protein Interaction with the Antiviral Sensor LGP2 Disrupts MDA5 Signaling Enhancement but Is Not Relevant to LGP2-Mediated RLR Signaling Inhibition', Journal of Virology. Edited by D. S. Lyles, 88(14), pp. 8180–8188. doi: 10.1128/JVI.00737-14.

Rossignol, J.-F. (2014) 'Nitazoxanide: A first-in-class broad-spectrum antiviral agent', Antiviral Research, 110, pp. 94–103. doi: 10.1016/j.antiviral.2014.07.014.

Rota, J. S. et al. (2009) 'Investigation of a mumps outbreak among university students with two measles-mumps-rubella (MMR) vaccinations, Virginia, September-December 2006', Journal of Medical Virology, 81(10), pp. 1819–1825. doi: 10.1002/jmv.21557.

Rubin, S. et al. (2015) 'Molecular biology, pathogenesis and pathology of mumps virus.', The Journal of pathology. NIH Public Access, 235(2), pp. 242–52. doi: 10.1002/path.4445.

Rubin, S. A. et al. (2012) 'Recent mumps outbreaks in vaccinated populations: no evidence of immune escape.', Journal of virology. American Society for Microbiology Journals, 86(1), pp. 615–20. doi: 10.1128/JVI.06125-11.

Rubin, S. A. (2018) 'Mumps Vaccines', Plotkin's Vaccines. Elsevier, pp. 663-688.e11. doi: 10.1016/B978-0-323-35761-6.00039-0.

Runkler, N. et al. (2007) 'Measles virus nucleocapsid transport to the plasma membrane requires stable expression and surface accumulation of the viral matrix protein.', Cellular microbiology, 9(5), pp. 1203–14. doi: 10.1111/j.1462-5822.2006.00860.x.

Russell, C. J., Jardetzky, T. S. and Lamb, R. A. (2001) 'Membrane fusion machines of paramyxoviruses: Capture of intermediates of fusion', EMBO Journal, 20(15), pp. 4024–34. doi: 10.1093/emboj/20.15.4024.

Ryon, J. J. et al. (2002) 'Functional and phenotypic changes in circulating lymphocytes from hospitalized zambian children with measles', Clin Diagn Lab Immunol, 9(5), pp. 994–1003. doi: 10.1128/CDLI.9.5.994.

Sakaguchi, M. et al. (1986) 'Growth of Measles Virus in Epithelial and Lymphoid Tissues of Cynomolgus Monkeys', Microbiology and Immunology, 30(10), pp. 1067–73. doi: 10.1111/j.1348-0421.1986.tb03036.x.

Sarov, M. and Stewart, A. F. (2005) 'The best control for the specificity of RNAi.', Trends in biotechnology, 23(9), pp. 446–8. doi: 10.1016/j.tibtech.2005.06.007.

Satoh, T. et al. (2010) 'LGP2 is a positive regulator of RIG-I- and MDA5-mediated antiviral responses.', Proceedings of the National Academy of Sciences of the United States of America, 107(4), pp. 1512–7. doi: 10.1073/pnas.0912986107.

Schwartzberg, P. L. et al. (2009) 'SLAM receptors and SAP influence lymphocyte interactions, development and function', Nature Reviews Immunology, 9(1), pp. 39–46. doi: 10.1038/nri2456.

Schwarz, D. S. et al. (2002) 'Evidence that siRNAs function as guides, not primers, in the Drosophila and human RNAi pathways.', Molecular cell, 10(3), pp. 537–48. doi: 10.1016/S1097-2765(02)00651-2.

Schwarz, D. S. et al. (2003) 'Asymmetry in the assembly of the RNAi enzyme complex.', Cell, 115(2), pp. 199–208. doi: 10.1016/S0092-8674(03)00759-1.

Seo, K. Y. et al. (2010) 'Eye Mucosa: An Efficient Vaccine Delivery Route for Inducing Protective Immunity', The Journal of Immunology, 185(6), pp. 3610–9. doi: 10.4049/jimmunol.1000680.

Sessions, O. M. et al. (2009) 'Discovery of insect and human dengue virus host factors', Nature, 458(7241), pp. 1047–1050. doi: 10.1038/nature07967.

Seyhan, A. A. et al. (2011) 'A genome-wide RNAi screen identifies novel targets of neratinib sensitivity leading to neratinib and paclitaxel combination drug treatments.', Molecular bioSystems, 7(6), pp. 1974–89. doi: 10.1039/c0mb00294a.

Shalem, O., Sanjana, N. E. and Zhang, F. (2015) 'High-throughput functional genomics using CRISPR–Cas9', Nature Reviews Genetics, 16(5), pp. 299–311. doi: 10.1038/nrg3899.

Sharma, S. and Rao, A. (2009) 'RNAi screening: tips and techniques', Nature Immunology, 10(8), pp. 799–804. doi: 10.1038/ni0809-799.

Shi, Z. et al. (2017) 'Heterogeneous Ribosomes Preferentially Translate Distinct Subpools of mRNAs Genome-wide.', Molecular cell, 67(1), pp. 71-83.e7. doi: 10.1016/j.molcel.2017.05.021.

Shi, Z. and Barna, M. (2015) 'Translating the Genome in Time and Space: Specialized Ribosomes, RNA Regulons, and RNA-Binding Proteins', Annual Review of Cell and Developmental Biology, 31(1), pp. 31–54. doi: 10.1146/annurev-cellbio-100814-125346.

Sidhu, M. S. et al. (1993) 'Canine distemper virus L gene: Sequence and comparison with related viruses', Virology, 193(1), pp. 50–65. doi: 10.1006/viro.1993.1102.

Sidorenko, S. P. and Clark, E. A. (2003) 'The dual-function CD150 receptor subfamily: the viral attraction', Nature Immunology, 4(1), pp. 19–24. doi: 10.1038/ni0103-19.

Singh, B. K. et al. (2015) 'The Nectin-4/Afadin Protein Complex and Intercellular Membrane Pores Contribute to Rapid Spread of Measles Virus in Primary Human Airway Epithelia.', Journal of virology. American Society for Microbiology (ASM), 89(14), pp. 7089–96. doi: 10.1128/JVI.00821-15.

Skabkin, M. A. et al. (2013) 'Reinitiation and other unconventional posttermination events during eukaryotic translation', Molecular Cell, 51(2), pp. 249–64. doi: 10.1016/j.molcel.2013.05.026.

Sledz, C. A. and Williams, B. R. G. (2004) 'RNA interference and double-stranded-RNA-activated pathways.', Biochemical Society transactions, 32(Pt 6), pp. 952–6. doi: 10.1042/BST0320952.

Le Sommer, C. et al. (2012) 'G protein-coupled receptor kinase 2 promotes flaviviridae entry and replication.', PLoS neglected tropical diseases. Edited by S. F. Michael, 6(9), p. e1820. doi: 10.1371/journal.pntd.0001820.

Sourimant, J. and Plemper, R. K. (2016) 'Organization, Function, and Therapeutic Targeting of the Morbillivirus RNA-Dependent RNA Polymerase Complex.', Viruses. Multidisciplinary Digital Publishing Institute (MDPI), 8(9), p. E251. doi: 10.3390/v8090251.

Spann, K. M. et al. (2004) 'Suppression of the induction of alpha, beta, and lambda interferons by the NS1 and NS2 proteins of human respiratory syncytial virus in human epithelial cells and macrophages [corrected].', Journal of virology, 78(8), pp. 4363–9. doi: 10.1128/jvi.78.8.4363-4369.2004.

Staeheli, P. et al. (1988) 'Influenza virus-susceptible mice carry Mx genes with a large deletion or a nonsense mutation.', Molecular and cellular biology, 8(10), pp. 4518–23. doi: 10.1128/mcb.8.10.4518.

Stillman, E. A. and Whitt, M. A. (1999) 'Transcript initiation and 5'-end modifications are separable events during vesicular stomatitis virus transcription.', Journal of virology, 73(9), pp. 7199–209. PMID: 10438807.

Stobart, C. C. et al. (2015) 'CX3CR1 is an important surface molecule for respiratory syncytial virus infection in human airway epithelial cells', Journal of General Virology, 96(9), pp. 2543–2556. doi: 10.1099/vir.0.000218.

Strasfeld, L. and Chou, S. (2010) 'Antiviral drug resistance: mechanisms and clinical implications.', Infectious disease clinics of North America. NIH Public Access, 24(2), pp. 413–37. doi: 10.1016/j.idc.2010.01.001.

Strunk, B. S. et al. (2012) 'A translation-like cycle is a quality control checkpoint for maturing 40S ribosome subunits.', Cell, 150(1), pp. 111–21. doi: 10.1016/j.cell.2012.04.044.

De Swart, R. L. et al. (2007) 'Predominant infection of CD150+ lymphocytes and dendritic cells during measles virus infection of macaques', PLoS Pathogens, 3(11), p. e178. doi: 10.1371/journal.ppat.0030178.

Tahara, M., Takeda, M. and Yanagi, Y. (2007) 'Altered Interaction of the Matrix Protein with the Cytoplasmic Tail of Hemagglutinin Modulates Measles Virus Growth by Affecting Virus Assembly and Cell-Cell Fusion', Journal of Virology, 81(13), pp. 6827–6836. doi: 10.1128/JVI.00248-07.

Tai, A. W. et al. (2009) 'A functional genomic screen identifies cellular cofactors of hepatitis C virus replication.', Cell host & microbe, 5(3), pp. 298–307. doi: 10.1016/j.chom.2009.02.001.

Takeda, M. et al. (2005) 'Long untranslated regions of the measles virus M and F genes control virus replication and cytopathogenicity.', Journal of virology, 79(22), pp. 14346–54. doi: 10.1128/JVI.79.22.14346-14354.2005.

Tannous, L. K., Barlow, G. and Metcalfe, N. H. (2014) 'A short clinical review of vaccination against measles.', JRSM open. SAGE Publications, 5(4), p. 2054270414523408. doi: 10.1177/2054270414523408.

Tatsuo, H. et al. (2000) 'SLAM (CDw150) is a cellular receptor for measles virus.', Nature, 406(6798), pp. 893–7. doi: 10.1038/35022579.

Tayyari, F. et al. (2011) 'Identification of nucleolin as a cellular receptor for human respiratory syncytial virus', Nature Medicine, 17(9), pp. 1132–1135. doi: 10.1038/nm.2444.

Techaarpornkul, S., Barretto, N. and Peeples, M. E. (2001) 'Functional Analysis of Recombinant Respiratory Syncytial Virus Deletion Mutants Lacking the Small Hydrophobic and/or Attachment Glycoprotein Gene', Journal of Virology, 75(15), pp. 6825–6834. doi: 10.1128/JVI.75.15.6825-6834.2001.

Teng, M. N., Whitehead, S. S. and Collins, P. L. (2001) 'Contribution of the respiratory syncytial virus G glycoprotein and its secreted and membrane-bound forms to virus replication in vitro and in vivo', Virology, 289(2), pp. 283–96. doi: 10.1006/viro.2001.1138.

Terenzi, F., Saikia, P. and Sen, G. C. (2008) 'Interferon-inducible protein, P56, inhibits HPV DNA replication by binding to the viral protein E1', The EMBO Journal, 27(24), pp. 3311–3321. doi: 10.1038/emboj.2008.241.

Thakur, C. S. et al. (2007) 'Small-molecule activators of RNase L with broad-spectrum antiviral activity', Proceedings of the National Academy of Sciences, 104(23), pp. 9585–9590. doi: 10.1073/pnas.0700590104.

Thompson, M. K. et al. (2016) 'The ribosomal protein Asc1/RACK1 is required for efficient translation of short mRNAs', eLife, 5, p. e11154. doi: 10.7554/eLife.11154.

Tian, Y., Han, X. and Tian, D. L. (2012) 'The biological regulation of ABCE1', IUBMB Life, 64(10), pp. 795–800. doi: 10.1002/iub.1071.

Torres, J. P. et al. (2010) 'Respiratory Syncytial Virus (RSV) RNA loads in peripheral blood correlates with disease severity in mice', Respiratory Research, 11(1), p. 125. doi: 10.1186/1465-9921-11-125.

Tripp, R. A. et al. (2001) 'CX3C chemokine mimicry by respiratory syncytial virus G glycoprotein', Nature Immunology, 2(8), pp. 732–738. doi: 10.1038/90675.

Tuteja, R. (2009) 'Identification and bioinformatics characterization of translation initiation complex eIF4F components and poly(A)-binding protein from Plasmodium falciparum', Communicative and Integrative Biology, 2(3), pp. 245–260. doi: 10.4161/cib.2.3.8843.

de Vries, R. D. et al. (2012) 'Measles Immune Suppression: Lessons from the Macaque Model', PLoS Pathogens, 8(8), p. e1002885. doi: 10.1371/journal.ppat.1002885.

Wang, J. T., McElvain, L. E. and Whelan, S. P. J. (2007) 'Vesicular stomatitis virus mRNA capping machinery requires specific cis-acting signals in the RNA.', Journal of virology, 81(20), pp. 11499–506. doi: 10.1128/JVI.01057-07.

Watson-Creed, G. et al. (2006) 'Two successive outbreaks of mumps in Nova Scotia among vaccinated adolescents and young adults', Canadian Medical Association Journal, 175(5), pp. 483–488. doi: 10.1503/cmaj.060660.

Welliver, R. C. (2008) 'The immune response to respiratory syncytial virus infection: Friend or foe?', Clinical Reviews in Allergy and Immunology, 34(2), pp. 163–73. doi: 10.1007/s12016-007-8033-2.

Whelan, S. P. J. (2008) 'Response to "Non-segmented negative-strand RNA virus RNA synthesis in vivo".', Virology, 371(2), pp. 234–7. doi: 10.1016/j.virol.2007.11.027.

Whimbey, E. et al. (1995) 'Respiratory syncytial virus pneumonia in hospitalized adult patients with leukemia', Clinical Infectious Diseases, 21(2), pp. 376–9. doi: 10.1093/clinids/21.2.376.

White, R. G. and Boyd, J. F. (1973) 'The effect of measles on the thymus and other lymphoid tissues.', Clinical and experimental immunology. Wiley-Blackwell, 13(3), pp. 343–57. PMID: 4701743.

WHO (2018a) Measles. Available at: https://www.who.int/news-room/fact-sheets/detail/measles (Accessed: 12 February 2019).

WHO (2018b) 'WHO | SAGE DoV GVAP Assessment report 2018', WHO. World Health Organization. Available at: https://www.who.int/immunization/documents/who_ivb_18.11/en/ (Accessed: 11 March 2019).

WHO (2018c) 'WHO | Weekly Epidemiological Record, 30 November 2018, vol. 93, 48 (pp. 649–660)', WHO. World Health Organization. Available at: https://www.who.int/wer/2018/wer9348/en/ (Accessed: 4 April 2019).

Xu, P. et al. (2011) 'Rescue of wild-type mumps virus from a strain associated with recent outbreaks helps to define the role of the SH ORF in the pathogenesis of mumps virus.', Virology. NIH Public Access, 417(1), pp. 126–36. doi: 10.1016/j.virol.2011.05.003.

Xue, S. et al. (2015) 'RNA regulons in Hox 5' UTRs confer ribosome specificity to gene regulation.', Nature, 517(7532), pp. 33–8. doi: 10.1038/nature14010.

Xue, S. and Barna, M. (2012) 'Specialized ribosomes: a new frontier in gene regulation and organismal biology.', Nature reviews. Molecular cell biology. NIH Public Access, 13(6), pp. 355–69. doi: 10.1038/nrm3359.

Yanagi, Y. et al. (2002) 'Measles virus receptor SLAM (CD150).', Virology, 299(2), pp. 155–61. doi: 10.1006/viro.2002.1471

Yi, R. et al. (2003) 'Exportin-5 mediates the nuclear export of pre-microRNAs and short hairpin RNAs', Genes & Development, 17(24), pp. 3011–3016. doi: 10.1101/gad.1158803.

Yin, H. S. et al. (2006) 'Structure of the parainfluenza virus 5 F protein in its metastable, prefusion conformation', Nature, 439(7072), pp. 38–44. doi: 10.1038/nature04322.

Yoon, J.-J. et al. (2009) 'Target Analysis of the Experimental Measles Therapeutic AS-136A', Antimicrobial Agents and Chemotherapy, 53(9), pp. 3860–3870. doi: 10.1128/AAC.00503-09.

Young, D. J. et al. (2015) 'Rli1/ABCE1 Recycles Terminating Ribosomes and Controls Translation Reinitiation in 3'UTRs In Vivo.', Cell, 162(4), pp. 872–84. doi: 10.1016/j.cell.2015.07.041.

Zhang, J.-H., Chung and Oldenburg (1999) 'A Simple Statistical Parameter for Use in Evaluation and Validation of High Throughput Screening Assays.', Journal of biomolecular screening, 4(2), pp. 67–73. doi: 10.1177/108705719900400206.

Zhou, H. et al. (2008) 'Genome-scale RNAi screen for host factors required for HIV replication.', Cell host & microbe, 4(5), pp. 495–504. doi: 10.1016/j.chom.2008.10.004.

Zhu, Y. X. et al. (2011) 'RNAi screen of the druggable genome identifies modulators of proteasome inhibitor sensitivity in myeloma including CDK5.', Blood, 117(14), pp. 3847–57. doi: 10.1182/blood-2010-08-304022.

Zimmerman, C. et al. (2002) 'Identification of a host protein essential for assembly of immature HIV-1 capsids.', Nature, 415(6867), pp. 88–92. doi: 10.1038/415088a.

8. APPENDIX

8.1. List of Figures

8.2. List of Tables

8.3. Publications and presentations

Parts of this thesis were published in mBIO:

Anderson DE, Pfeffermann K, Kim SY, Sawatsky B, Pearson J, Kovtun M, Corcoran DL, Krebs Y, Sigmundsson K, Jamison SF, Yeo ZZJ, Rennick LJ, Wang L-F, Talbot PJ, Duprex WP, Garcia-Blanco MA, von Messling V. 2019. Comparative loss-of-function screens reveal ABCE1 as an essential cellular host factor for efficient translation of Paramyxoviridae and Pneumoviridae. mBIO 10:e00826-19. https://doi.org/10.1128/mBio.00826-19.

Parts of this thesis were orally presented at scientific conferences:

ASV (American Society for Virology) Annual Meeting 2018, College Park, Maryland, U.S.

Comparative Loss of Function Screens Reveal ABCE1 as Essential Cellular Host Factor for Efficient Translation of Paramyxoviridae and Pneumoviridae.

National Symposium on Zoonoses Research 2017, Berlin, Germany

Comparative loss of function screens reveal common pathways required by Paramyxoviridae and Pneumoviridae.

GFV (Gesellschaft für Virologie e.V.) Annual Meeting 2017, Marburg, Germany

Comparative loss of function screens reveal common pathways required by Paramyxoviridae and Pneumoviridae.

Parts of this thesis were presented by a poster at scientific conferences:

GFV (Gesellschaft für Virologie e.V.) Annual Meeting 2018, Würzburg, Germany

ABCE1 is an essential Paramyxo- and Pneumoviridae host factor.

9. AFFIRMATION

9.1. Declaration of authorship

I herewith declare that I have not previously participated in any doctoral examination procedure in a mathematics or natural science discipline.

.....

Place, Date, Signature

I, Kristin Pfeffermann, herewith declare that I have produced my doctoral dissertation on the topic of

Characterization of the role of host factors in the paramyxovirus life cycle

independently and using only the tools indicated therein. In particular, all references borrowed from external sources are clearly acknowledged and identified.
I confirm that I have respected the principles of good scientific practice and have not made use of the services of any commercial agency in respect of my doctorate.

.....

Place, Date, Signature

9.2. Erklärung und Versicherung

Ich, Kristin Pfeffermann, erkläre hiermit, dass ich mich bisher keiner Doktorprüfung im Mathematisch-Naturwissenschaftlichen Bereich unterzogen habe.

.....

Ort, Datum, Unterschrift

Ich, Kristin Pfeffermann, erkläre hiermit, dass ich die vorgelegte Dissertation

Characterization of the role of host factors in the paramyxovirus life cycle

selbständig angefertigt und mich anderer Hilfsmittel als der in ihr angegebenen nicht bedient habe, insbesondere, dass alle Entlehnungen aus anderen Schriften mit Angabe der betreffenden Schrift gekennzeichnet sind.
Ich versichere, die Grundsätze der guten wissenschaftlichen Praxis beachtet, und nicht die Hilfe einer kommerziellen Promotionsvermittlung in Anspruch genommen zu haben.

.....

Ort, Datum, Unterschrift